Recent star formation in cluster early-type galaxies

George, Koshy

rijksuniversiteit
groningen

Recent star formation in cluster early-type galaxies

Evidence from dynamics and stellar populations over the past 7 Gyr

Proefschrift

ter verkrijging van het doctoraat in de
Wiskunde en Natuurwetenschappen
aan de Rijksuniversiteit Groningen
op gezag van de
Rector Magnificus, dr. E. Sterken,
in het openbaar te verdedigen op
maandag 29 april 2013
om 11.00 uur

door

Koshy George

geboren op 16 maart 1979
te Chengannur, India

Promotor:	Prof. dr. S.C. Trager
Beoordelingscommissie:	Prof. dr. R.F. Peletier Prof. dr. M.A.W. Verheijen Prof. dr. S. Zaroubi

ISBN: 978-90-367-6199-4 (printed version)
ISBN: 978-90-367-6202-1 (electronic version)

Cover: Galaxy cluster formation over cosmic time.
Image credit: Hubble extreme deep field.
Designed by Niels Bos and concept by Koshy George.

Contents

Chapter 1

Introduction

Our story starts long, long ago, when human beings still lived in caves. On dark moonless nights they would stare at the night sky and wonder about its majestic beauty. They must have attempted to count those multitudes of stars, frightened by the strange signs from the heavens: a dim "milky" glowing band of light, faint and fuzzy nebulae, shooting streaks of light. Much time has passed since then: the wheel was invented, many wars were fought, man moved from caves to fancy mansions, the telescope was invented, stars were catalogued. The glowing band of light was named the Milky Way galaxy, and most of those faint fuzzy nebulous features were discovered to be stellar systems outside the Milky Way. As civilisation progressed we couldn't resist uncovering the secrets of the Universe. Today we have gigantic telescopes in remote places – beautiful Hawaii, the deserted Chilean Andes and the calm of outer space – to study and understand these majestic objects at which our forefathers stared with fear and wonder.

Edwin Hubble is often credited for establishing the field of extragalactic astronomy by observing and studying the nebulae in the night sky, which were in fact galaxies beyond the Milky Way. Hubble not only observed galaxies but classified them based on the morphological appearance in photographic images. Today we call this the "Hubble sequence" which is represented by the "tuning fork" diagram shown in Figure 1.1. Ellipticals (E) are situated to the left, lenticulars (S0) at the base of the fork, and spirals with (SB) and without (S) bar structures are separated along the two prongs. It is now customary to call those galaxies falling on the left of the Figure 1.1 early-type galaxies (ellipticals and lenticulars), whereas those on the right are referred to as late-type galaxies (spirals).

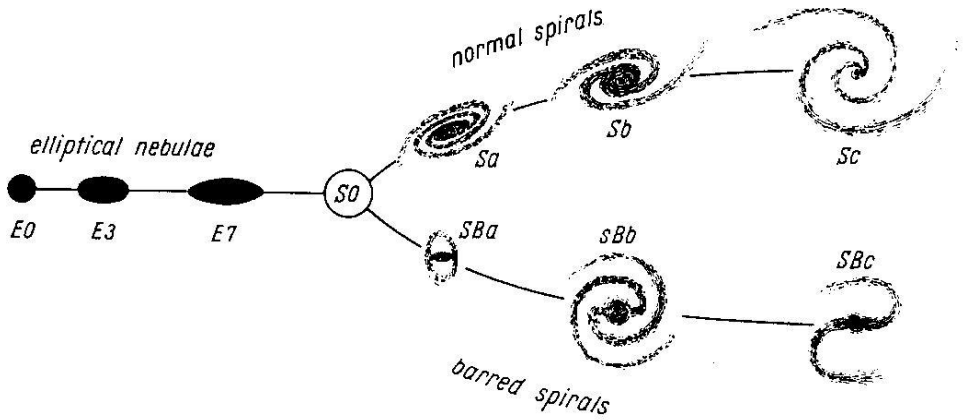

Figure 1.1: The Hubble tuning fork diagram. Galaxies to the left (ellipticals and lenticulars) are called early-type galaxies and those to the right (spirals) are called late-type galaxies. [Image credit: Hubble E.P., The Realm of the Nebulae (New Haven, 1936.)]

1.1 Galaxy formation and evolution

We now think that everything started with a violent explosion – the "Big Bang" – believed to have happened 13.7 Gyrs ago. In the beginning the Universe was in an extremely hot, dense state which began expanding rapidly during a phase now known as inflation. This was followed by a remarkably homogeneous phase, radiation from which can be observed today as the Cosmic Microwave Background (the fluctuations of which are less than one part in one hundred thousand). Density fluctuations in this cool, homogeneous Universe laid the seeds for galaxy formation. This is explained by the theoretical framework, which is in general agreement with observed properties of galaxies, known as the Λ Cold Dark Matter (ΛCDM) cosmology (see, e.g., Blumenthal et al. 1984). The primordial density fluctuations gravitationally attracted dark matter to the denser areas with in which gas got trapped and formed proto-galaxies. At this point the Universe was almost exclusively composed of hydrogen, helium, and dark matter. Soon after the first proto-galaxies formed, the hydrogen and helium gas within them began to condense and make the first stars. Further clustering and subsequent merging of protogalaxies is responsible for the formation and evolution of galaxies and determine their shape and structure until the present epoch of observation in the local Universe (e.g., White & Rees 1978; Binney 1977; Blumenthal et al. 1984). Galaxies are not isolated objects in space; rather, galaxies are distributed in a great cosmic web of filaments throughout the Universe. The locations where the filaments meet are dense clusters of galaxies that also began as density fluctuations in the early Universe. Hence the distribution of galaxies is closely related to the physics of the early Universe.

1.2 Galaxy clusters

Galaxy clusters are the largest gravitationally-bound objects in the Universe. Observationally galaxy clusters are dense, massive ($M \sim 10^{15}\,M_{\odot}$), bound structures, extending over few Mpc in size, consisting of hundreds to thousands of galaxies. Galaxy clusters formed from the highest-density peaks of the density fluctuations discussed above within which tiny fluctuations collapse into galaxies. However ΛCDM predicts that these high-density fluctuations which collapse into galaxy clusters are very rare in early Universe. Clusters are then formed relatively recently, less than 10 billion years ago, through accretion of galaxies and galaxy groups. Many galaxy clusters in the local Universe appear to be accreting galaxy groups, implying an on-going assembly process as late as $z \sim 0$ (Tran et al. 2008; Kautsch et al. 2008).

Clusters in general are rich in early-type galaxies, the fraction of which increases as one goes to the dense cluster cores. This is now understood to happen at the expense of late-type galaxies, which fall in to the cluster potential and undergo gas removal processes while interacting with the hostile cluster environment. Their star formation is therefore truncated, and they are transformed to early-type galaxies. Thus galaxy clusters, the densest environments at any redshift, are ideal laboratories to understand the formation and evolution of galaxies. The richest nearby galaxy cluster – often used as a local Universe reference point – is the Coma cluster.

1.3 Early-type galaxies

The morphology-density relation (e.g. Dressler 1980) means that the centres of galaxy clusters are full of red, gas-poor early-type galaxies (ETGs). ETGs are red because they are made up mostly of old stars, both low-mass stars still on the main sequence and giant stars in advanced stages of evolution. This understanding largely comes from studies based on observed optical colours and broad-band light. ETGs are observed to fall on a tight red sequence in the colour–magnitude diagram of galaxies. These observations give the impression that all the stars in ETGs are formed at one epoch, when the Universe was less than half of its current age and are simply aging with the age of the Universe to the present epoch (Renzini 2006). This is in strong conflict with the current understanding of galaxy formation and evolution theory according to ΛCDM, in which ETGs should be assembling not at one epoch, but over a range of epochs. The results from photometric surveys have demonstrated that the stellar mass of galaxies on the "red sequence" – mostly ETGs – has doubled during the last 8 billion years, which is only possible due to merging, accretion and *in situ* star formation events.(Bell et al. 2004; Faber et al. 2007).

A major challenge in studying the stellar contents of ETGs is that they are too distant to resolve into individual stars using current optical telescopes. M32, a compact elliptical galaxy satellite of the Andromeda Galaxy, is the exception. The resolved studies of M32 demonstrate that the stellar population is not fully formed at one epoch, but instead contains both intermediate-age and old stars (from ∼ 2–10 Gyr old: Monachesi et al. 2012). This means integrated light studies based on colours do not give us the real

picture of the underlying stellar population of ETGs. This was brought into firm focus by Worthey (1994), who showed that colours are degenerate to compensating changes of the age and chemical composition of the underlying stellar content. A change in age or metallicity of the stellar population can leave the same imprint on the observed colours of ETGs (Faber 1973a; O'Connell 1986; Worthey 1994). This degeneracy makes colours unusable for studying recent (1–2 Gyr old) star formation in ETGs. However, one can disentangle the age from the metallicity of the stellar population of an ETG by using a pair of metal-line and Balmer-line index strengths measured from its integrated optical spectrum. ETGs analysed in this way have indeed found to have recent star formation events (e.g., Trager et al. 2000a,b).

Young stars in early-type galaxies form as a consequence of accretion of cold (molecular) gas or interactions with other galaxies in their neighbourhood. Studying galaxies in dense environments like galaxy clusters should help to understand the evolution of ETGs, where interactions may have been very common in the past as a result of the cluster building process.

1.3.1 Integrated stellar population analysis

In its simplest form integrated stellar population analysis could be made by assuming all the stars in a galaxy are formed at one epoch and make up a single stellar population (SSP). The analysis techniques are model dependent and can be visualised as follows. First, evolutionary tracks for stellar interiors over a range in mass and a single (fixed) metallicity are sampled at a single age, resulting in an isochrone. Next, an initial mass function is chosen to specify the number of stars at each position along the isochrone. Third, empirical or synthetic stellar spectra are assigned to stars at each position on the isochrones. The spectra are then integrated weighted by the number of stars at each position along the isochrone, resulting in a model spectrum of the stellar population (e.g., Worthey 1994; Bruzual & Charlot 2003; Maraston & Strömbäck 2011; Vazdekis et al. 2012). This model spectrum is then compared with the observed spectra of galaxies to derive the underlying (single-stellar-population-equivalent) stellar population parameters. The stellar population parameters can be derived using complete spectral fitting (e.g., Koleva et al. 2009; Conroy & van Dokkum 2012) or using the classic Lick/IDS indices (e.g., Worthey 1994; Trager et al. 2000a; Thomas et al. 2005).

1.3.2 The Fundamental Plane

ETGs obey scaling relations between different observables. Fundamental Plane (FP) is one such scaling relation, in which ETGs follow a plane in the three-dimensional phase space relating velocity dispersion (σ), due to the random motion of stars in the galactic potential to the effective radius (R_e) and mean surface brightness ($\langle I_e \rangle$) (FP: Dressler et al. 1987; Djorgovski & Davis 1987; Faber et al. 1987). The FP can be represented as follows:

$$\langle I_e \rangle \propto \sigma^{\alpha} R_e^{\beta} \tag{1.1}$$

Self-gravitating, virialised stellar systems like ETGs should follow the Virial Theorem, with galaxies populating a Virial Plane with coefficients $\alpha = 2$ and $\beta = -1$ in the above

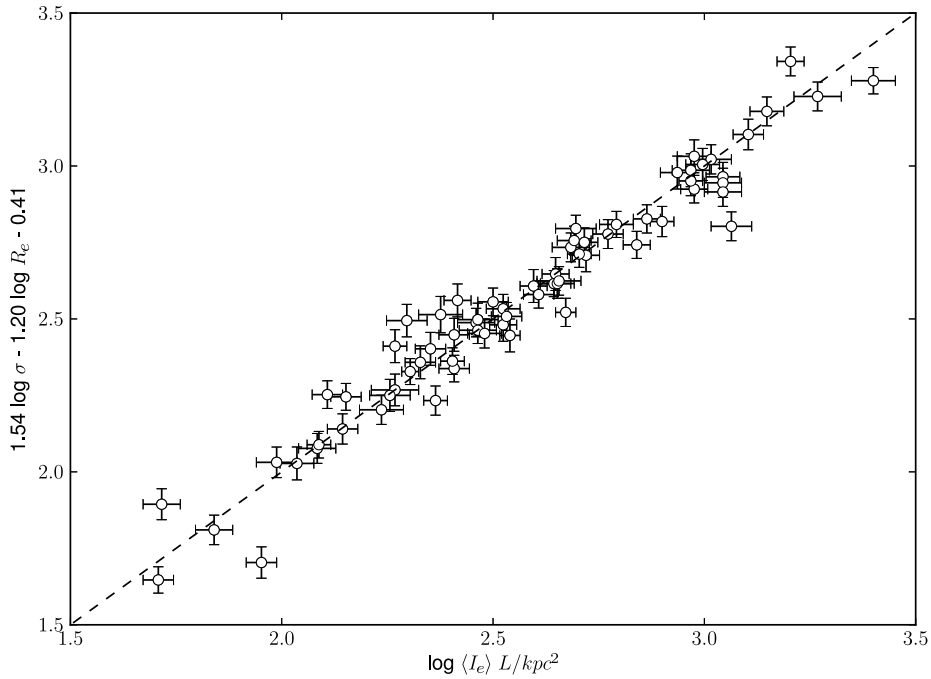

Figure 1.2: An edge-on view of the Coma R-band Fundamental plane. The plane has a finite thickness, with a scatter larger than can be explained purely by observational errors [Data from Jorgensen et al. (1996)].

equation. However, observations of ETGs show that galaxies rather fall on the Fundamental Plane with coefficients different from Virial Plane expectations; for example, the coefficients for R-band FP of the Coma Cluster are $\alpha = 1.54$ and $\beta = -1.20$. This is known as the "tilt" of the Fundamental Plane, and it appears to be due to a systematic variation of mass-to-light ratios with mass of ETGs (Cappellari et al. 2006; Graves et al. 2009; Graves & Faber 2010). Figure 1.2 shows an edge-on view of the R-band FP of ETGs in the Coma Cluster.

The FP is only weakly affected by the age–metallicity degeneracy since it is dictated by the mass-to-light ratios of the galaxy which in turn is highly sensitive to the age, more specifically the temperature of the main sequence turnoff of the underlying stellar population. The FP can therefore be used to understand ETGs evolution over cosmic time by converting it into a mass–mass-to-light relation (e.g., Kelson et al. 1997; van Dokkum et al. 1998; Gebhardt et al. 2003; Wuyts et al. 2004; Treu et al. 2005; van der Wel et al. 2005). The measured dynamical mass-to-light ratios from the FP parameters are a proxy for understanding the varying stellar content of ETGs, such that any variation in the (σ, R_e, $\langle I_e \rangle$) coordinate of a galaxy can be related to its star-formation history. This is because recent star formation should enhance the luminosity of a galaxy,

reducing its mass-to-light ratios and moving the galaxy off the plane. This implies the intrinsic scatter of the FP may be due to varying mass-to-light ratios of galaxies and the stellar contribution of which could be driven by recent star formation episodes. The stellar contribution of the dynamical mass-to-light ratios (stellar mass-to-light ratios) can be computed using stellar population analysis. The intrinsic scatter about Coma cluster FP shown in Figure 1.2 is ∼10–15% (Jorgensen et al. 1996).

The dynamic and stellar mass-to-light ratios along with the intrinsic scatter of the FP can therefore be used to understand recent star formation in ETGs. In this thesis, we attempt to understand the recent star formation in ETGs belonging to the very dense environments of galaxy clusters using a combined dynamical and stellar population analysis over the past 7 Gyr.

1.4 This Thesis

This thesis studies massive ETGs in four rich, optically-selected clusters in three redshift bins. The cluster ETGs were selected based on their early-type morphologies and/or colours and their positions relative to the cluster core. Imaging and spectroscopic data on ETGs are from the 10m-diameter Keck telescopes in Hawai'i, USA, the 8m-diameter Very Large Telescope (VLT) on Paranal, Chile, and the Hubble Space telescope (HST).

1.4.1 Chapter 2

We study the impact of stellar populations on the FP of ETGs in Abell 550, a galaxy cluster at $z \sim 0.1$. We construct the FP using structural parameters and velocity dispersions of ETGs. Dynamical mass-to-light ratios are calculated using the kinematic measurements, and stellar mass-to-light ratios are inferred using stellar-population models. Our stellar-population measurements yield ages, metallicities, and α-element enhancements derived from absorption-line strengths measured from our high signal-to-noise spectra. The ETGs in Abell 550 exhibit a scatter about the FP due to the intrinsic variations of their *stellar* mass-to-light ratios: recent star formation decreases the stellar mass-to-light ratios and increases the scatter of galaxies about the FP, yielding a finite thickness of the FP for this cluster. Additionally, we find that the tilt of the FP (with respect to the one expected from virial theorem) for this cluster can also be attributed to recent star formation: the stellar mass-to-light ratios vary systematically with their dynamical mass. Both results indicate that the ETGs in Abell 550 are still falling onto the FP relation at $z \sim 0.1$.

1.4.2 Chapter 3

We go further back in time, studying ETGs in the well-known merging cluster Abell 851 at $z \sim 0.4$. Our FP and stellar population analysis here again result in strong evidence for recent star formation in this cluster. The FP residuals are correlated with the stellar mass-to-light ratios derived from stellar-population models, and the stellar mass-to-light ratios are nearly constant over the range of measured dynamical masses.

These two empirical results imply that ETGs in Abell 851 have undergone recent star-formation episodes independent of their mass, and that this recent star formation is responsible for the increased scatter in the FP via the change in the stellar mass-to-light ratios. This can be explained by morphological and stellar-population transformations of the ETGs in Abell 851 due to the on-going cluster assembly at $z \sim 0.4$.

1.4.3 Chapter 4

We extend our study to higher redshifts, studying ETGs in two galaxy clusters at $z \sim 0.7$, GHO 1322+3027 and GHO 1322+3114. We find that the combined FP of ETGs in these clusters also has a large intrinsic scatter. The stellar and dynamical mass-to-light ratios follow similar trends as a function of dynamical mass. Thus, similar to the results in the previous two chapters, we find the ETGs in GHO 1322+3027 and GHO 1322+3114 have undergone recent star-formation episodes. The reason for this recent star formation can be explained by morphological and stellar-population transformations happening in the cluster cores due to the on-going cluster assembly processes.

1.4.4 Chapter 5

We trace the evolution of the dynamical and stellar mass-to-light ratios in cluster ETGs as a function of redshift. The analysis includes ETGs from all four rich, massive clusters studied here and the Coma Cluster, over the full redshift range of $0 < z < 0.7$. We find that the ETGs in our study exhibit no significant evolution in the mean dynamical or stellar mass-to-light ratios. The mean SSP ages of the ETGs are constant within the errors, whereas their mean metallicity decreases toward higher redshifts. The average α-enhancement increases toward higher redshift, suggesting an on-going build-up of chemical elements from recently-terminated star formation in the cluster galaxies at each epoch.

These results are only possible if these ETGs, at each epoch, experience star-formation events within the last 2 Gyr. The cluster ETGs at all redshifts exhibit complex star-formation histories, as supported by the evolution of their dynamical and stellar mass-to-light ratios. We suggest that these recent star formation episodes are due to morphological and stellar-population transformations arising from the ongoing assembly of galaxy clusters; this evolution is seen at all redshifts, meaning that ETGs continue to evolve well into the current epoch ($z \sim 0$).

Chapter 2

The relation between the early-type galaxies Fundamental Plane and stellar populations in Abell 550 at $z = 0.1$

Abstract

We present a study of the structural and stellar population parameters of 15 early-type galaxies (ETGs) in Abell 550, a rich massive Coma-like galaxy cluster at $z \sim 0.1$. The motivation for this study is to understand the role of stellar populations in shaping the Fundamental Plane (FP) of ETGs. We used spectroscopy and photometry to derive the structural parameters of ETGs and estimate the star-formation histories from single-stellar-population (SSP) models. ETGs in Abell 550 are found to follow a FP with similar coefficients and negligible zero-point offset with respect to those in the Coma cluster. Stellar population parameters based on high-quality spectroscopic data (S/N $>$ 50/Å) demonstrate for the first time an anti-correlation between the stellar mass-to-light ratios of the ETGs and their residuals from the FP. The direct implication of this result is that recent star formation plays a major role in determining the thickness of the FP. The scatter of ETGs on the FP can be used as a tool to quantify the presence of very recent star formation in cluster ETGs at higher redshifts where stellar population studies are expensive. The one-to-one correspondence between the dynamical and stellar mass-to-light ratios of ETGs in Abell 550 explains the tilt in the FP as the result of a systematic variation of stellar mass-to-light ratio with the dynamical mass of the

*Based on observations obtained from ESO program 072.A-0646(D), PI S.C.Trager

galaxies. Furthermore, the results reported here are inconsistent with passive evolution of the stellar populations of ETGs belonging to galaxy clusters.

2.1 Introduction

Early-type galaxies (ETGs) in the local Universe are hypothesized to be old, red and dead stellar systems. They are supposed to be formed at early epochs when the Universe was less than half of its current age and to have evolved passively until the present epoch (see Renzini 2006 for a detailed review). The color–magnitude diagram of galaxies supports this picture: ETGs are red and follow a tight sequence with small intrinsic scatter in the diagram, while galaxies which are actively forming stars are blue and have a broad distribution in color at fixed magnitude (Faber 1973b; Sandage & Visvanathan 1978; Bower et al. 1992; Baldry et al. 2004). This has led to a pervasive view that ETGs are ancient stellar systems formed in an intense burst of star formation in the early Universe, evolving to the present epoch with no further star formation.

However, according to the current paradigm of a Λ-Cold Dark Matter (ΛCDM) cosmology, structures form hierarchically, with small dark matter clumps merging together to form large dark matter halos. The associated baryons within the dark matter halos cool down dissipatively to form stellar systems, which we observe as galaxies. In this picture, galaxies are baryonic condensates at the center of large dark matter halos. ETG formation and evolution should then be hierarchical in nature with merging, accretion and *in situ* star formation all playing major roles in shaping this baryonic content (White & Rees 1978). In the hierarchical framework, ETGs join the red sequence on the color–magnitude diagram and the Fundamental Plane (FP: Dressler et al. 1987; Djorgovski & Davis 1987; Faber et al. 1987) over cosmic time. This can occur either through the secular evolution of star-forming blue galaxies or through equal-mass galaxy mergers. In both cases an intense starburst or feedback induced by an active galactic nucleus could remove most of the fuel for further star formation, making galaxies change color and migrate to the red sequence and also to fall on the FP. The existence of these scaling relations and their properties, like the location of recent arrivals on this relation, can be used to understand ETG formation and evolution.

The theoretical framework desribed above implies that star formation history of ETGs has to be more complex than simple passive evolution, with a build-up of the stellar mass content over cosmic time. Observational evidence from deep surveys like DEEP2 and COMBO-17 supports this build-up of stellar mass in ETGs during the last eight billion years (Bell et al. 2004; Faber et al. 2007). The presence of recent star formation (Kaviraj 2010) and intermediate-age stellar populations (e.g., Trager et al. 2000a) in many ETGs in the local Universe lends further support for this paradigm. Stellar population studies of ETGs on the red sequence using line strengths have shown that their colors are degenerate in age and metallicity (Worthey 1994). This naturally implies that colors cannot be used to detect recent star formation episodes occuring longer than 1–2 Gyr ago – and so appearing on the red sequence does not necessarily imply that an ETG is a *purely* old stellar system. Studying ETGs through colors may not give the necessary information unless the age-metallicity degeneracy is broken

using line strengths. When this is possible, stellar population studies of integrated galaxy spectra have shown that ETGs span a wide range of ages in the local Universe (e.g., Trager et al. 2000a,b).

On the other hand, the FP is only weakly affected by the age–metallicity degeneracy and can be used to understand ETG formation and evolution over cosmic times. The FP is a tight relation in the three-dimensional phase space between the velocity dispersion σ, effective radius R_e and the mean surface brightness $\langle I_e \rangle$ of galaxies. This relation is observed to be tilted with respect to the one expected from the virial theorem and has a $\sim$ 10–15 % intrinsic scatter in local clusters (Jorgensen et al. 1996). The observed FP of ETGs in Coma cluster has the form

$$R_e \propto \sigma^{1.24} \langle I_e \rangle^{-0.82} \tag{2.1}$$

(Jorgensen et al. 1996), but the relation for ETGs expected from virial theorem should have the form

$$R_e \propto \sigma^2 \langle I_e \rangle^{-1}. \tag{2.2}$$

The coefficients of these relations differ; this is known as tilt of the FP with respect to the Virial Plane of ETGs. The existence of this tilt and the scatter around the FP can be used to understand the formation and evolution of ETGs. The position of a galaxy in this plane can be related to its star formation history. Any recent star formation should enhance the luminosity of the galaxy thus increasing the surface brightness $\langle I_e \rangle$ for a given R_e and σ. This means recent star formation should move the galaxies off the plane. In this work we examine this possibility using high-quality imaging and spectroscopic data to construct the Fundamental Plane and infer the star formation histories of ETGs falling on it.

The reason why ETGs fall on the Fundamental Plane rather than on the Virial Plane is a topic of intense discussion in the literature (see, e.g., Ciotti et al. 1996; Trujillo et al. 2004; Cappellari et al. 2006; Graves et al. 2009; Graves & Faber 2010). There are several proposed reasons why this might the case:

1. a systematic variation in the dynamic structure of galaxies with total mass (this is known as "broken homology");

2. varying IMF or dark matter content within the effective radius of galaxies with total mass; and/or

3. varying stellar population properties of galaxies along the FP.

The Sloan Lens ACS Survey (SLACS) study of ETGs that are gravitational lenses have ruled out broken homology for galaxies over a range in velocity dispersion ($\sigma \approx$ 180–390 $\mathrm{km\,s^{-1}}$): Bolton et al. (2007) showed that the tilt of the FP is due to a systematic variation in the total mass-to-light ratio with mass of ETGs. However, it is important to note that these lensing studies are limited to very massive ETGs, and they cover a range of redshifts ($z_{\mathrm{lens}} \sim$ 0.1–0.4) where stellar population evolutionary effects cannot be completely ruled out.

To understand the impact of stellar populations on the FP of ETGs, we need a homogeneous sample of galaxies over a range in mass belonging to the same environment.

This can be achieved by obtaining high-resolution imaging and sufficiently-high signal-to-noise spectroscopy of ETGs belonging to a single galaxy cluster. The FP can then be constructed in conjunction with an independent measurement of dynamical mass-to-light ratio $(M/L)_{\rm dyn}$ and stellar mass-to-light ratio $(M/L)_{\rm stellar}$, allowing us to study their separate roles in shaping the FP. Furthermore $(M/L)_{\rm stellar}$ is sensitive to recent star formation; hence this is also a study of impact of recent star formation on the FP. With this goal in mind, we have carried out a detailed dynamic and stellar population analysis of ETGs belonging to the Abell 550 galaxy cluster at $z \sim 0.1$. Observing at this redshift allows us to efficiently target many cluster member ETGs with only a few telescope pointings.

We adopt a flat Universe cosmology with $H_o = 71\,{\rm km\,s^{-1}\,Mpc^{-1}}$, $\Omega_M = 0.27$, $\Omega_\Lambda = 0.73$ (Komatsu et al. 2011). This chapter is organised as follows. The observations are described in Section 2, data reduction and analysis in Section 3, the Fundamental Plane in Section 4 and stellar population studies in Section 5, followed by discussion in Section 6 and conclusion in Section 7.

2.2 Observations

Data acquistion was performed with the VIMOS imager/spectrograph mounted on the Nasmyth focus B of UT3 Melipal, one of the 8.2-m Very Large Telescopes (VLT) at Paranal, Chile. VIMOS is a wide field imager and multi-object spectrograph (MOS) which performs imaging and multi-slit spectroscopy of targets over four quadrants with a field of view of $\sim 15 \times 16\,{\rm arcmin^2}$ (Le Fèvre et al. 2003). Imaging of the galaxy cluster Abell 550 was carried out in B and R filters under good seeing conditions of ~ 0.6arcsec. The location of the cluster field is shown in Figure 2.1. We have aquired three frames in each of the B and R bands, each with an integration time of 25s and 60s respectively. ETGs in Abell 550 was selected based on their B-R color for each quadrant, which places them on the red sequence in the color–magnitude diagram. Galaxies within ± 0.25 mag of the color–magnitude relation $(B-R) = 2.823 - 0.104R$ ($2''$ apertures) in quadrant 3 (the cluster core), and within ± 0.50 mag in quadrants 1/2/4 had top priority; those within a factor of two farther from the red sequence had lower priority. However, limitations on slit placement due to a wavelength solution restriction in the mask generation code prevented us from observing the very center of cluster. Two slit masks were prepared for each quadrant with $0\farcs5$-wide slitlets placed on the astrometric positions of the color-selected ETGs. Spectroscopy was carried out using the HR blue grism, which provides a dispersion of 0.51 pixel^{-1} and a wavelength coverage of 4100–6300 Å, depending on the position of the slit. The spectra were taken over 11 nights using the two slit masks with 40 minutes integration time in each exposure. A total of ~ 200 minutes of integration time was taken through mask 1, and a total of ~ 240 minutes of integration time was taken through mask 2. We reject the data obtained on one night due to bad quality caused by an instrument failure. Calibration frames taken along with the science observations were used for the data reduction process.

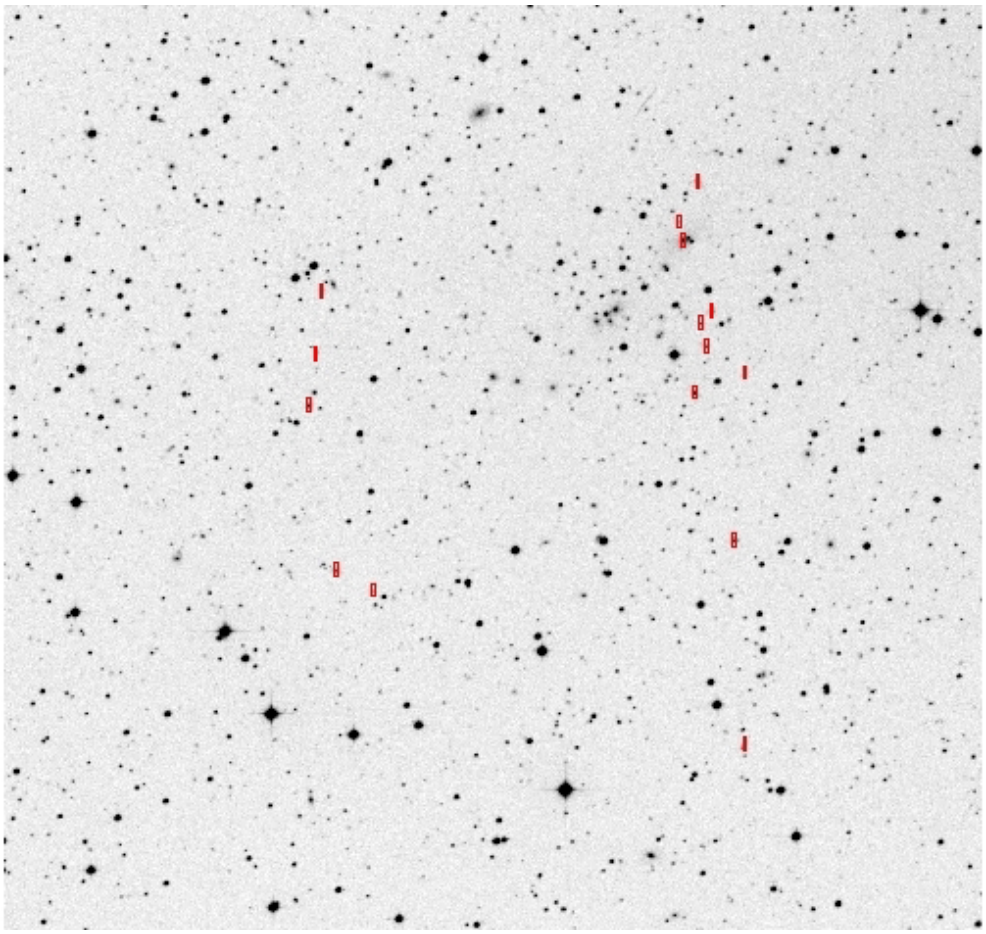

Figure 2.1: Location of our Abell 550 field: The region around $15 \times 16\,\mathrm{arcmin}^2$ field of Abell 550 observed with VIMOS in the R filter. The cluster core can be seen to the upper right of the center of the image. VIMOS MOS images are overlaid over a shallower DSS image of the same field. Red rectangles correspond to 15 ETGs with spectral S/N $> 50/$Å.

2.3 Data reduction and analysis

2.3.1 Data reduction

We reduced the imaging data through a series of standard reduction procedures which involves bias subtraction, flat-fielding and cosmic ray rejection. Images were corrected for pixel offset between frames using forground stars located at different positions on the image. Co-aligned images were median-combined to create images of the cluster field with high signal-to-noise ratio. The R-band images observed under better seeing conditions were used for further analysis.

The spectroscopic data were reduced using *CarnegiePython*. This package is designed for robust optimal extraction of multi-slit spectral data. Bad pixels which could create spurious artifacts were first masked, followed by bias correction using a master bias frame. The distortions along the spatial and the dispersion axis on the two-dimensional multi-slit data were quantified by tracing the distortions of individual slitlets using flat-field and arc-lamp frames. The distortion is primarily caused by the spectrograph optics; there is also a shift between frames due to the flexure of the instrument during the course of integration. Flat-fielding was then carried out using the observed dome flat frames. Wavelength calibration was performed using emission lines from a Helium-Neon arc-lamp spectrum with a zero-point correction for each slitlet using bright sky lines in the two-dimensional science frames. The background sky was modeled taking into account the measured distortion along the spatial and spectral direction for each slitlet (Kelson 2003). The modeled sky frame was then subtracted from the program frame, leaving just the (2D) galaxy spectra. This process of removing the sky in the final step of data reduction ensures that spectral information is not lost to improper sky subtraction. Finally, the two-dimensional spectra from each slitlet were combined and extracting in a single step, creating one-dimensional wavelength-calibrated galaxy spectra. Flux calibration was performed using a white dwarf spectrophotometric standard observed along with the science frames. The spectra were then converted to rest-frame wavelengths by measuring the redshift of the galaxy, obtained from a match with stellar population models. Only ETGs belonging to Abell 550 at $z \sim 0.1$ are used in this study. We attempted spectroscopy of over 170 red sequence galaxies using two slit masks over the four quadrants of VIMOS. However, many galaxies either were misaligned with their slitlets or had very low signal-to-noise, making it difficult to trace the spectral profile during the reduction procedure. We obtained 39 ETGs with spectroscopically confirmed redshifts belonging to Abell 550. The spectra of 15 ETGs have signal-to-noise ratio S/N > 50/Å. We used the high-quality imaging and spectral data of these 15 galaxies for studying the dynamical and stellar population properties of ETGs in Abell 550.

http://code.obs.carnegiescience.edu/python/

2.3.2 Photometry: Structural parameters

The surface brightness profile (I_r) of ETGs can be parameterised by a Sérsic function (Sersic 1968). The surface brightness decreases with galactic radius r from a value I_o at the center as

$$I_r \propto I_o \exp(-r^{1/n}), \tag{2.3}$$

with the power-law slope index n as the only free parameter (once the central surface brightness has been specified). The total flux within the parameterized Sérsic profile can be used to derive the total magnitude of the galaxy. Galaxy structural parameters like radius at which the surface brightness drops to half of its central value, defined as effective radius (R_e), and the effective (mean) surface brightness within this radius ($\langle I_e \rangle$), can be measured very accurately using various fitting methods. We used GALFIT (Peng et al. 2002), a robust two-dimensional fitting code, to determine effective radius and surface brightness. GALFIT fits a function (in our case a Sérsic) to the galaxy image, and then optimally chooses the best-fitting profile (in a reduced-χ^2 sense) as the model profile of the galaxy. The process involves convolving a modelled galaxy image for telescope response and atmospheric seeing variations, thereby retaining the true optimal profile. The best-fit convolved model is computed and the parameters of the original, unconvolved model are reported. The image profile of a star close to the galaxy in each quadrant is used to estimate the point spread function (PSF) of the telescope. This choice is required to control the PSF variation due to the significant distortions and focus variations across the VIMOS field of view. Nearby objects (stars or galaxies) were simultaneously fitted/masked with an appropriate profile along with the galaxy under study. This takes care of contamination from nearby sources and helps determine the actual profile of the galaxy.

Initial guesses for the galaxy profile, like position, magnitude, effective radius, and Sérsic index, are fed into GALFIT, which converges to optimal values of the structural parameters after a few iterations. Structural parameters were measured only on the R-band images, which had the best seeing. The total flux measured within the effective radius was used to calculate the mean surface brightness of the galaxy.

In the absence of photometric standard stars in our imaging data, we were forced to rely on the zero-point measurements reported in the VIMOS calibration archive for the dates of our observation run. This was further cross-calibrated with the objects that overlapped with a published photometric study of Abell 550 by Pimbblet et al. (2002, data kindly provided by Dr. Pimmblet).

We corrected for the effects of bandpass shifting using the kcorrect.v4.2 routine, which accounts for the k-correction of the galaxy (Blanton & Roweis 2007). Galactic extinction in the direction of Abell 550 was corrected using the extinction values for B- and R-bands from NED. Finally, the correction in surface brightness for cosmological dimming is done by subtracting $2.5\log(1+z)^4$ from the measured values. The derived structural parameters of the galaxy from R band images are listed in Table 1.

The residual images from GALFIT for many of the ETGs show spiral arms and disk structures; these are shown in Figure 2.2 and Figure 2.3. ETGs are defined to be

http://howdy.physics.nyu.edu/index.php/Kcorrect
http://ned.ipac.caltech.edu/

morphologically-selected elliptical or lenticular galaxies. The presence of structures in many color-selected Abell 550 cluster ETGs indicate that galaxies on the red sequence deviate from a pure morphological classification.

2.3.3 Spectroscopy: Velocity dispersions

The velocity dispersions of the ETGs were measured using GANDALF (Sarzi et al. 2006), a simultaneous emission-and-absorption line full-spectrum fitting algorithm designed to separate the relative contributions of the stellar continuum and nebular emission in the spectra of galaxies, while measuring the gas emission and kinematics. The ETG spectra in our sample show emission-line features that could potentially contaminate absorption-line strengths (like Hβ) needed for stellar population analysis. MILES stellar population models corresponding to different stellar population ages and metallicities were used as templates for GANDALF (Vazdekis et al. 2010). GANDALF measures the line-of-sight velocity dispersion by broadening the templates to match the galaxy spectra using a χ^2-minimization technique. The net result of this process is a spectrum cleaned of emission lines along with the best-fit stellar population model template and the line-of-sight central velocity dispersion (LOSVD) of stars in random orbits, projected on the plane of the sky (σ). Figure 2.4 gives an example of the GANDALF fitting technique.

We first quantified the line spread function due to the finite resolution of the instrument using the widths of night sky emission lines. MILES model templates were smoothed to the measured instrument resolution before running GANDALF. The emission-line corrected ETG spectra are shown in Figure 2.5, and the measured velocity dispersions (σ) are listed in Table 2.1.

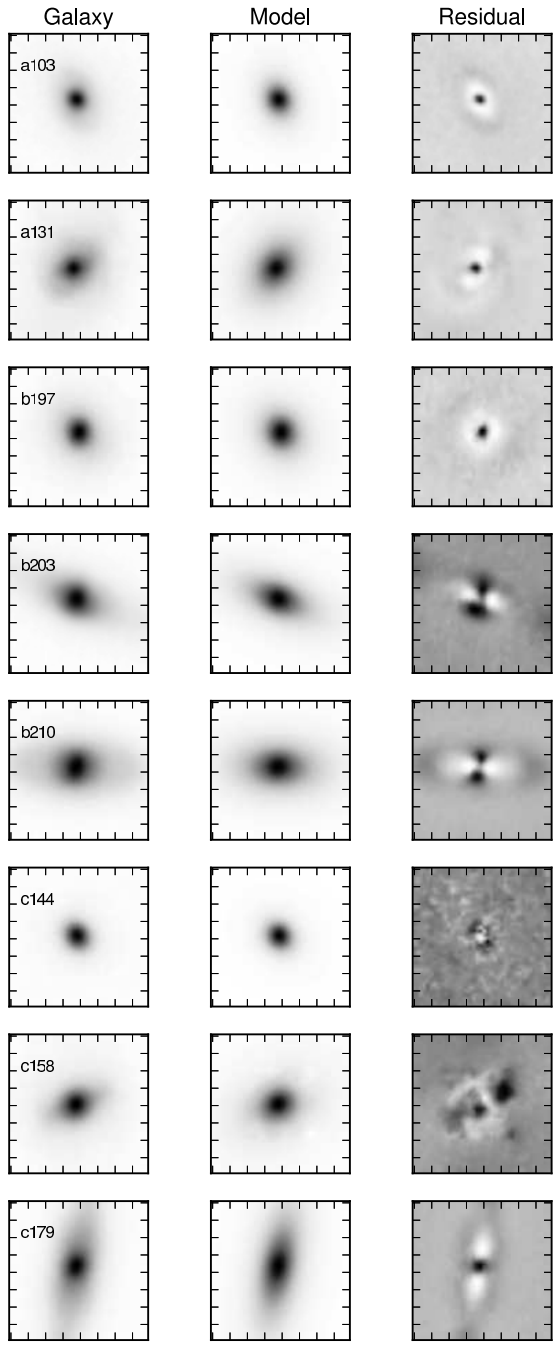

Figure 2.2: GALFIT surface photometry. Observed images of Abell 550 ETGs are shown in the left panel, GALFIT-modeled images in the middle panel, and the residual images in right panel. Residual images are displayed with different grey-scale stretches to enhance structures in the observed galaxy image profile not properly modeled solely with a Sérsic profile. Many ETGs in Abell 550 show disk-like structures and may be morphologically S0 or even early-type spiral galaxies.

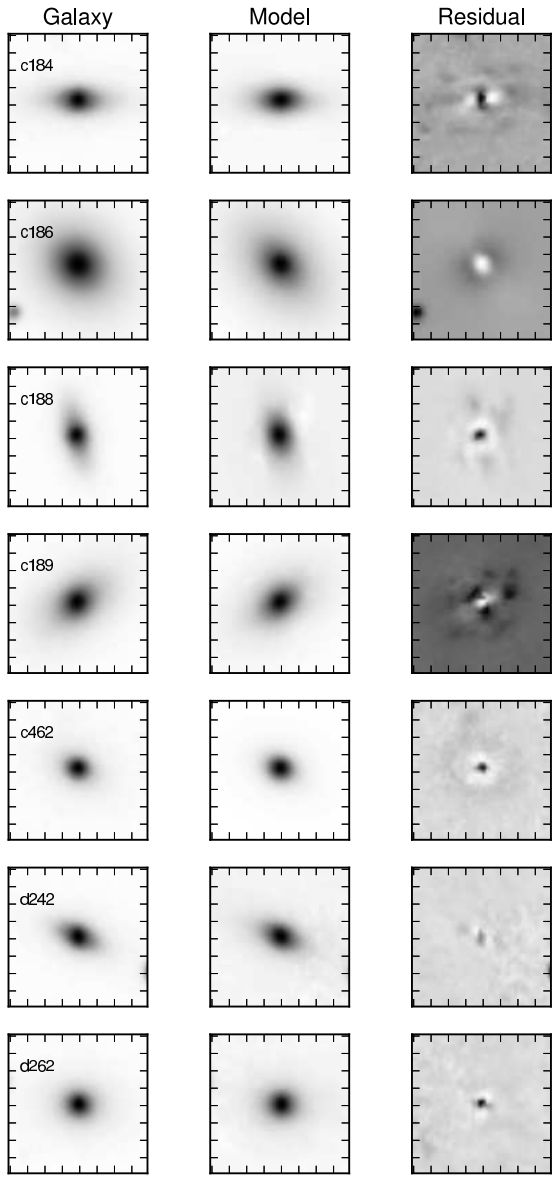

Figure 2.3: GALFIT surface photometry. Observed images of Abell 550 ETGs are shown in the left panel, GALFIT-modeled images in the middle panel, and the residual images in right panel. Residual images are displayed with different grey-scale stretches to enhance structures in the observed galaxy image profile not properly modeled solely with a Sérsic profile. Many ETGs in Abell 550 show disk-like structures and may be morphologically S0 or even early-type spiral galaxies.

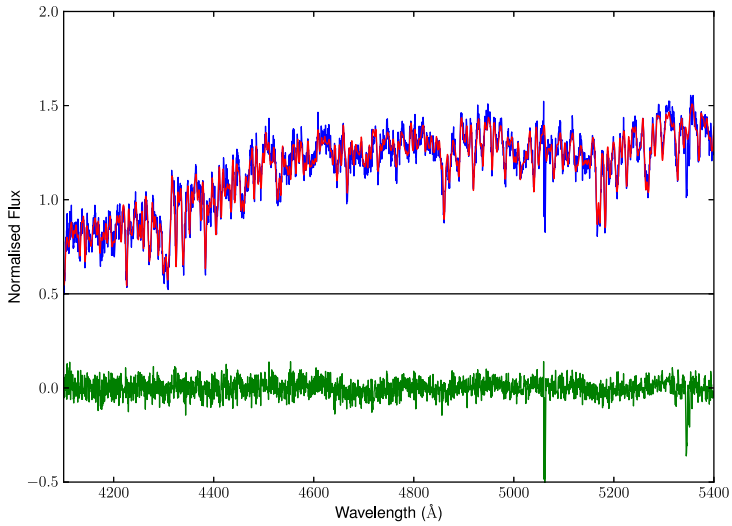

Figure 2.4: The spectrum of galaxy a103 (blue) is fitted with a stellar population model template (red). Residuals (green) from the fitting process show artifacts other than emission lines from the galaxy. This is due to mismatch between the template and the observed real galaxy spectra caused by sky lines and/or instrumental artifacts like ghosts or overlapping orders. These regions were masked while deriving velocity dispersions of galaxies.

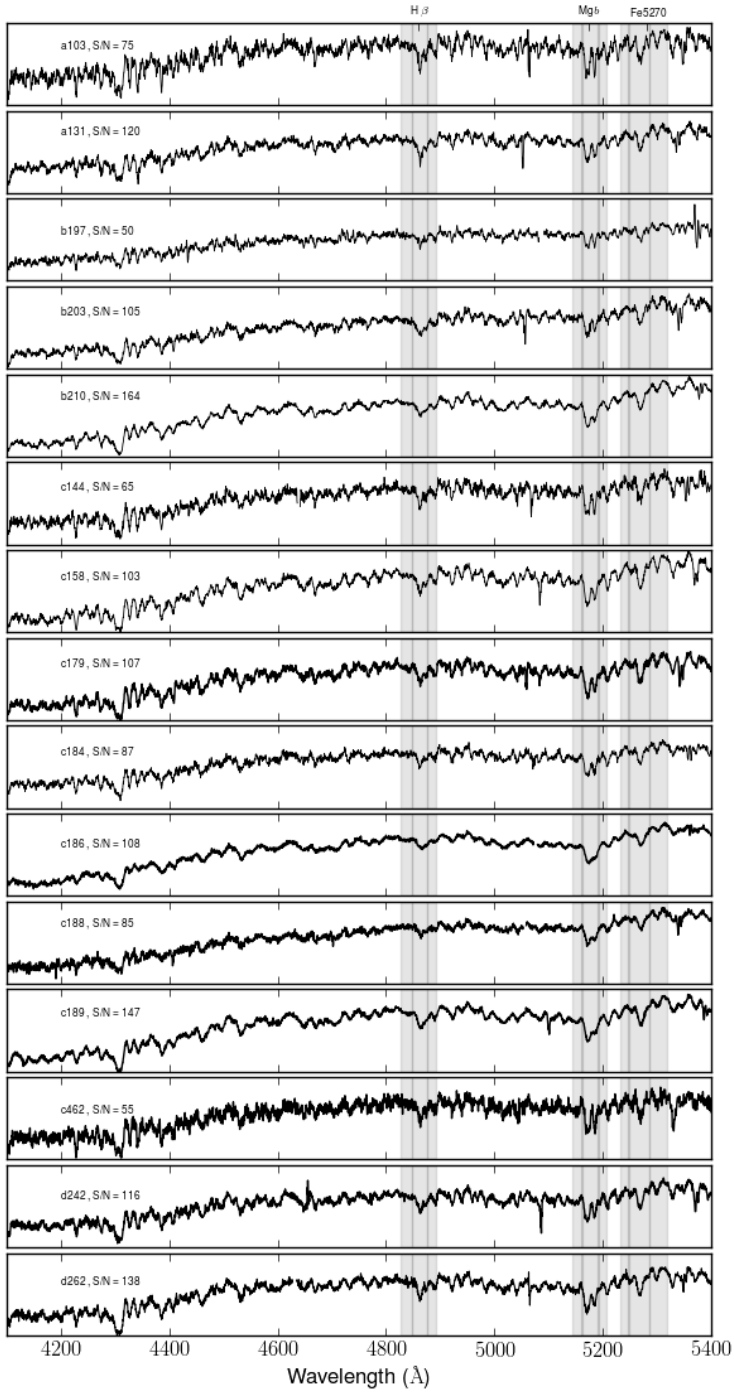

Figure 2.5: The emission line corrected spectra of Abell 550 ETGs. The spectral region corresponding to the Hβ, Mgb and Fe5270 indices are highlighted.

Table 2.1: Properties of Abell 550 ETGs

Galaxy ID	RA	Dec	z	R (mag)	ϵ_R (mag)	R_e (kpc)	ϵ_{R_e} (kpc)	n	ϵ_n	q	ϵ_q	σ ($\mathrm{km\,s^{-1}}$)	ϵ_σ ($\mathrm{km\,s^{-1}}$)
a103	05:53:24.754	−21:12:09.03	0.102	18.13	0.06	1.95	0.21	2.69	0.37	0.71	0.05	83.00	5
a131	05:53:28.876	−21:11:39.87	0.104	17.03	0.03	3.80	0.22	2.27	0.13	0.72	0.02	127.60	3
b197	05:53:30.513	−21:04:30.45	0.097	17.52	0.04	3.09	0.23	3.68	0.25	0.81	0.02	106.40	3
b203	05:53:31.143	−21:06:07.62	0.104	17.09	0.02	3.93	0.17	2.98	0.14	0.41	0.01	136.30	3
b210	05:53:31.786	−21:07:26.32	0.096	16.50	0.01	4.37	0.13	2.84	0.08	0.51	0.01	229.00	2
c144	05:52:44.306	−21:06:33.22	0.101	18.47	0.06	1.22	0.11	3.42	0.68	0.78	0.06	114.25	3
c158	05:52:48.012	−21:04:58.52	0.097	16.57	0.04	6.10	0.50	4.29	0.22	0.72	0.02	157.00	2
c179	05:52:49.660	−21:01:39.78	0.103	16.92	0.02	5.61	0.21	2.07	0.08	0.30	0.01	130.60	3
c184	05:52:48.539	−21:05:52.29	0.100	17.73	0.03	2.40	0.12	2.33	0.17	0.35	0.01	140.30	4
c186	05:52:51.143	−21:03:10.28	0.099	14.89	0.02	15.61	0.56	3.61	0.07	0.75	0.01	335.60	5
c188	05:52:49.133	−21:05:17.51	0.104	17.71	0.03	2.17	0.11	2.61	0.18	0.48	0.01	190.70	6
c189	05:52:49.757	−21:07:03.54	0.094	15.79	0.03	10.23	0.80	6.31	0.25	0.59	0.01	244.20	2
c462	05:52:51.689	−21:02:42.17	0.106	18.70	0.06	1.36	0.14	2.92	0.67	0.64	0.06	102.49	4
d242	05:52:43.926	−21:16:02.54	0.097	17.58	0.02	1.58	0.05	2.93	0.27	0.40	0.02	164.20	3
d262	05:52:45.255	−21:10:49.12	0.102	17.22	0.02	2.30	0.12	4.78	0.27	0.74	0.02	170.00	3

Notes.
Measured photometric and spectroscopic structural parameters for 15 ETGs belonging to Abell 550 having reliable S/N ratios (> 50/Å). Column (1) is an identifier for each galaxy, labeled by the VIMOS quadrants (a,b,c,d); columns (2) and (3) are galaxy coordinates (epoch J2000); column (4) is the spectroscopic redshift; columns (5) and (6) are the R-band magnitude and its uncertainty; columns (7) and (8) are the effective radius and its uncertainty in kpc; columns (9) and (10) are the Sérsic index n and its uncertainty; columns (11) and (13) are the axis ratio between major and minor axes and its uncertainty; and columns (13) and (14) are the velocity dispersion in $\mathrm{km\,s^{-1}}$ and its uncertainty.

Galaxy Name	S/N	Hβ	eHβ	Mgb	eMgb	Fe5270	eFe5270
a103	75	2.38	0.06	4.10	0.06	3.07	0.07
a131	120	2.43	0.04	3.56	0.04	2.44	0.04
b197	50	2.72	0.08	4.77	0.08	3.58	0.08
b203	105	2.50	0.04	3.81	0.04	2.59	0.05
b210	164	1.59	0.03	4.81	0.03	2.66	0.03
c144	65	1.97	0.07	4.16	0.07	2.88	0.08
c158	103	2.13	0.04	5.08	0.04	3.16	0.05
c179	107	1.66	0.04	4.75	0.04	3.06	0.05
c184	87	1.82	0.05	4.44	0.05	2.85	0.06
c186	108	1.37	0.04	5.29	0.04	2.64	0.04
c188	85	1.35	0.05	5.31	0.05	2.53	0.05
c189	147	1.66	0.03	4.42	0.03	2.75	0.04
c462	55	2.04	0.08	4.54	0.08	2.08	0.09
d242	116	2.06	0.04	4.34	0.04	2.78	0.04
d262	138	1.75	0.03	4.06	0.04	2.72	0.04

Table 2.2: Fully-corrected line strength data for 15 Abell 550 ETGs with S/N > 50/Å.

2.3.4 Spectroscopy: Line strengths

We measured the absorption-line strengths of Abell 550 ETGs on the Lick/IDS index system (Burstein et al. 1984; Worthey 1994; Trager et al. 1998). In order to compare the indices to stellar population models, which are based on stellar spectra, we need to correct the measured indices for the broadening induced by the velocity dispersions of the galaxies. We corrected for velocity broadening by using the technique described in Kelson et al. (2006). First the index strengths were measured from the flux calibrated, emission-line corrected galaxy spectra ($\mathrm{Index_{gal}}$), as described in Trager et al. (2008). This was followed by index measurements on the broadened ($\mathrm{Index_{tempbroad}}$) and non-broadened ($\mathrm{Index_{temp}}$) best-fit template spectra from GANDALF. The difference in index strengths measured on the broadened and non-broadened template spectra gives the velocity dispersion correction, which was applied to each ETG spectrum. The final corrected index strength is

$$\mathrm{Index_{galcorr}} = \mathrm{Index_{gal}} + (\mathrm{Index_{temp}} - \mathrm{Index_{tempbroad}}). \quad (2.4)$$

The corrected line strengths are given in Table 2.2. The rest-frame galaxy spectra are contaminated by atmospheric emission lines which made many of the line strengths (for example, Fe5335) unusable for stellar population anaylsis. The problems become more severe for stellar-population studies based on line-strength data at higher redshifts.

2.4 The Fundamental Plane of Abell 550 ETGs

We constructed the FP of ETGs in Abell 550 using the structural parameters from the R-band images and the velocity dispersions from the spectra. The best-fitting plane

was computed by minimizing the total squared perpendicular distance from all data points spanning the three dimensional phase space of R_e, $\langle I_e \rangle$ and σ (cf. Jorgensen et al. 1996). We ran 1000 Monte Carlo realizations for the position of each galaxy along with associated errors in the FP. We are interested in understanding the role of stellar populations in shaping the FP, and therefore we parameterise the FP as a relation between a stellar population-dependent parameter and the structural parameters of the galaxies. This was done by keeping the mean surface brightness as an independent parameter:

$$\langle I_e \rangle \propto \sigma^{\alpha} R_e^{\beta} \tag{2.5}$$

Self-gravitating, virialised stellar systems like ETGs are supposed to follow the Virial Theorem, with galaxies populating a Virial Plane with coefficients $\alpha = 2$ and $\beta = -1$. However, observations of ETGs in clusters show that galaxies rather fall on the Fundamental plane with coefficients different from Virial Plane expectations. This is known as the "tilt" of the Fundamental Plane. The FP coefficients for Abell 550 ETGs are $\alpha = 1.44 \pm 1.06$ and $\beta = -0.57 \pm 0.31$. These values agree with those for the Coma Cluster FP to within the error bars (Jorgensen et al. 1996). We therefore adopt the Coma cluster coefficients for the FP of Abell 550. The edge-on FP projection of Abell 550 ETGs is shown in Figure 2.6.

High-redshift clusters show a similar FP tilt to the Coma cluster but exhibit a significant zero-point offset. This zero-point offset is attributed to the evolution of galaxy mass-to-light ratios in the sense that galaxies are younger and have lower mass-to-light ratios at higher redshifts (Treu et al. 2005; van Dokkum & Stanford 2003). However, ETGs in the Abell 550 R-band FP appear not to have evolved when compared with the FP of Coma Cluster ETGs. We find that Abell 550 ETGs located at a lookback time of 1.2 Gyr have an FP zero-point (-0.41 ± 0.01) comparable to the zero-point of Coma Cluster ETGs (-0.41). The scatter of ETGs from the FP is measured ($\sigma_{FP} = 0.113$) and is found to be higher in comparison with the R band FP of Coma cluster ETGs ($\sigma_{FP} = 0.084$).

2.5 Stellar population studies of Abell 550 ETGs

We used the Hβ, Mgb and Fe5270 line strengths for our stellar population analysis. Hβ is highly sensitive to age while Mgb and Fe5270 are more sensitive to metallicity, with a mild dependence on age. The combination of these indices can disentangle the stellar population parameters age, metallicity and alpha-enhancement ratio (e.g., Worthey 1994; Trager et al. 2000b). The rest-frame galaxy spectra are contaminated by atmospheric emission lines which made many of the otherwise potential line strengths inaccessible for stellar population analysis. We place the measured indices on single-stellar-population (SSP-) equivalent age and metallicity model grids. We compare Abell 550 ETG indices with the high-quality Coma ETG data from Trager et al. (2008). Figure 2.7 shows an index-index diagram for Abell 550 (red) and Coma (blue) ETGs. The Abell 550 cluster ETGs span a range in ages comparable to but slightly larger than the Coma cluster ETGs.

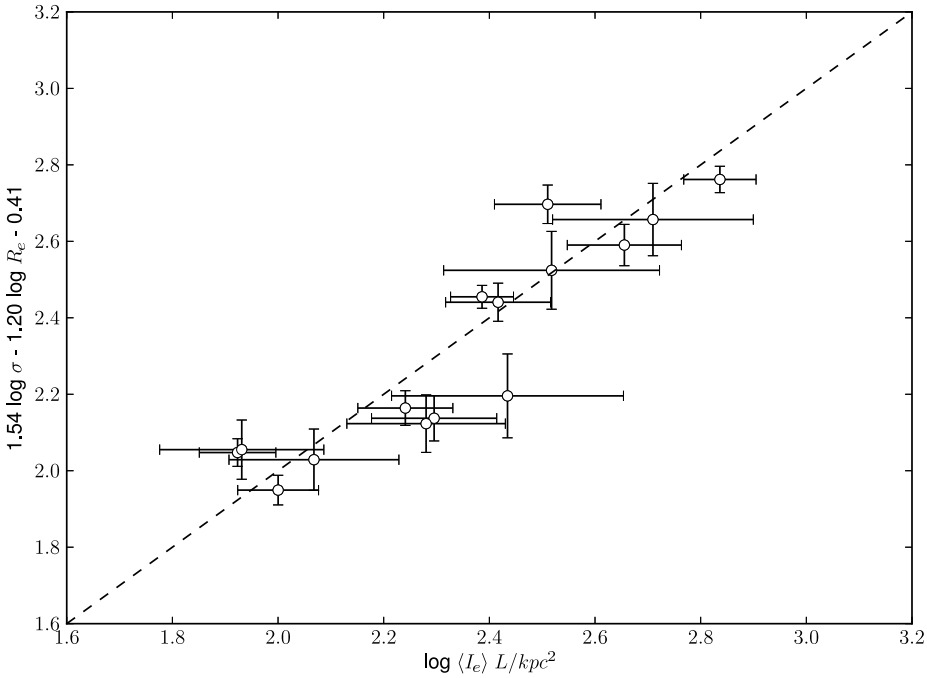

Figure 2.6: Edge-on projection of the R band Fundamental Plane for Abell 550 ETGs with a one to one line overlaid for visual comparison of galaxies off from the Plane.

Next we model the SSP-equivalent star formation histories for Abell 550 cluster ETGs. We assume a Chabrier IMF and Bruzual & Charlot (2003, BC03) models with Padova isochrones (Bertelli et al. 1994) and followed the prescriptions and methodology described in detail in (Trager et al. 2008). Once the SSP-equivalent ages (t_{ssp}), metallicties ([Z/H]) and alpha-enhancements ([E/Fe]) were determined, BC03 models were used to infer stellar mass-to-light ratios in the B-band (M/L_B). We use these results to perform a quantitative analysis of the derived structural and stellar population parameters of Abell 550 cluster ETGs.

2.6 Discussion

We investigate the stellar population properties of galaxies along the thickness of the FP by measuring the scatter $\Delta\langle I_e\rangle$ from the best-fit FP. The scatter is a measure of varying surface brightness of galaxies having a fixed R_e and σ and is closely related to the stellar population of a galaxy. The stellar mass-to-light ratios derived from stellar population models correlate with the FP scatter (Figure 2.8). We quantify the relation using a least-squares fit, running 1000 Monte Carlo realizations considering the errors

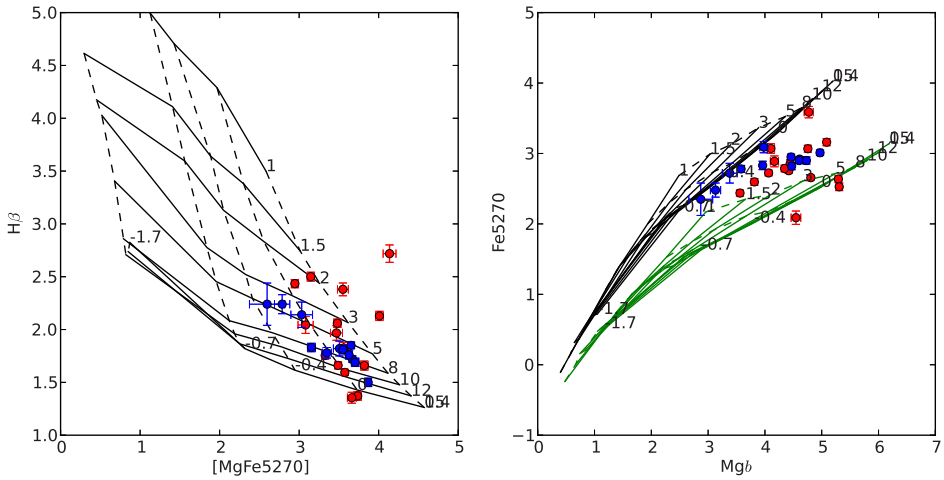

Figure 2.7: Index-index diagrams for Abell 550 ETGs constructed using measured [MgFe5270] $= \sqrt{\mathrm{Mg}b \times \mathrm{Fe5270}}$ and Hβ, Fe5270 and Mgb indices. Stellar population model grids based on Bruzual & Charlot (2003, BC03) models for constant age (solid lines) and constant metallicity (dashed lines) and different enhancement ratios [E/Fe] = 0 (black) and +0.3 (red) are plotted. Blue points correspond to the high-quality data of 12 Coma cluster ETGs from Trager et al. (2008). Red points are Abell 550 ETGs, which span a broader range in Hβ line strengths (proxy for age) than Coma Cluster ETGs.

in both dimensions.

$$\log M/L_{\mathrm{ssp}} = (-0.66 \pm 0.30) \times FP_{\mathrm{Residual}} + (0.43 \pm 0.05). \tag{2.6}$$

This correlation implies that scatter on the FP is driven by star formation episodes in the recent past. The relation can be used to determine the presence of recent star formation (at least in galaxy clusters) in ETGs at large lookback times where stellar population studies are too expensive.

Furthermore, this result implies that ETGs in Abell 550 $z \sim 0.1$ are still falling onto the FP relation. The increased FP scatter towards low stellar mass-to-light ratios implies that recent star formation is "puffing up" the FP relation. These galaxies will eventually fade, increase their mass-to-light ratios and fall onto the FP relation. This result is in strong conflict with the hypothesis that all ETGs form their stars at high redshift and passively evolve to the present day.

Having found a correlation between FP scatter and stellar population properties of ETGs, we now examine the tilt of the FP. It has been convincingly shown by detailed lensing and dynamical mass modelling studies that the tilt of the Fundamental Plane from the Virial Plane is due to a systematic change in the mass-to-light ratio of the galaxy with mass (Cappellari et al. 2006; Bolton et al. 2007). However, the mass-to-light ratio is a measure of galaxy luminosity per unit galaxy mass, and there can

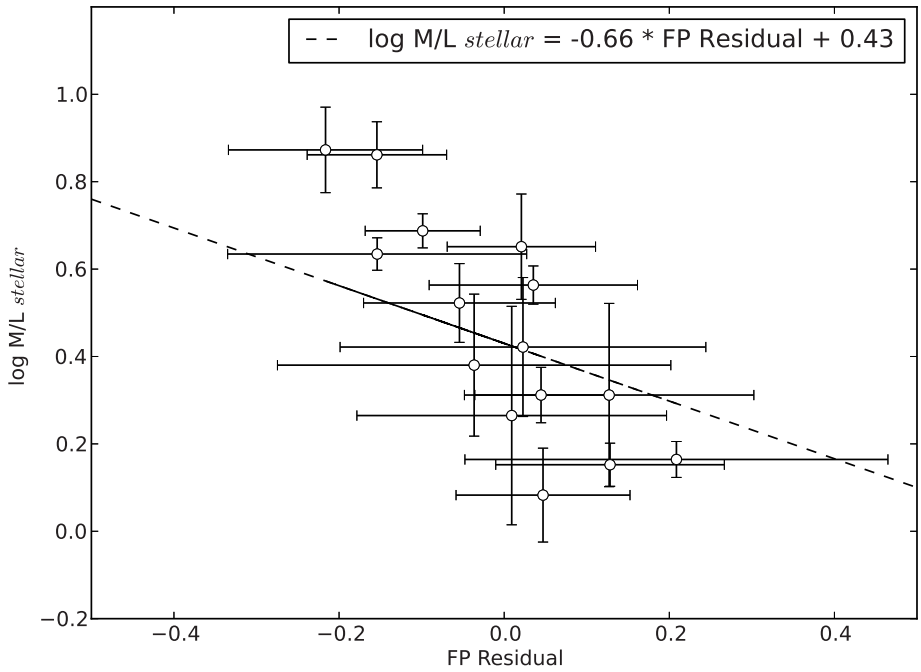

Figure 2.8: Abell 550 ETGs residual on the Fundamental Plane versus stellar mass-to-light ratio (SSP-equivalent) in the B-band.

be contributions from both dark matter and stellar content to the mass of the galaxy (Graves & Faber 2010). We quantify the stellar contribution to the galaxy mass-to-light ratio and try to determine how much this contributes to the tilt of the FP. We first check this by comparing dynamical with stellar mass-to-light ratios. We find that the dynamical and stellar mass-to-light ratios follow a one-to-one correlation. However, stellar mass-to-light ratios are model-dependent and derived with the assumption of a single stellar population with a Chabrier IMF (in the present study) for all galaxy masses.

Under the assumption of homology, we paramterise the dynamical mass-to-light ratio variation with dynamical mass for Abell 550 ETGs. We combined the measured R_e, $\langle I_e \rangle$ and σ values into a physically meaningful three-dimensional space called κ-space (Bender et al. 1992). The parameters in κ space are obtained by a orthogonal cordinate transformation of the measured parameters, which also emphasis the FP while retaining physically meaningful variables:

$$\kappa_1 \propto \log M_{\rm dyn} \tag{2.7}$$

$$\kappa_2 \propto \log M/L_{\rm dyn} I^3 \tag{2.8}$$

$$\kappa_3 \propto \log M/L_{\rm dyn} \tag{2.9}$$

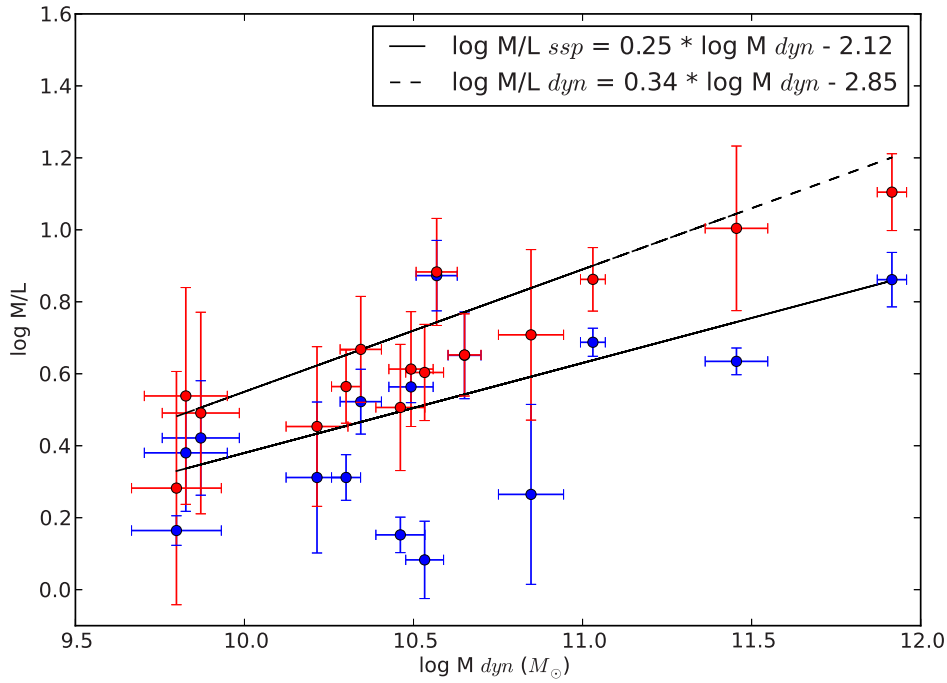

Figure 2.9: Dynamical (red points) and stellar (blue) mass-to-light variation with ETG mass for Abell 550 cluster.

The mass, mass-to-light ratios can then be derived by placing the measured parameters in κ space (Burstein et al. 1997).

$$\log M_{\rm dyn} = \sqrt[2]{\kappa_1} + 5.67 \tag{2.10}$$

$$\log M/L_{\rm dyn} = \sqrt[3]{\kappa_3} - 0.83 \tag{2.11}$$

We determined the dynamical mass, mass-to-light ratios by putting the measured quantities into the above equations.

We next determine the dependence of both stellar and dynamical mass-to-light ratios on ETG dynamical mass. As shown in Figure 2.9, both follow similar trends with galaxy mass. The stellar mass-to-light dependence on ETG dynamical mass can be parameterized as

$$\log M/L_{\rm ssp} = (0.25 \pm 0.05) \log M_{\rm dyn} - (2.12 \pm 0.54). \tag{2.12}$$

while the dynamical mass-to-light dependence on ETG dynamical mass can be parameterized as

$$\log M/L_{\rm dyn} = (0.34 \pm 0.10) \log M_{\rm dyn} - (2.85 \pm 1.10), \tag{2.13}$$

The stellar and dynamical mass-to-light ratios show similar correlations with the dynamical mass of ETGs within the measurement errors. This relation is robust within the limitations of ground-based imaging and spectroscopy which we conducted for 15 ETGs in Abell 550.

We then compared this observed corelation with what we could have derived putting the FP coefficients from Coma Cluster ETGs (Jorgensen et al. 1996). For Coma Cluster ETGs, the mass-to-light–mass relation is of the form

$$\log M/L = 0.24 \times \log M + \text{constant}. \tag{2.14}$$

The coefficient of this mass-to-light–mass relation is the same within the errors as those we found for both stellar and dynamic mass to light ratios with ETGs mass in Abell 550. The tilt of the Abell 550 FP from the Virial Plane is therefore due to the systematic variation of stellar mass-to-light ratio with galaxy mass or, in other words recent star formation. Dark matter and broken homology seem to play negligible roles in shaping the Fundamental Plane in Abell 500.

We have checked whether our results are biased from the selection criteria used in this study. Our sample is limited both in magnitude and a narrow range in color. If there were low-mass ETGs with redder colors, their corresponding mass-to-light ratios will be higher than those we picked for our study. However, semi-analytic models of galaxy formation in massive clusters have demonstrated that such very red, low-mass galaxies are very rare, at least at $z \sim 0$ (Trager & Somerville 2009). We therefore suggest that our results are unlikely to be seriously affected by our selection effects; however, the presence of such red, low-mass ETGs both in observations and semi-analytic models of galaxy clusters is an interesting topic for further work.

The existence of a mass-to-light–mass relation along with an increased FP scatter towards lower stellar mass-to-light ratios is evidence for downsizing of ETGs in Abell 550 galaxy cluster. The massive ETGs must be in place from the initial phase of cluster growth (hypothesized to take place at $z > 2$) followed by a continuing accretion of low-mass galaxies in the cluster. The cluster build-up over cosmic time can be understood from the star formation histories or equivalently from the mass-to-light–mass relation of galaxies.

2.7 Conclusions

We have presented a detailed structural and stellar population analysis for ETGs in Abell 550, a rich galaxy cluster at $z \sim 0.1$. We constructed the Fundamental Plane for ETGs in this cluster and studied their stellar population properties along and across the thickness of the FP. Our principal conclusions are (1) Abell 550 ETGs exhibit a scatter around the FP which is due to the intrinsic variations of their stellar mass-to-light ratios. The relation is such that any recent star formation will decrease the stellar mass-to-light ratios and increase the scatter of galaxies around the FP. The finite thickness of the FP is thus due to the presence of star formation episodes in the recent past. This points towards a scenario in which Abell 550 cluster ETGs are still in the process of settling on to the FP. In other words, galaxies are still falling on to the FP relation at $z \sim 0.1$,

which is in strong conflict with the hypothesis that all ETGs form their stars at high redshift and passively evolve to the present day; and (2) the tilt of the FP for Abell 550 ETGs is due to recent star formation and is demonstrated as a systematic variation of the stellar mass-to-light ratios of the galaxies as a function of their dynamical masses.

Chapter 3

Stellar populations and the Fundamental Plane of early-type galaxies in Abell 851 at $z = 0.406$

Abstract

We have studied the stellar populations and Fundamental Plane (FP) of 12 early-type galaxies (ETGs) in Abell 851, a rich, massive Coma-like galaxy cluster at $z \sim 0.41$. The main motivation for this study is to understand the FP and stellar population properties of ETGs in a dynamically-unrelaxed, intermediate-redshift galaxy cluster. We used spectroscopy and photometry to derive the structural parameters of ETGs and estimate the star-formation histories from single-stellar-population (SSP) models. ETGs in Abell 851 follow a FP with a higher instrinsic scatter and similar coefficients to the FP of the Coma Cluster. Stellar population studies based on high-quality spectroscopic data (S/N $>$ 40Å) demonstrate an anti-correlation between the stellar mass-to-light ratios of the ETGs and their residuals from the FP. The stellar mass-to-light ratios derived from stellar population modelling are nearly constant, but with a large scatter, over the range of dynamical masses studied in this work. These relations show that ETGs in Abell 851 have undergone recent star-formation episodes, regardless of their mass, that are responsible for the increased scatter of the FP and stellar mass-to-light ratios. These results can be explained by morphological and stellar-population tranformations happening in Abell 851 due to the on-going cluster assembly at $z \sim 0.41$ and cannot

*The data presented herein were obtained at the W.M. Keck Observatory, which is operated as a scientific partnership among the California Institute of Technology, the University of California and the National Aeronautics and Space Administration. The Observatory was made possible by the generous financial support of the W.M. Keck Foundation.

be explained by high formation redshifts and subsequent passive evolution for ETGs in Abell 851.

3.1 Introduction

The Fundamental Plane (FP) can be used as a probe to understand the formation and evolution of early-type galaxies (ETGs) (FP: Dressler et al. 1987; Djorgovski & Davis 1987; Faber et al. 1987). The FP's tilt with respect to the Virial Plane and its finite thickness are due to variations in the mass-to-light ratios of constituent galaxies (Cappellari et al. 2006; Graves et al. 2009; Graves & Faber 2010). Recent star formation can lower the mass-to-light ratios (depending on the strength and time since the last burst) and determine the location of ETGs on the FP (Chapter 2). Thus studies of the FP in conjunction with stellar population properties can be used as a direct probe to understand the presence of recent star formation in ETGs.

Studies of the FP of ETGs in dense galaxy clusters, like the Coma Cluster, in the local Universe (Jorgensen et al. 1996) and in comparison with clusters at high redshifts demonstrated that ETGs (particularly the massive ones) are passively-evolving stellar systems with a formation redshift $z > 2$ (van Dokkum & Franx 1996; Kelson et al. 1997; van Dokkum et al. 1998). This was further probed up to $z \sim 1.2$ by van Dokkum & Stanford (2003), who showed that cluster ETGs mass-to-light ratios are compatible with passive evolution. The mass-to-light ratio evolution in these studies relied on measuring the changing zero-point offsets of the FP at different redshifts with respect to the FP of ETGs in the Coma cluster. These studies showed that ETGs, particularly those in dense galaxy cluster cores, have a high formation redshift and are passively evolving as "red and dead" galaxies to the current epoch. However all these studies were done on one cluster per redshift bin, with an assumption that all clusters follow the same evolutionary path in time. These studies therefore lack statistical support for strong claims about ETG formation and evolution in dense cluster environment.

The current paradigm of Λ-Cold Dark Matter (ΛCDM) cosmology predicts galaxy cluster assembly to be ongoing as late as $z \sim 0.4$. This implies individual galaxies and galaxy groups should be falling into a common potential well, even at these relatively low redshifts. Observationally, many intermediate-redshift galaxy clusters are not relaxed and in fact are undergoing mergers (Hsu et al. 2013; Bradač et al. 2008). The end result of this cluster assembly process is rapid evolution in the morphology and stellar populations of cluster galaxies. The increase of blue galaxies in cluster cores at $z \sim 0.5$ in comparison with local Universe clusters, manifested as the Butcher-Oemler effect, lends further support to this paradigm (Butcher & Oemler 1978a,b). Thus, recently assembled intermediate-redshift clusters should host ETGs which are recently quenched star-forming blue galaxies. This is compatible with the picture explained in detail in Faber et al. (2007), who showed ETGs could have different evolutionary scenarios: out of which, galaxy mergers and stripping of the gas reservoir could be the major processes shutting down (quenching) star formation in hostile environments like galaxy clusters. The FP of ETGs in intermediate-redshift clusters should therefore show signatures of recent star formation events: ETGs with recent star formation engender large (intrinsic)

scatter in the FP.

In this chapter we present the FP of ETGs from Abell 851, a well-studied, intermediate-redshift ($z \sim 0.406$) galaxy cluster that is believed to have undergone a recent merger event (Kodama et al. 2001; Schindler et al. 1998). Abell 851 has been extensively studied for the ongoing starburst activities in the cluster core and outskirts (Oemler et al. 2009; Dressler et al. 2009). Rapid evolution of the morphology and stellar population should follow the starburst phase in the dense environment of the cluster core. The ETGs of Abell 851 should carry the signatures of such transformations, such that many of them have likely undergone recent star formation events. This can be confirmed by a detailed FP and stellar population analysis. Our aim is to construct the FP of ETGs in Abell 851, study the mass-to-light ratio variations of ETGs on the FP, and connect these with stellar population properties.

We adopt a flat Universe cosmology with $H_o = 71\,\mathrm{km\,s^{-1}\,Mpc^{-1}}$, $\Omega_M = 0.27$, $\Omega_\Lambda = 0.73$ (Komatsu et al. 2011). This chapter is organised as follows. The observations are described in Section 2, data reduction and analysis in Section 3, the construction of the Fundamental Plane of Abell 851 in Section 4 and a stellar population analysis of the cluster ETGs in Section 5, a combined stellar population and dynamic analysis in section 6, followed by discussion in Section 7 and a conclusion in Section 8.

3.2 Observations

Spectroscopic data acquistion was performed with the Low-Resolution Imaging spectrograph (LRIS) (Oke et al. 1995) on the Cassegrain focus of Keck I, one of the 10-m telescopes at Mauna Kea, Hawai. LRIS is a imager and multi-object spectrograph (MOS) which performs imaging and multi-slit spectroscopy of targets over a field of view of $\sim 6 \times 7.8\,\mathrm{arcmin}^2$. We used the red side of the instrument, the only wavelength region accessible during the period of our observations.

Galaxies were selected based on their early-type morphology from the HST/WFPC2 imaging observations of the Abell 851 cluster field (Dressler et al. 1994). We used HST/WFPC2 F702W images for this purpose, and these together with a later ACS F814W observation of the same field with higher spatial resolution were used to derive the structural parameters of the Abell 851 ETGs (below). The location of the cluster field is shown in Figure 3.1.

Spectroscopy was carried out using multi-slit masks made corresponding to the astrometric position of selected ETGs. We used LRIS with a 600 lines mm^{-1} grating and a slit width of $0\farcs7$, which provides a dispersion of 1.25 pixel^{-1} and a wavelength coverage of 5300–8000Å, depending on the position of the slit. Galaxies were observed for 2400 s per exposure and the typical seeing was $0\farcs7$–$1\farcs0$. The spectral data were taken over three nights using the two slit masks. A total of ~ 240 minutes of integration time was taken through mask 1, and a total of ~ 120 minutes of integration time was taken through mask 2. Calibration frames taken along with the science observations were used for the data reduction process.

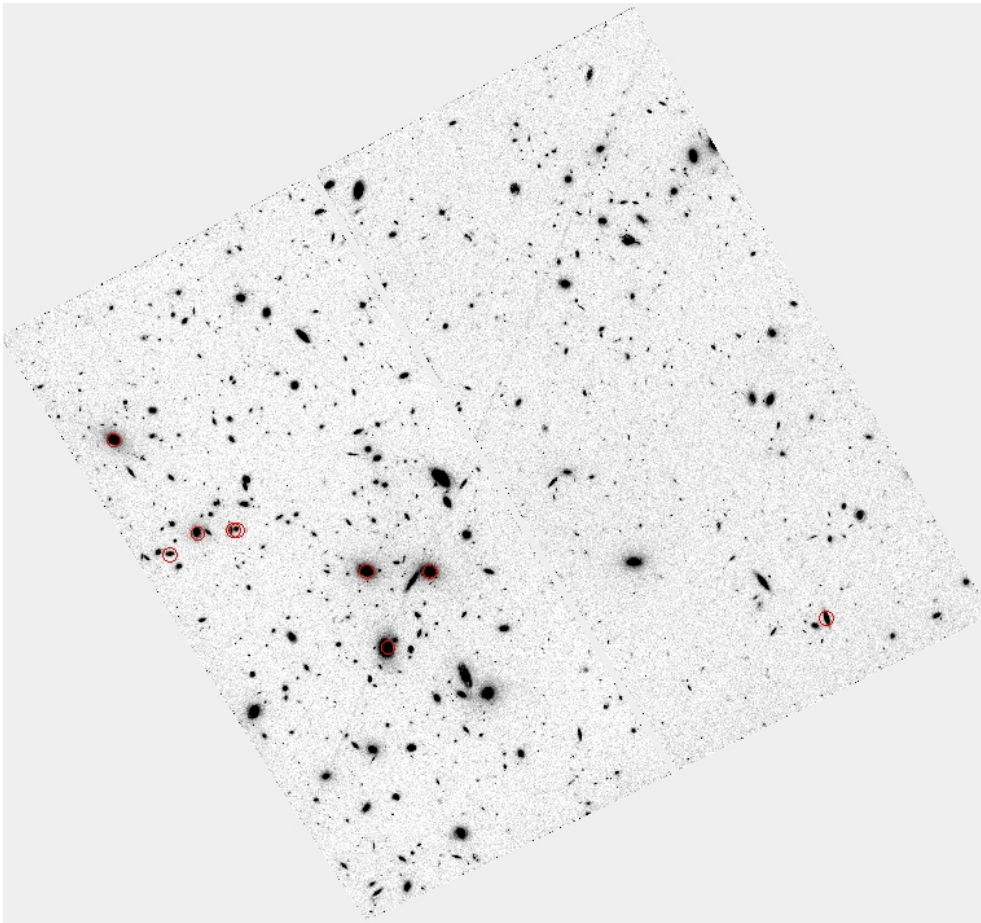

Figure 3.1: The field of Abell 851: The region around the central field of Abell 851 observed with HST/ACS F814W filter is shown. The cluster core can be seen at the center of the image. Red circles correspond to 9 ETGs with S/N $>$ 40/Å used in this study. The other ETGs used in this study were imaged with HST/WFPC2 in the F702W filter.

3.3 Data reduction and analysis

3.3.1 Data reduction

Imaging data were taken from HST archives and used for deriving the structural parameters. The spectroscopic data were reduced using *CarnegiePython* as described in Chapter 2. Wavelength calibration was performed using emission lines from the sky that fill the regions of the slitlets along with the galaxy spectrum in the two-dimensional science frames. Three pairs of galaxy spectra share the same slitlets, and the contribution of each galaxy needs to be extracted carefully. Flux calibration was performed using a spectrophotometric standard observed along with the science frames. The spectra were then converted to rest-frame wavelengths by measuring the redshift of the galaxy, obtained from a match with stellar population models. The spectra of 12 ETGs have signal-to-noise ratio S/N > 40/Å. We used this high-quality imaging and spectral data for constructing the FP and studying the stellar population properties of ETGs in Abell 851.

3.3.2 Photometry: Structural parameters

We used GALFIT (Peng et al. 2002) to determine effective radius(R_e) and surface brightness($\langle I_e \rangle$). A Sérsic profile was fit to the ACS F814W and WFPC2 F702W images of ETGs using the method described in detail in Chapter 2. Point spread function for each galaxy was generated using *TinyTim*. A few ETGs in our sample are very close together in ACS images and have overlapping profiles. These galaxy profiles are fitted simulatanously inorder to retain the optimal profile of these close galaxies. We calibrated the photometry using zeropoints from the HST archives.

We corrected for bandpass shifting using a fitting function derived from B, R_c, F702W and F814W colors for BC03 models with metallicties of $Z = 0.008$, 0.02, and 0.05, and ages from 1–9 Gyr at $z = 0$ and $z = 0.405$:

$$\begin{aligned} R_{c(z=0)} &= F814W_{(z=0.405)} - 0.72[(F702W_{(z=0.405)} - F814W_{(z=0.405)}) - 0.52] \\ &\quad \times[(F702W_{(z=0.405)} - F814W_{(z=0.405)}) - 0.40] \\ &\quad -0.93[(F702W_{(z=0.405)} - F814W_{(z=0.405)}) - 0.47] + 0.68, \end{aligned} \tag{3.1}$$

with a root mean square scatter of 0.003 mag. Once the observed F702W and F814W are known, we computed R_c in the rest frame.

Galactic extinction in the direction of Abell 851 was corrected using the extinction values from NED. Finally, the correction in surface brightness for cosmological dimming is done by adding the $\log(1+z)^4$ term to the measured values. The derived structural parameters of the galaxy from HST images are listed in Table 1.

The residual images from GALFIT for many of the ETGs show disk structures; these are shown in Figure 3.2 and Figure 3.3.

http://code.obs.carnegiescience.edu/python/
http://www.stsci.edu/hst/observatory/focus/TinyTim
http://ned.ipac.caltech.edu/

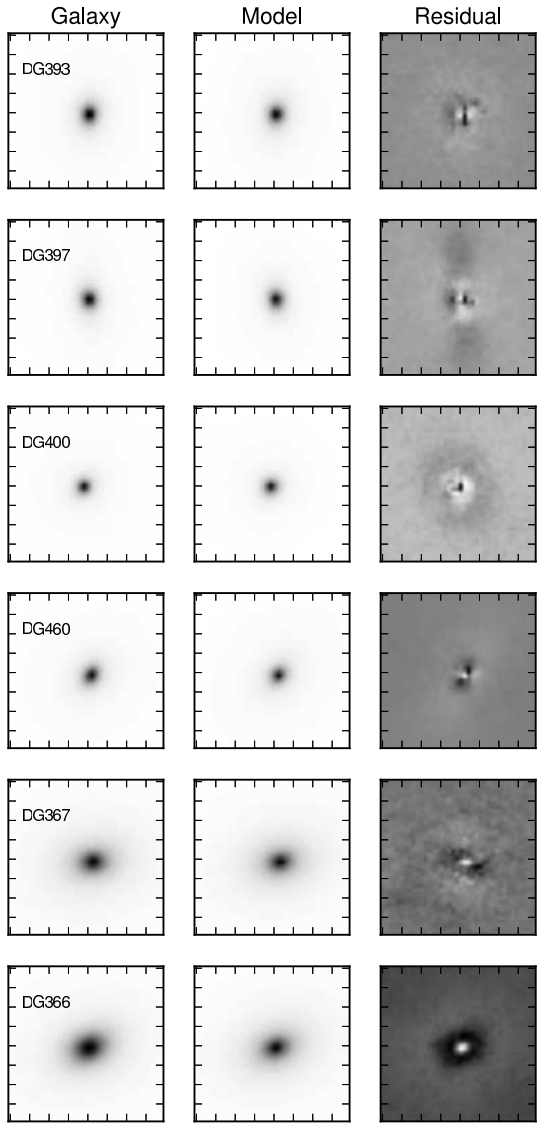

Figure 3.2: GALFIT surface photometry. Observed images of Abell 851 ETGs are shown in the left panel, GALFIT-modeled images in the middle panel, and the residual images in right panel. Residual images are displayed with different grey-scale stretches to enhance structures in the observed galaxy image profile not properly modeled solely with a Sérsic profile.

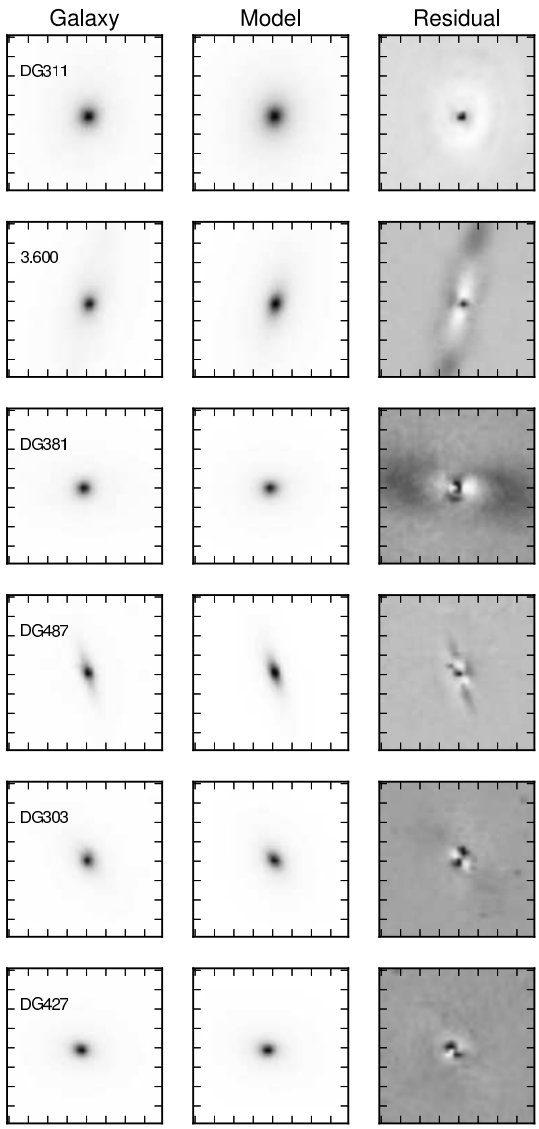

Figure 3.3: GALFIT surface photometry. Observed images of Abell 851 ETGs are shown in the left panel, GALFIT-modeled images in the middle panel, and the residual images in right panel. Residual images are displayed with different grey-scale stretches to enhance structures in the observed galaxy image profile not properly modeled solely with a Sérsic profile.

3.3.3 Spectroscopy: Velocity dispersions

We used the same techniques described in Chapter 2 for measuring the velocity dispersions of the ETGs. GANDALF (Sarzi et al. 2006) was used to clean the ETG spectra of emission-lines and to measure the line-of-sight central velocity dispersion (LOSVD) of stars in random orbits, projected on the plane of the sky (σ). The line spread function due to the finite resolution of the instrument was measured using the widths of night sky emission lines. MILES model templates were smoothed to the measured instrument resolution before running GANDALF. The emission-line corrected ETG spectra are shown in Figure 3.4, and the measured velocity dispersions (σ) are listed in Table 3.1.

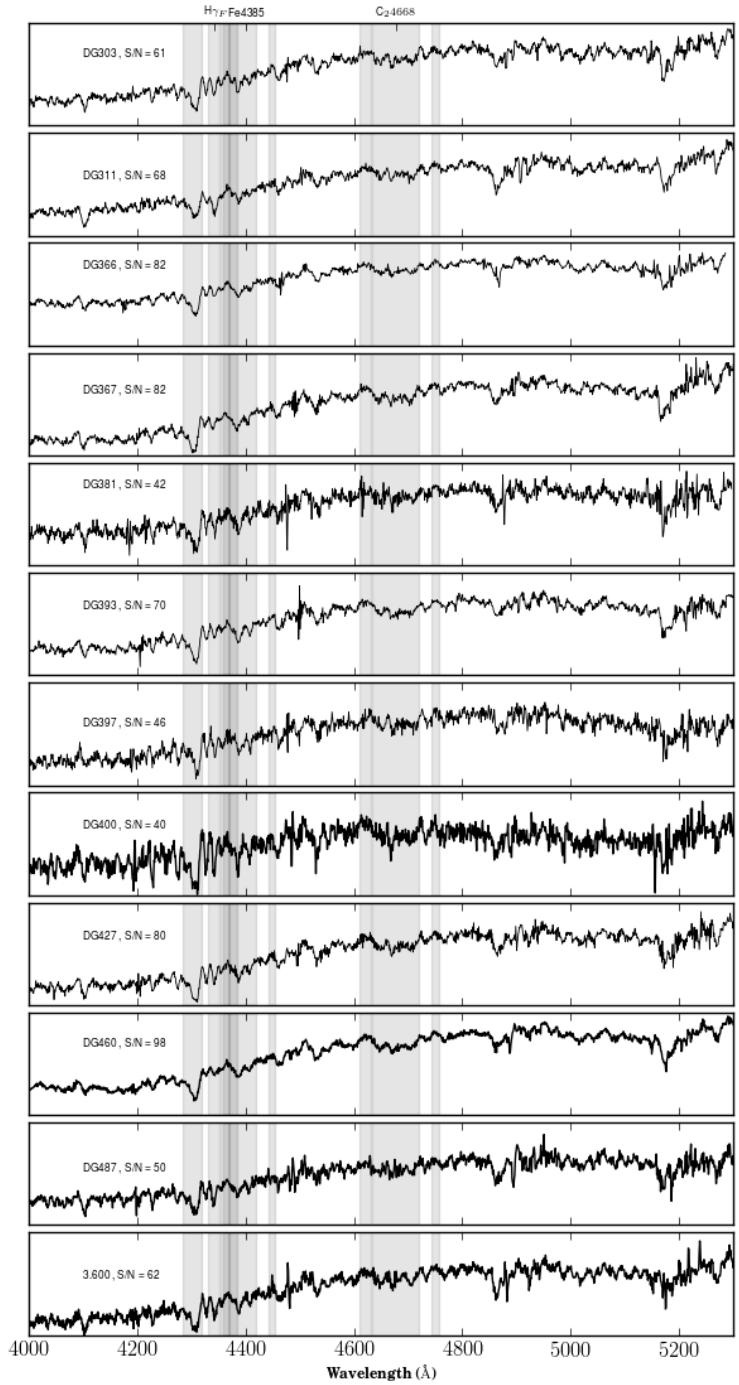

Figure 3.4: The emission line corrected spectra of Abell 851 ETGs. The spectral regions corresponding to the $H\gamma_F$, $C_2$4668 and Fe4383 indices are highlighted.

Table 3.1: Properties of Abell 851 ETGs

Galaxy ID	RA	Dec	z	R (mag)	ϵ_R (mag)	R_e (kpc)	ϵ_{R_e} (kpc)	n	ϵ_n	q	ϵ_q	σ (km s^{-1})	ϵ_σ (km s^{-1})
DG303	09:43:07.6	+46:58:45	0.408	19.93	0.008	2.77	0.03	1.65	0.03	0.58	0.006	138.20	14
DG311	09:42:57.4	+46:58:50	0.400	20.44	0.012	1.45	0.03	2.80	0.05	0.63	0.007	186.80	9
DG366	09:42:58.0	+46:59:12	0.412	18.68	0.009	5.24	0.07	2.42	0.02	0.70	0.004	223.10	6
DG367	09:42:56.2	+46:59:12	0.404	18.50	0.008	8.64	0.10	3.08	0.02	0.73	0.004	238.30	8
DG381	09:43:03.6	+46:59:17	0.409	20.32	0.025	2.41	0.11	4.74	0.13	0.76	0.011	162.80	16
DG393	09:43:02.8	+46:59:23	0.401	19.45	0.013	3.01	0.07	4.24	0.06	0.68	0.005	199.40	9
DG397	09:43:01.8	+46:59:24	0.408	20.44	0.012	1.45	0.03	2.79	0.05	0.63	0.007	186.30	9
DG400	09:43:01.7	+46:59:24	0.406	20.68	0.019	1.19	0.04	3.56	0.10	0.87	0.012	133.30	12
DG427	09:43:09.0	+46:59:35	0.402	19.47	0.007	3.36	0.04	2.37	0.03	0.67	0.006	166.40	13
DG460	09:43:05.2	+46:59:50	0.406	18.64	0.009	7.32	0.12	5.68	0.04	0.71	0.002	289.50	7
DG487	09:43:10.0	+46:59:58	0.404	20.27	0.015	2.71	0.05	1.37	0.04	0.21	0.006	113.40	23
3.600	09:42:44.9	+46:58:58	0.407	19.16	0.005	11.49	0.11	5.47	0.02	0.38	0.001	143.20	12

Notes.
Measured photometric and spectroscopic structural parameters for 15 ETGs belonging to Abell 851 having reliable S/N ratios (> 40/Å). Column (1) is an identifier (DG: Dressler & Gunn) for each galaxy as defined in Dressler & Gunn (1992), columns (2) and (3) are galaxy coordinates (epoch J2000); column (4) is the spectroscopic redshift; columns (5) and (6) are the R-band magnitude and its uncertainty; columns (7) and (8) are the effective radius and its uncertainty in kpc; columns (9) and (10) are the Sérsic index n and its uncertainty; columns (11) and (13) are the axis ratio between major and minor axes and its uncertainty; and columns (13) and (14) are the velocity dispersion in km s^{-1} and its uncertainty.

Galaxy Name	S/N	Hγ_F	eHγ_F	$C_2$4668	e$C_2$4668	Fe4383	eFe4383
DG303	61	-0.20	0.09	5.52	0.23	3.71	0.20
DG311	68	1.58	0.08	5.62	0.21	3.08	0.17
DG366	82	-0.82	0.07	5.86	0.18	3.50	0.15
DG367	82	-0.30	0.07	6.25	0.17	2.07	0.15
DG381	42	-0.82	0.15	4.93	0.37	3.18	0.31
DG393	70	-1.62	0.09	7.04	0.21	4.26	0.17
DG397	46	-0.77	0.24	8.25	0.55	4.75	0.47
DG400	40	-1.27	0.27	7.53	0.68	3.47	0.56
DG427	80	-0.61	0.07	6.41	0.17	3.58	0.15
DG460	98	-1.07	0.06	7.35	0.14	3.46	0.12
DG487	50	0.37	0.11	5.68	0.27	2.80	0.24
3.600	62	0.14	0.09	5.59	0.22	3.46	0.19

Table 3.2: Fully-corrected line strength data for 12 Abell 851 ETGs with S/N > 40/Å.

3.3.4 Spectroscopy: Line strengths

We measured the absorption-line strengths of Abell 851 ETGs on the Lick/IDS index system (Burstein et al. 1984; Worthey 1994; Trager et al. 1998) as explained in Chapter 2. The velocity-dispersion-broadening-corrected line strengths are given in Table 3.2. The rest-frame galaxy spectra are contaminated by atmospheric emission and absorption lines which made many of the line strengths (for example, Mgb, Fe5270 and Fe5335) unusable for stellar population anaylsis.

3.4 The Fundamental Plane of Abell 851 ETGs

We constructed the FP of ETGs in Abell 851 using the measured structural parameters from the HST images and the velocity dispersions from the spectra. We have statistically too low a number of ETGs (12) to fit a FP and to study any possible deviations of the slopes with look-back time. However, previous studies have demonstrated that the FP slope is not evolving at least up to $z \sim 1$ for ETGs in galaxy clusters, but the FP zero-points change (Holden et al. 2010). We therefore adopted the Coma cluster FP coefficients for the FP of Abell 851 (Jorgensen et al. 1996). We calculated the zeropoint offset of Abell 851 FP using the following equation (Treu et al. 2005),

$$\log\langle I_{\rm e}\rangle - \alpha \log \sigma - \beta \log R_{\rm e} = \gamma \tag{3.2}$$

Adopting the Coma cluster values of $\alpha = 1.54$ and $\beta = -1.20$, we found $\gamma = 0.116 \pm 0.004$ for Abell 851. The scatter of ETGs from the FP is measured ($\sigma_{FP} = 0.12$) and is found to be higher in comparison with the R band FP of Coma cluster ETGs ($\sigma_{FP} = 0.084$). The edge-on FP projection of Abell 851 ETGs is shown in Figure 3.5.

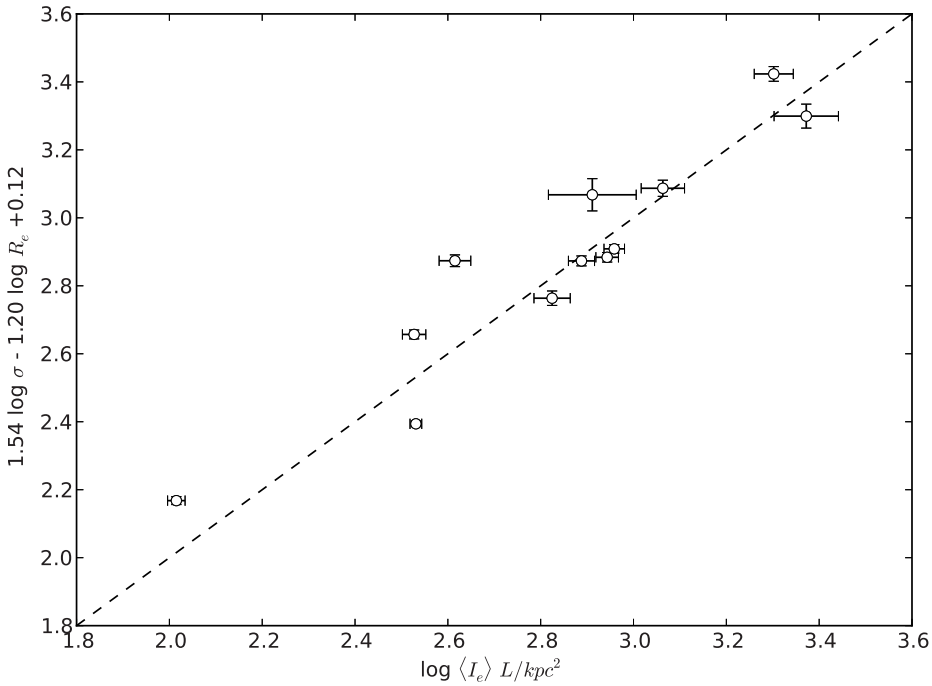

Figure 3.5: Edge-on projection of the rest-frame R-band Fundamental Plane for Abell 851 ETGs. The line represents a one-to-one relation to help visualize deviations from the FP.

3.5 Stellar population studies of Abell 851 ETGs

We used the Hγ_F, $C_2$4668, and Fe4383 line strengths for our stellar population analysis. Hγ_F is highly sensitive to age while $C_2$4668 and Fe4383 are more sensitive to metallicity, with a mild dependence on age. The combination of these indices can disentangle the stellar population parameters age, metallicity and alpha-enhancement ratio (e.g., Worthey 1994; Trager et al. 2000b; Kelson et al. 2006). The rest-frame galaxy spectra are contaminated by atmospheric emission and absorption lines which make many of the otherwise potential line strengths inaccessible for stellar population analysis. We place the measured indices on single-stellar-population (SSP-) equivalent age and metallicity model grids. We compare Abell 851 ETG indices with the high-quality Coma ETG data from Trager et al. (2008). Figure 3.6 shows an index-index diagram for Abell 851 (red) and Coma (blue) ETGs. The Abell 851 cluster ETGs span a range in ages much larger than the Coma cluster ETGs.

The indices we use here are different than those we used in Chapter 2 for the stellar population study of Abell 550. The metallicty indicator, Fe4383, and alpha-enhancement sensitive index, $C_2$4668, need to be confirmed to be reliable before drawing

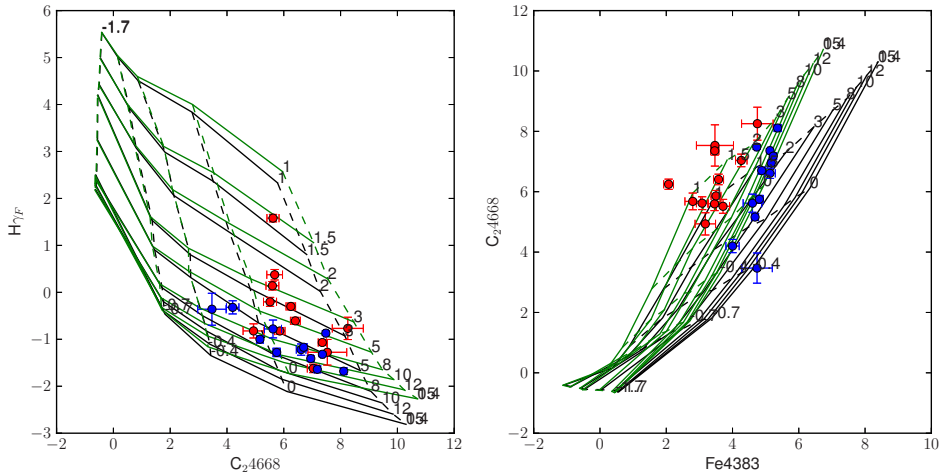

Figure 3.6: Index-index diagrams for Abell 851 ETGs constructed using measured Fe4383, Hγ_F, and $C_2$4668 indices. Stellar population model grids based on Bruzual & Charlot (2003, BC03) models for constant age (solid lines) and constant metallicity (dashed lines) and different enhancement ratios [E/Fe] = 0 (black) and +0.3 (green) are plotted. Blue points correspond to the high-quality data of 12 Coma Cluster ETGs from Trager et al. (2008). Red points are Abell 851 ETGs, spanning a broader range in Hγ_F line strengths (a proxy for age) than Coma Cluster ETGs.

any conclusion on stellar population analysis. We therefore use the high quality data of 12 ETGs on Coma cluster from Trager et al. (2008) to determine SSP-equivalent ages ($t_{\rm ssp}$), metallicities ([Z/H]) and alpha-element enhancement ratios ([E/Fe]). These data are taken using the same instrument (but a different grating blaze wavelength) and have high signal-to-noise (S/N > 40Å), and further cover a broad range in wavelength unaffected by atmospheric lines (or any other contamination). We use the combination of Hγ_F, $C_2$4668, and Fe4383 line strengths (used in this study on Abell 851) and also the combination of Hβ, Mgb and Fe5270 line strengths (used in the previous chapter for Abell 550) of 12 Coma ETGs to derive these SSP-equivalent parameters. We assume a Chabrier IMF and use the Bruzual & Charlot (2003, BC03) models with Padova isochrones (Bertelli et al. 1994) and follow the prescriptions and methodology described by Trager et al. (2008). Once $t_{\rm ssp}$, [Z/H], and [E/Fe] were determined, BC03 models are used to infer stellar mass-to-light ratios in the B-band (M/L_B). We find that the M/L_B ratios derived from the two combinations of line strengths agree within the modelled uncertainities for Coma ETGs sample from Trager et al. (2008) as shown in Figure 3.7. We therefore believe the combination of line strengths we used in this study are appropriate for deriving the SSP parameters of Abell 851 ETGs.

Next we model the SSP-equivalent star formation histories followed by M/L_B ratios for Abell 851 cluster ETGs. We use these results to perform a quantitative analysis of the derived structural and stellar population parameters of Abell 851 cluster ETGs.

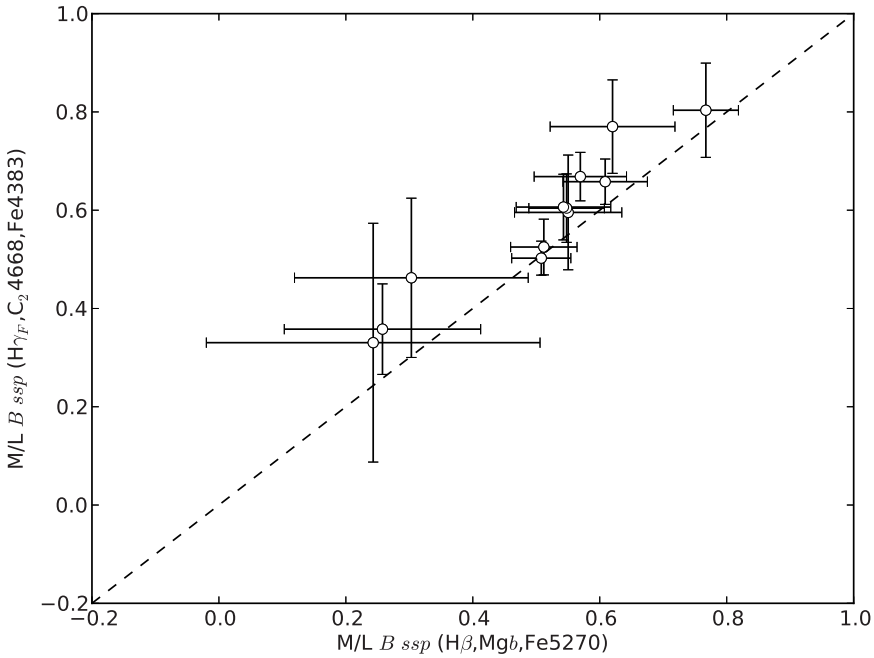

Figure 3.7: M/L_B ratios derived from the combination of Hγ_F, C$_2$4668, and Fe4383 line strengths (used in this study of Abell 851) and the combination of Hβ, Mgb and Fe5270 line strengths (used in Chapter 2 for Abell 550) of 12 Coma Cluster ETGs from Trager et al. (2008).

3.6 Impact of stellar population on Dynamical relations for Abell 851 ETGs

Under the assumption of homology, we paramterise the mass-to-light ratio variation with dynamical mass for Abell 851 ETGs. We combined the measured R_e, $\langle I_e \rangle$ and σ values into a physically meaningful three-dimensional space called κ-space (Bender et al. 1992). The parameters in κ space is obtained by a orthogonal cordinate transformation of the measured parameeters, which also emphasis the FP while retaining physically meaningful variables:

$$\kappa_1 \propto \log M_{\rm dyn} \tag{3.3}$$

$$\kappa_2 \propto \log M/L_{\rm dyn} \times I^3 \tag{3.4}$$

$$\kappa_3 \propto \log M/L_{\rm dyn} \tag{3.5}$$

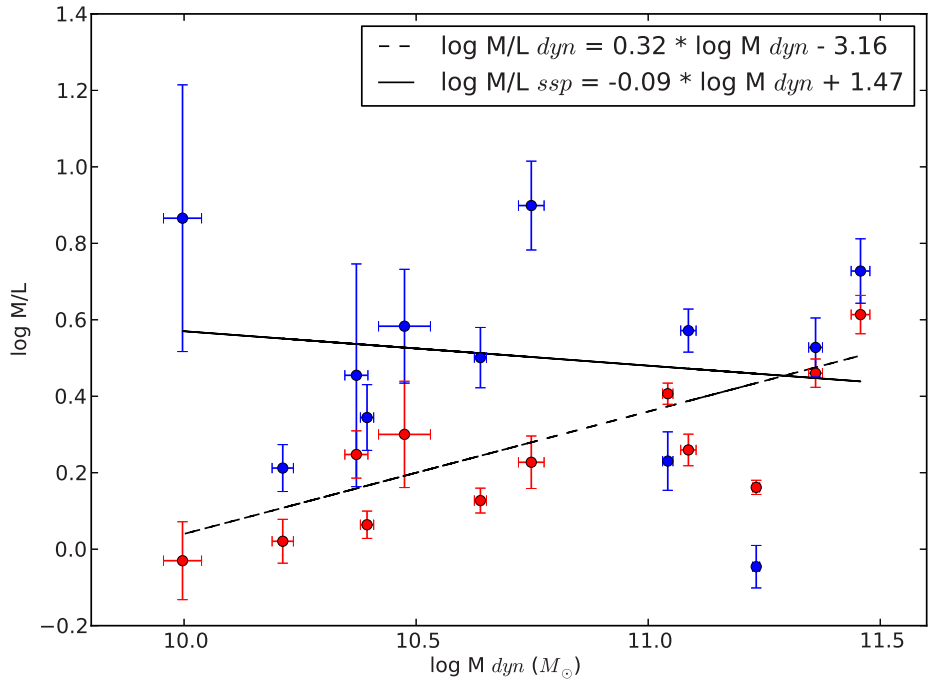

Figure 3.8: Dynamical (red points) and stellar (blue) mass-to-light variation with ETG mass for Abell 851 cluster.

The mass, mass-to-light ratios can then be derived by placing the measured parameters in κ space (Burstein et al. 1997).

$$\log M_{\rm dyn} = \sqrt[2]{\kappa_1} + 5.67 \tag{3.6}$$

$$\log M/L_{\rm dyn} = \sqrt[3]{\kappa_3} - 0.83 \tag{3.7}$$

We determined the dynamical mass, mass-to-light ratios by putting the measured quantities into the above equations, as shown in Figure 3.8. We quantify the relation using a least-squares fit, running 1000 Monte Carlo realizations considering the errors in both dimensions. The dynamical mass-to-light dependence on ETG dynamical mass can be parameterized as

$$\log M/L_{\rm dyn} = (0.32 \pm 0.04) \times \log M_{\rm dyn} - (3.16 \pm 0.47), \tag{3.8}$$

The stellar mass-to-light dependence on ETG dynamical mass can be parameterized as

$$\log M/L_{\rm ssp} = (-0.09 \pm 0.11) \times \log M_{\rm dyn} + (1.47 \pm 1.27). \tag{3.9}$$

The dependence of both stellar and dynamical mass-to-light ratios on ETG dynamical mass is shown in Figure 3.8.

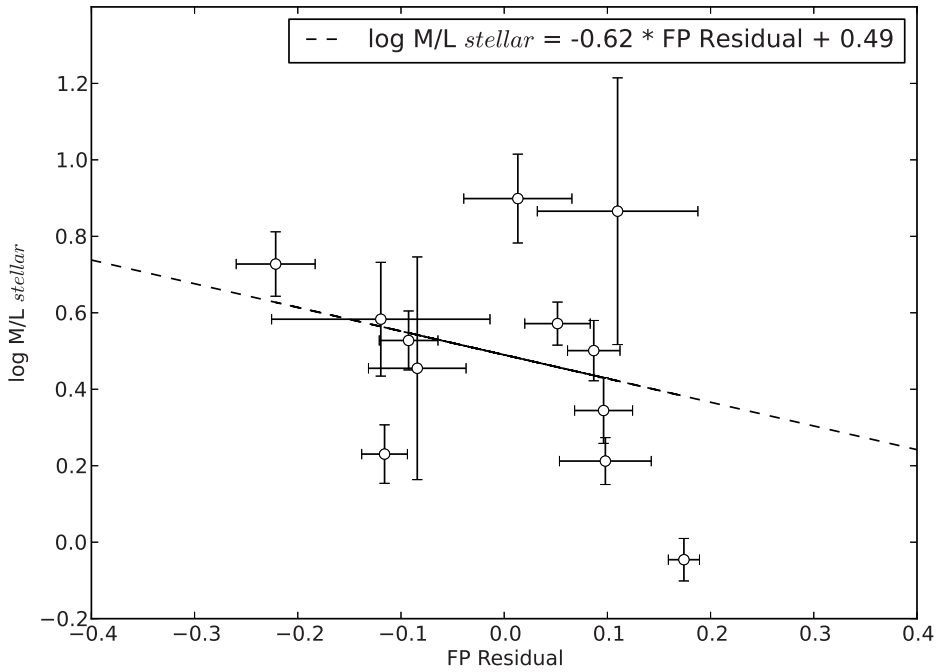

Figure 3.9: Abell 851 ETGs residual on the Fundamental Plane versus stellar mass-to-light ratio in the B-band.

3.7 Discussion

We investigate the stellar population properties of galaxies along the thickness of the FP by measuring the scatter $\Delta\langle I_e\rangle$ from the best-fit FP. The stellar mass-to-light ratios derived from stellar population models correlate with the FP scatter (Figure 3.9). We quantify the relation using a least-squares fit, running 1000 Monte Carlo realizations considering the errors in both dimensions.

$$\log M/L_{\rm ssp} = (-0.62 \pm 0.42) \times FP_{\rm Residual} + (0.49 \pm 0.05). \tag{3.10}$$

At a redshift of $z = 0.406$, we are observing galaxies in Abell 851 ~ 4.3 billion years back in time. Previous studies have demonstrated that Abell 851 is a dynamically young cluster, still in the process of assembly (Kodama et al. 2001; Schindler & Wambsganss 1996; Schindler et al. 1998). Many galaxies in this cluster must have recently accreted from the field or even from infalling groups (Koyama et al. 2011; Oemler et al. 2009). Once galaxies are part of the cluster they are prone to morphological and stellar population transformations in the hostile cluster environment (Dressler et al. 1997). This means we may be witnessing the last star formation events in many of the ETGs in Abell 851 (Oemler et al. 1997). We first checked for any such recent star formation

events from our FP analysis, such that recent star formation should manifest itself as a enhanced FP scatter as we demonstrated in Chapter 2. We found that the intrinsic scatter of Abell 851 ETGs in the FP is higher than those found for ETGs in the Coma Cluster. We then carried out a detailed stellar population analysis of these 12 ETGs to confirm the presence of recent star formation. We found that in Abell 851, the stellar mass-to-light ratios are nearly constant with mass, with a large scatter irrespective of mass. This is possible if there is star formation happening on different time scales (or alternatively bursts with varying strengths) for ETGs irrespective of their mass.

We further found that the residuals from the FP anti-correlate with the stellar mass-to-light ratios of ETGs. When combined with the fact that stellar mass-to-light has a large scatter over the observed range in dynamical mass, this shows that throughout (along and within) the FP, ETGs have a variety of star formation histories. The lack of an increasing trend in stellar mass-to-light ratio with dynamical mass of ETGs points towards a scenario in which there is no downsizing for ETGs located in the core of Abell 851.

Abell 851 must then be in the very early phase of its assembly process, with infalling galaxies still undergoing morphological and stellar population tranformations at the epoch of observation. We are witnessing the aftermath of a recent phase of intense star formation in the ETGs, just after the galaxies lost their molecular gas in the hostile cluster environmnet. Further studies on a statistically large sample of ETGs in merging clusters at intermediate redshifts should give more insight into this scenario.

3.8 Conclusions

We have presented a detailed structural and stellar population analysis for ETGs in Abell 851, a rich galaxy cluster at $z \sim 0.406$. The FP of ETGs in this cluster has a larger instrinsic scatter than the FP of the Coma Cluster. This FP residual is anti-corellated with the stellar mass-to-light ratio derived from stellar population modelling. The stellar mass-to-light ratios have a constant trend over the range of ETGs dynamical mass studied in this work. These relations show that ETGs in Abell 851 have undergone recent star-formation episodes, regardless of their mass. This recent star formation is responsible for the increased scatter around the FP and the stellar mass-to-light ratios. These results can be explained by morphological and stellar-population tranformations happening in Abell 851 due to the on-going cluster assembly at $z \sim 0.406$ but cannot be explained by high formation redshifts for ETGs in Abell 851.

Chapter 4

Stellar populations and the Fundamental Plane of early-type galaxies in two rich galaxy clusters at $z \sim 0.7$

Abstract

We present here a study of the structural and stellar population parameters of early-type galaxies (ETGs) in two rich galaxy clusters at $z \sim 0.7$. The motivation for this study is to understand the structural and stellar population properties of ETGs in rich galaxy clusters at these redshifts. We use spectroscopy and photometry to construct the Fundamental Plane (FP) and estimate the star formation history from single stellar population (SSP) models. ETGs from GHO 1322+3027 (at $z = 0.76$) and GHO 1322+3114 (at $z = 0.70$) follow FPs with intrinsic scatter comparable to that of the Coma Cluster. The stellar mass-to-light ratios derived from stellar population modelling shows a one-to-one relation with dynamical mass-to-light ratios over the range of dynamical mass studied in this work.

*The data presented herein were obtained at the W.M. Keck Observatory, which is operated as a scientific partnership among the California Institute of Technology, the University of California and the National Aeronautics and Space Administration. The Observatory was made possible by the generous financial support of the W.M. Keck Foundation.

4.1 Introduction

In the preceding chapters we have demonstrated that early-type galaxies (ETGs) in low- and intermediate-redshift galaxy clusters show signatures of recent star formation (Chapters 2 and 3). ETGs at any epoch after $z \sim 1$ are thought to be passively evolving stellar systems, and those residing in very hostile high-density environments should not be exceptions. The presence of a trace amount of young stars in these otherwise passively-evolving stellar systems points towards a scenario where star-forming galaxies undergo rapid morphological and stellar population transformations in the dense cluster environment. These transformations are likely to be the direct result of cluster assembly processes in which galaxy groups or infalling galaxies from the field contribute towards the formation of massive galaxy clusters (Kodama et al. 2001). Many intermediate redshift clusters show evidence for such merging events (like radio relics and halos) in the recent past and also their ETGs show signatures of recent star formation (Giovannini et al. 2009). Looking further back in time by studying the ETGs in high redshift clusters will help in understanding the formation of ETGs and cluster assembly process in greater detail.

Galaxy clusters GHO 1322+3114 ($z \sim 0.7$) and GHO 1322+3027 ($z \sim 0.75$) should be dynamically young clusters compared with clusters at $z \sim 0.1$ and 0.4, such as those studied in Chapters 2 and 3. These clusters have been studied in the optical and X-rays to determine their richnesses and total masses (Gunn et al. 1986; Castander et al. 1994). They are rich and massive galaxy clusters observed when the Universe was roughly half of its current age. The current paradigm of Λ-Cold Dark Matter (ΛCDM) cosmology predicts galaxy clusters to be dynamically young with cluster assembly processes actively happening at this epoch. The ongoing or recent assembly of these $z \sim 0.7$ clusters should be manifested as recent star-formation events in the cluster ETGs (Chapter 3). Under the (extreme) assumption that clusters of similar masses are coeval at a given epoch, we expect to see stronger evidence of recent star formation in the cluster ETGs compared to the lower redshift cluster galaxies studied in previous chapters. This can be understood by studying the scatter of ETGs from the Fundamental Plane (FP) and from their associated stellar population properties. The increased scatter on the FP and the corresponding young ages of the stellar population content are direct proof of the cluster youth (Chapters 2 and 3).

We present a detailed study based on the FPs and stellar populations of ETGs in GHO 1322+3114 and GHO 1322+3027 based on deep spectral data from the Keck 10-m telescopes and high-resolution imaging from HST. We follow the same procedure as in previous chapters, except that our stellar population analysis relies on different line strengths, owing to the presence of residuals from the forest of sky lines in the red part of the galaxy spectra and contamination from the atmospheric A and B bands. Furthermore, the faintness of the galaxies due to the surface-brightness dimming at those high redshifts causes many of the intrinsically bright galaxies to be at the detection threshold of spectroscopy from 10-m telescopes. This is further complicated by a lack of HST imaging for the majority of the galaxies with spectral data. Thus this study is based on 6 ETGs from two clusters.

We adopt a flat Universe cosmology with $H_o = 71\,\mathrm{km\,s^{-1}\,Mpc^{-1}}$, $\Omega_M = 0.27$,

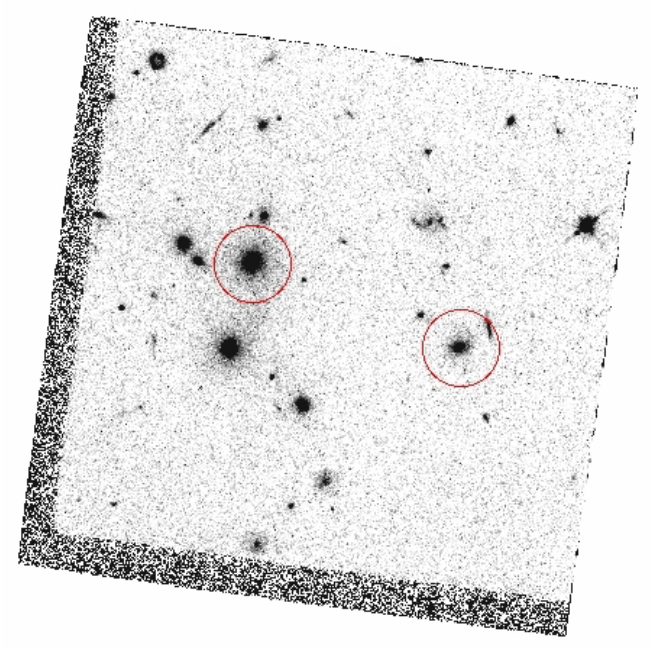

Figure 4.1: The WFPC2 F814W planetary camera image of the field of GHO 1322+3027: The region around the cluster core. Red circles correspond to the ETGs used in this study.

$\Omega_\Lambda = 0.73$ (Komatsu et al. 2011). This chapter is organised as follows. The observations are described in Section 2, data reduction and analysis in Section 3, the construction of the Fundamental Plane of high-redshift clusters in Section 4 and a stellar population analysis of the cluster ETGs in Section 5, combined stellar population and dynamic analysis in section 6, followed by discussion in Section 7 and conclusions in Section 8.

4.2 Observations

Spectroscopic data acquisition was performed with the Low-Resolution Imaging spectrograph (LRIS: Oke et al. 1995) on the Cassegrain focus of Keck I, one of the 10-m telescopes at Mauna Kea, Hawai'i. LRIS performs imaging and multi-slit spectroscopy of targets over a field of view of $\sim 6 \times 7.8\,\mathrm{arcmin}^2$. We used the red side of the instrument, the only wavelength region accessible during the period of our observations.

Galaxies were selected based on their early-type morphology from HST/WFPC2 imaging observations of the cluster fields (Trager et al. 1996) and pre-existing spectroscopic redshifts from Dressler & Gunn (1990). HST/WFPC2 F814W observations of the cluster fields were used to derive the structural parameters of the clusters ETGs (below). The locations of the ETGs in the cluster fields are shown in Figure 4.1 and Figure 4.2. We note that GHO 1322+3027 cluster ETGs were imaged with the plan-

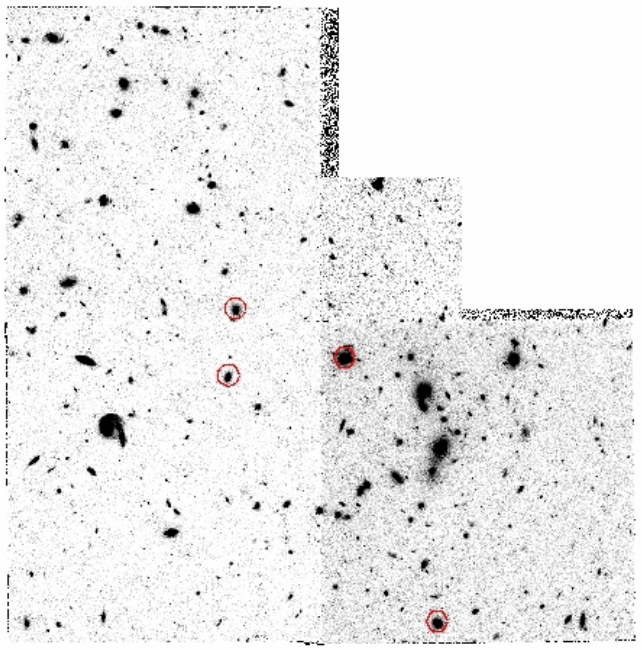

Figure 4.2: The WFPC2 F814W mosaic images of the field of GHO 1322+3114: The region around the cluster core. Red circles correspond to the ETGs used in this study.

etary camera (PC) of WFPC2, whereas GHO 1322+3114 cluster ETGs were imaged with the wide-field (WF) chips of WFPC2.

Spectroscopy was carried out using multi-slit masks made corresponding to the astrometric position of selected ETGs. We used LRIS with a 600 lines mm^{-1} grating and a slit width of $1''$, which provided a dispersion of 1.25 $pixel^{-1}$ and a wavelength coverage of 6000–9000Å, depending on the position of the slit. Galaxies were observed for 2400 s per exposure and the typical seeing was $0''.7$–$1''.0$. The spectral data were taken over three nights using two slit masks. For GHO 1322+3027 galaxies, a total of $\sim$ 480 minutes of integration time was taken and a total of $\sim$ 680 minutes of integration time was taken for GHO 1322+3114 galaxies. Calibration frames taken along with the science observations were used for the data reduction process.

4.3 Data reduction and analysis

4.3.1 Data reduction

Imaging data were taken from HST archives and used for deriving the structural parameters. This data were photometrically calibrated and of high spatial resolution.

The spectroscopic data were reduced using *CarnegiePython* as described in Chap-

http://code.obs.carnegiescience.edu/python/

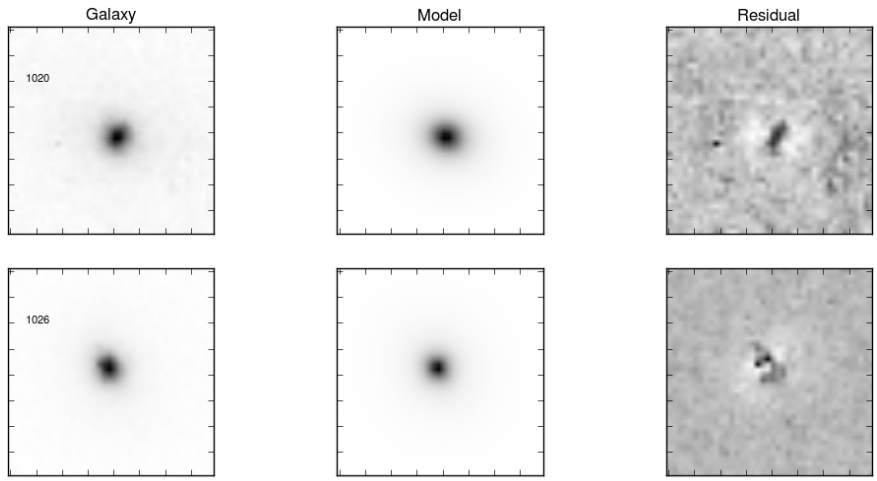

Figure 4.3: GALFIT surface photometry. Observed images of GHO 1322+3027 cluster ETGs are shown in the left panel, GALFIT-modelled images in the middle panel, and the residual images in right panel. Residual images are displayed with different grey-scale stretches to enhance structures in the observed galaxy image profile not properly modelled solely with a Sérsic profile.

ter 2. Wavelength calibration was performed using emission lines from the sky that fill the regions of the slitlets along with the galaxy spectrum in the two-dimensional science frames. Flux calibration was performed using a spectrophotometric standard observed along with the science frames. The spectra were then converted to rest-frame wavelengths by measuring the redshift of the galaxy, obtained from a match with stellar population models. The spectra of 6 ETGs have signal-to-noise ratio $\mathrm{S/N} > 15/\text{Å}$. We used this imaging and spectral data for constructing the FP and studying the stellar population properties of ETGs in high-redshift clusters.

4.3.2 Photometry: Structural parameters

We used GALFIT (Peng et al. 2002) to determine effective radius(R_e) and surface brightness($\langle I_e \rangle$). A Sérsic profile was fit to the WFPC2 F814W and WFPC2 F606W images of ETGs using the method described in detail in Chapter 2. A point spread function for each galaxy was generated using *TinyTim*. The residual images from GALFIT are shown in Figure 4.3 and Figure 4.4.

We calibrated the photometry using zero points from the HST archives. We note that the observations were carried out using F814W and F606W filters in observed frame which are very close to the B and U bands in the rest frame. ETGs from GHO 1322+3027 and GHO 1322+3114 were corrected for bandpass-shifting using the fitting function derived from B_c, F606W and F814W colours for BC03 models with metallicities

http://www.stsci.edu/hst/observatory/focus/TinyTim

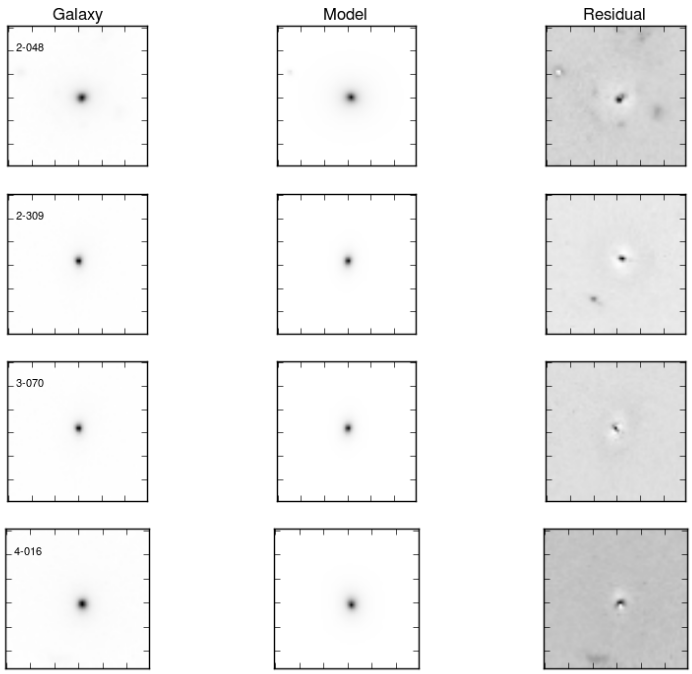

Figure 4.4: GALFIT surface photometry. Observed images of GHO 1322+3114 cluster ETGs are shown in the left panel, GALFIT-modelled images in the middle panel, and the residual images in right panel. Residual images are displayed with different grey-scale stretches to enhance structures in the observed galaxy image profile not properly modelled solely with a Sérsic profile.

of $Z = 0.008$, 0.02, and 0.05, and ages from 1–7 Gyr at $z = 0$ and $z = 0.75$ and $z = 0.69$. Once the observed F606W and F814W are known R_c in the rest frame is computed using following equations. For CL1322+3027 at z=0.755 the fitting function is as follows, with an RMS scatter of 0.06 mag:

$$\begin{aligned} B_{c(z=0)} &= F814W_{(z=0.75)} - 0.11[(F606W_{(z=0.75)} - F814W_{(z=0.75)}) - 2.14] \\ &\quad \times[(F606W_{(z=0.75)} - F814W_{(z=0.75)}) - 1.75] \\ &\quad +0.11[(F606W_{(z=0.75)} - F814W_{(z=0.75)}) - 1.90] + 1.86. \end{aligned} \tag{4.1}$$

For CL1322+3114 at z=0.695 the fitting function is as follows, with an RMS scatter of

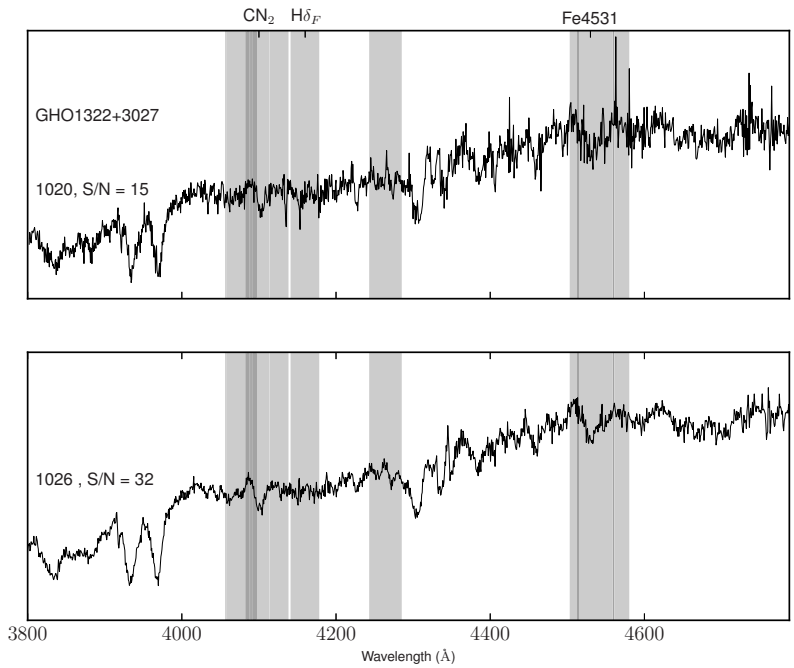

Figure 4.5: The emission-line-corrected spectra of high-redshift cluster ETGs in GHO 1322+3027.

0.04 mag:

$$\begin{aligned} B_{c(z=0)} &= F814W_{(z=0.69)} - 0.25[(F606W_{(z=0.75)} - F814W_{(z=0.75)}) - 2.03] \\ &\quad \times[(F606W_{(z=0.75)} - F814W_{(z=0.75)}) - 1.63] \\ &\quad +0.24[(F606W_{(z=0.75)} - F814W_{(z=0.75)}) - 1.80] + 1.91. \end{aligned} \tag{4.2}$$

Galactic extinction in the direction of these high-redshift clusters was corrected using the extinction values from NED ($A_\lambda = 0.037$). Finally, the correction in surface brightness for cosmological dimming is done by adding the $\log(1+z)^4$ term to the measured values. The derived structural parameters of the galaxy from HST images are listed in Table 1.

4.3.3 Spectroscopy: Velocity dispersions

We used the techniques described in Chapter 2 for measuring velocity dispersions of the ETGs. GANDALF (Sarzi et al. 2006) was used to clean the ETG spectra of emission-lines and to measure the line-of-sight central velocity dispersion (LOSVD) of stars in

http://ned.ipac.caltech.edu/

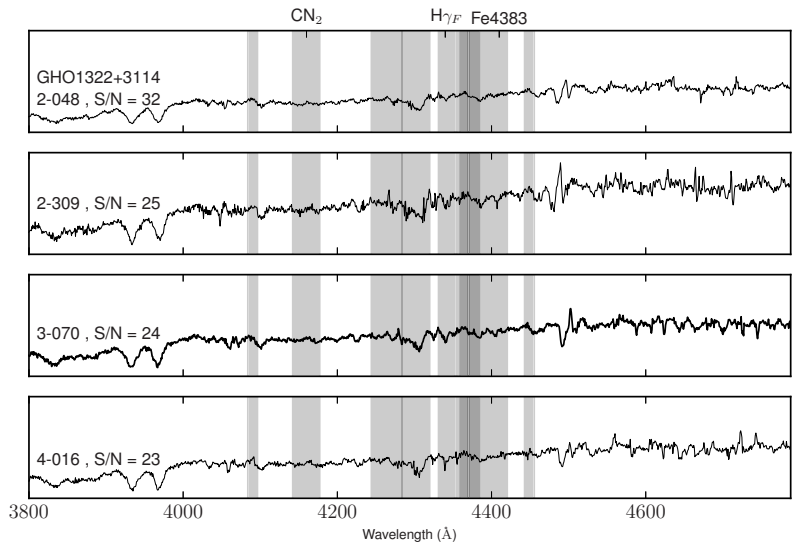

Figure 4.6: The emission-line-corrected spectra of high-redshift cluster ETGs in GHO 1322+3114.

random orbits, projected on the plane of the sky (σ). The line spread function due to the finite resolution of the instrument was measured using the widths of night sky emission lines. MILES model templates were smoothed to the measured instrument resolution before running GANDALF. The emission-line corrected ETG spectra are shown in Figure 4.5 and Figure 4.6 for GHO 1322+3027 and GHO 1322+3114, respectively, and the measured velocity dispersions (σ) are listed in Table 4.1.

Table 4.1: Properties of $z \sim 0.7$ cluster ETGs

Galaxy ID	RA	Dec	z	R (mag)	ϵ_R (mag)	R_e (kpc)	ϵ_{R_e} (kpc)	n	ϵ_n	q	ϵ_q	σ (km s^{-1})	ϵ_σ (km s^{-1})
1-020	13:24:47.74	+30:11:32.90	0.752	23.21	0.014	2.17	0.06	2.41	0.10	0.80	0.01	121	33
1-026	13:24:48.74	+30:11:38.41	0.753	21.69	0.014	4.01	0.15	4.45	0.13	0.85	0.01	238	10
2.048	13:24:48.96	+30:58:38.97	0.694	21.72	0.007	4.66	0.05	2.44	0.05	0.88	0.01	222	12
2.309	13:24:47.25	+30:59:41.91	0.696	22.53	0.010	3.15	0.04	1.53	0.03	0.80	0.01	172	17
3.070	13:24:51.14	+30:58:43.49	0.691	22.65	0.008	1.81	0.03	2.29	0.07	0.54	0.01	187	12
4.016	13:24:50.98	+30:58:27.47	0.692	22.50	0.010	2.79	0.04	2.07	0.04	0.74	0.01	201	12

Notes.
Measured photometric and spectroscopic structural parameters for 6 ETGs belonging to $z \sim 0.7$ having reliable S/N ratios (> 15/Å). Column (1) is an identifier for each galaxy as defined by the WFPC2 chip number and position used for imaging or if available the identification from Dressler & Gunn (1990), columns (2) and (3) are galaxy coordinates (epoch J2000); column (4) is the spectroscopic redshift; columns (5) and (6) are the R-band magnitude and its uncertainty; columns (7) and (8) are the effective radius and its uncertainty in kpc; columns (9) and (10) are the Sérsic index n and its uncertainty; columns (11) and (13) are the axis ratio between major and minor axes and its uncertainty; and columns (13) and (14) are the velocity dispersion in km s^{-1} and its uncertainty.

Table 4.2: Fully-corrected line strength data for four ETGs from GHO 1322 +3027 with S/N > 15/Å.

Galaxy Name	S/N	$H\delta_F$	$eH\delta_F$	CN_2	eCN_2	Fe4531	eFe4531
1020	15	1.33	0.28	0.12	0.02	3.55	0.54
1026	32	1.68	0.12	0.10	0.01	2.64	0.21

Table 4.3: Fully-corrected line strength data for five ETGs from GHO 1322 +3114 with S/N > 15/Å.

Galaxy Name	S/N	$H\gamma_F$	$eH\gamma_F$	CN_2	eCN_2	Fe4383	eFe4383
2-048	32	−1.34	0.17	0.14	0.01	3.89	0.28
2-309	25	−0.99	0.19	0.12	0.01	3.75	0.35
3-070	24	−0.08	0.22	0.08	0.01	3.96	0.36
4-016	23	−0.37	0.23	0.08	0.01	3.23	0.41

4.3.4 Spectroscopy: Line strengths

We measured the absorption-line strengths of high-redshift clusters ETGs on the Lick/IDS index system (Burstein et al. 1984; Worthey 1994; Trager et al. 1998) as described in Chapter 2. The velocity-dispersion-broadening-corrected line strengths are given in Table 4.2 and Table 4.3. The rest-frame galaxy spectra are contaminated by atmospheric emission and absorption lines which made many of the line strengths (for example, Mgb, Fe5270 and Fe5335) unusable for stellar population analysis. This was further complicated by the slightly different redshifts for the two clusters studied here. We therefore used different combination of line strengths for our stellar population analysis.

4.4 The Fundamental Plane of high-redshift ETGs

We constructed the FP of ETGs in two high-redshift galaxy clusters using the measured structural parameters from the HST images and the velocity dispersions from the spectra. We assume that both clusters are coeval and place the ETGs on to a common FP. We have 9 ETGs with spectroscopic data, but only six of these are present in the the HST imaging, required to measure their structural parameters. We therefore have statistically too-low a number of ETGs to fit a FP and to study any possible deviations of the slopes with look-back time. However, previous studies have demonstrated that the FP slope is not evolving at least up to $z \sim 1$ for ETGs in galaxy clusters, but the FP zero-points change (Holden et al. 2010). We therefore adopted the Coma cluster B band FP coefficients (Jorgensen et al. 1996). We calculated the zero point offset of FP using the following equation

$$\log\langle I_e \rangle - \alpha \log \sigma - \beta \log R_e = \gamma \tag{4.3}$$

Adopting the Coma cluster values of $\alpha = 1.41$ and $\beta = -1.19$, we found $\gamma = 0.08 \pm 0.01$ for $z \sim 0.7$ clusters. The scatter of ETGs from the FP ($\sigma_{FP} = 0.073$) is measured to be

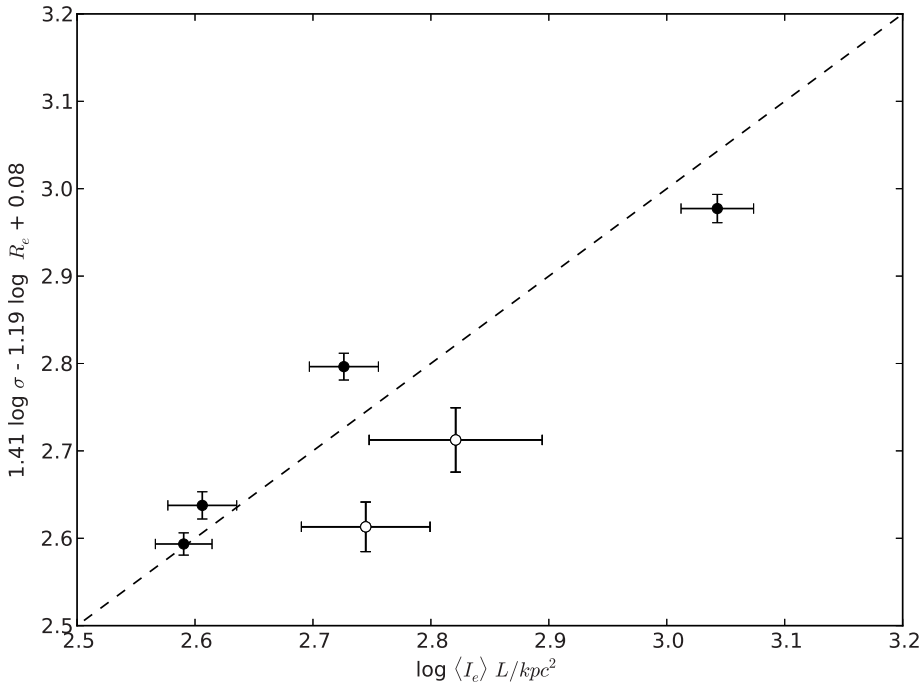

Figure 4.7: Edge-on projection of the B-band Fundamental Plane for high-redshift cluster ETGs. Open points correspond to ETGs from GHO 1322+3027, closed points to ETGs from GHO 1322+3114.

only marginally larger than the scatter around the B-band FP of Coma Cluster ETGs ($\sigma_{FP} = 0.071$). The edge-on FP projection of the high-redshift cluster ETGs is shown in Figure 4.7.

4.5 Stellar population studies of $z \sim 0.7$ cluster ETGs

The rest-frame galaxy spectra are contaminated by atmospheric emission and absorption lines which make many of the otherwise potential line strengths inaccessible for stellar population analysis. We are therefore unable to use the same indices for stellar population analysis as in previous chapters.

We used the Hδ_F, CN_2, and Fe4531 line strengths for stellar population analysis of ETGs in GHO 1322+3027. Hδ_F is sensitive to more to age than to metallicity, and CN_2 and Fe4531 are more sensitive to metallicity than to age. The combination of these indices can disentangle the stellar population parameters of age, metallicity and α-enhancement ratio (e.g., Worthey 1994; Trager et al. 2000b; Kelson et al. 2006). We place the measured indices on single-stellar-population (SSP) equivalent age and

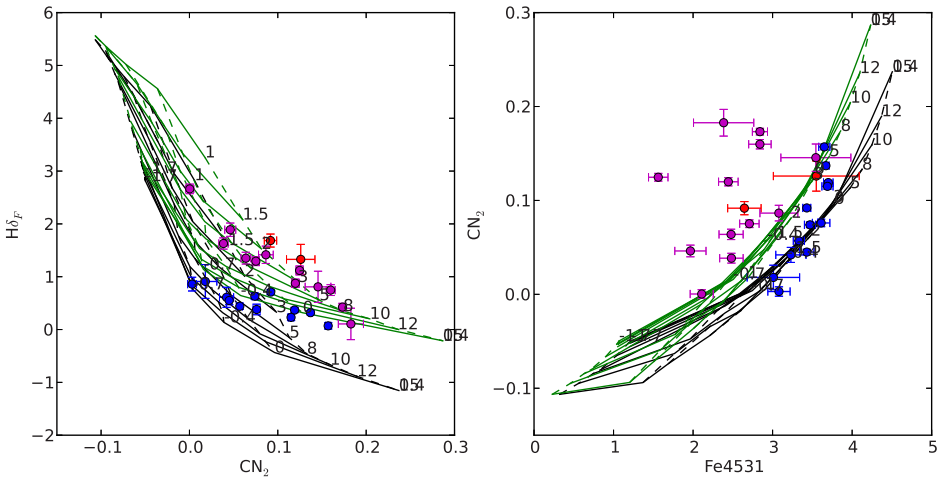

Figure 4.8: Index-index diagrams for GHO 1322+3027 cluster ETGs constructed using measured Fe4531, Hδ_F, and CN_2 indices. Stellar population model grids based on Bruzual & Charlot (2003, BC03) models for constant age (solid lines) and constant metallicity (dashed lines) and different enhancement ratios [E/Fe] = 0 (black) and +0.3 (green) are plotted. Blue points correspond to the high-quality data of the 12 Coma Cluster ETGs from Trager et al. (2008). Magenta points are Abell 851 ETGs from Chapter 3. Red points are GHO 1322+3027 ETGs, having higher Hδ_F line strengths than Coma Cluster ETGs.

metallicity model grids. We compare the indices of ETGs in this high-redshift cluster with the high-quality Coma ETG data from Trager et al. (2008). Figure 4.8 shows an index-index diagram for the ETGs in the high-redshift cluster (red) and Coma (blue). The high-redshift cluster ETGs span a range in ages much larger than the Coma Cluster ETGs.

We used the Hγ_F, CN_2, and Fe4383 line strengths for stellar population analysis of ETGs in GHO 1322+3114 cluster. Hγ_F is used as the primary age-sensitive index while CN_2 and Fe4383 are used as the metallicity- and [α/Fe]-sensitive indices. We compare the indices from the ETGs in this cluster with the high-quality Coma ETG data from Trager et al. (2008) in Figure 4.9. Again we find that the high-redshift cluster ETGs span a range in ages much larger than the Coma Cluster ETGs. This was followed by modelling the SSP-equivalent star formation histories for GHO 1322+3114 cluster ETGs as described in previous section.

We then model the SSP-equivalent star formation histories for cluster ETGs. We assume a Chabrier IMF and Bruzual & Charlot (2003, BC03) models with Padova isochrones (Bertelli et al. 1994) and followed the prescriptions and methodology described in detail in (Trager et al. 2008). Once the SSP-equivalent ages (t_{ssp}), metallicities ([Z/H]) and α-enhancements ([E/Fe]) were determined, BC03 models were used to infer stellar mass-to-light ratios in the B-band (M/L_B). We use these results to perform

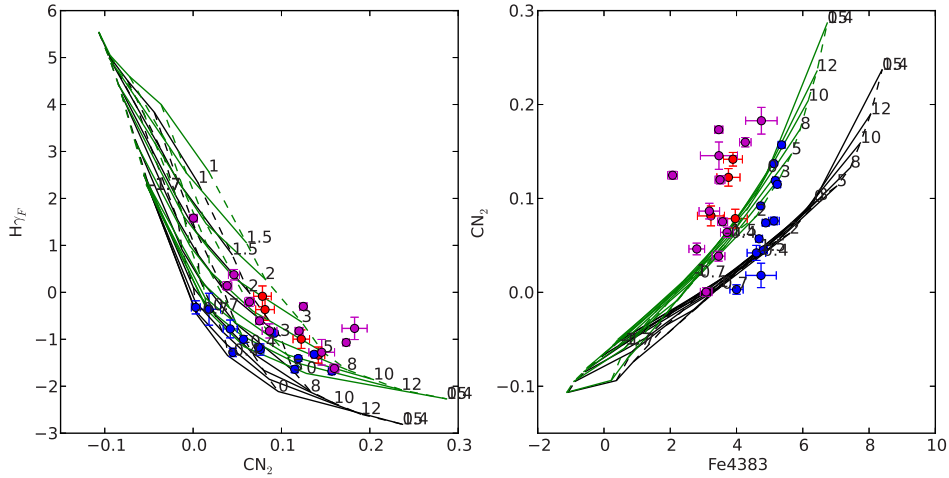

Figure 4.9: Index-index diagrams for GHO 1322+3114 cluster ETGs constructed using measured Fe4383, Hγ_F, and CN_2 indices. Stellar population model grids based on Bruzual & Charlot (2003, BC03) models for constant age (solid lines) and constant metallicity (dashed lines) and different enhancement ratios [E/Fe] = 0 (black) and +0.3 (green) are plotted. Blue points correspond to the high-quality data of 12 Coma cluster ETGs from Trager et al. (2008). Magenta points are Abell 851 ETGs from Chapter 3. Red points are GHO 1322+3114 ETGs, having higher Hγ_F line strengths than Coma Cluster ETGs.

a quantitative analysis of the derived structural and stellar population parameters of the GHO 1322+3027 and GHO 1322+3114 cluster ETGs.

The indices we use here for two clusters are different than those we used in Chapter 2 and 3 for the stellar population studies of Abell 550 and Abell 851. The mass-to-light ratios inferred from the age-sensitive (Hδ_F, Hγ_F), metallicity-sensitive (Fe4383, Fe4531), and α-enhancement-sensitive (CN_2) indices, need to be confirmed to be reliable before drawing any conclusion on stellar population analysis. We therefore use the high-quality data of the 12 ETGs in the Coma Cluster presented in Trager et al. (2008) to determine SSP-equivalent ages ($t_{\rm ssp}$), metallicities ([Z/H]) and α-element enhancement ratios ([E/Fe]). These data are taken using the same instrument (but a different grating blaze wavelength), have high signal-to-noise (S/N > 40Å), and further cover a broad range in wavelength unaffected by atmospheric lines or other spectral contamination. We use the combination of Hδ_F, CN_2, and Fe4531 line strengths (used in this study for ETGs in GHO 1322+3027) along with Hγ_F, CN_2, and Fe4383 line strengths (used in this study for ETGs in GHO 1322+3114) and also the combination of Hβ, Mgb and Fe5270 line strengths (used in Chapter 2 for Abell 550) of the 12 Coma Cluster ETGs to derive the SSP-equivalent parameters. We assume a Chabrier IMF and use the Bruzual & Charlot (2003, BC03) models with Padova 1994 isochrones (Bertelli et al. 1994) and follow the prescriptions and methodology described by Trager et al. (2008). Once $t_{\rm ssp}$,

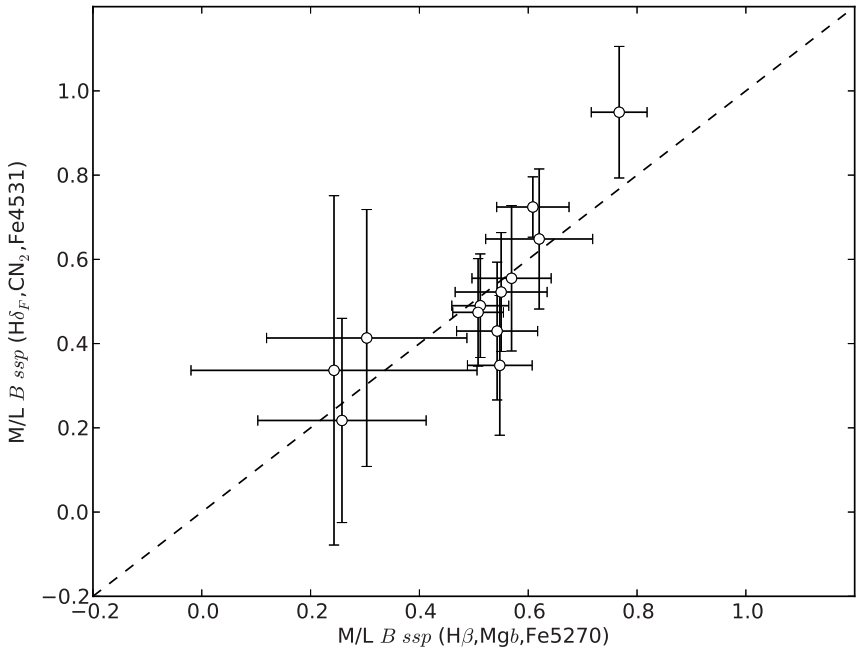

Figure 4.10: M/L_B ratios derived from the combination of Hδ_F, CN$_2$, and Fe4531 line strengths (used in this study of ETGs in GHO 1322+3027) and from the combination of Hβ, Mgb and Fe5270 line strengths (used in Chapter 2 for Abell 550) of 12 Coma Cluster ETGs from Trager et al. (2008).

[Z/H], and [E/Fe] have been determined, BC03 models are used to infer stellar mass-to-light ratios in the B-band (M/L_B). We find that the M/L_B ratios derived from the two combinations of line strengths agree within the modelled uncertainties for Coma ETGs sample from Trager et al. (2008) as shown in Figure 4.10 & Figure 4.11. We therefore believe the combination of line strengths we used in this study are appropriate for deriving the SSP parameters of ETGs.

Next we model the SSP-equivalent star formation histories followed by M/L_B ratios for $z \sim 0.7$ cluster ETGs. We use these results to perform a quantitative analysis of the derived structural and stellar population parameters of these high z cluster ETGs.

4.6 Impact of stellar population on Dynamical relations for high redshift clusters ETGs

Under the assumption of homology, we parameterise the mass-to-light ratio variation with dynamical mass for high redshift clusters ETGs. We combined the measured R_e,

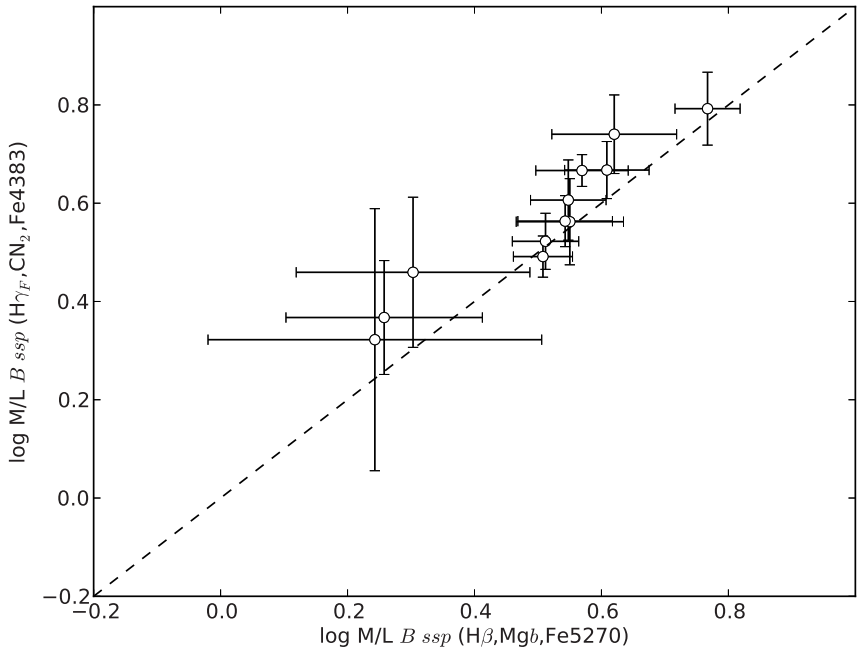

Figure 4.11: M/L_B ratios derived from the combination of Hγ_F, CN$_2$, and Fe4383 line strengths (used in this study of ETGs in GHO 1322+3114) and from the combination of Hβ, Mgb and Fe5270 line strengths (used in Chapter 2 for Abell 550) of 12 Coma Cluster ETGs from Trager et al. (2008).

$\langle I_e \rangle$ and σ values into a physically meaningful three-dimensional space called κ-space (Bender et al. 1992).

We determined the dynamical mass, mass-to-light ratios by placing the measured parameters in κ space. The inferred masses and mass-to-light ratios are shown in Figure 4.12. We quantify the relation using a least-squares fit, running 1000 Monte Carlo realisations considering the errors in both dimensions. The dynamical mass-to-light dependence on ETG dynamical mass can be parameterised as

$$\log M/L_{\rm dyn} = (0.33 \pm 0.11) \times \log M_{\rm dyn} - (3.03 \pm 1.17), \tag{4.4}$$

The stellar mass-to-light dependence on ETG dynamical mass can be parameterised as

$$\log M/L_{\rm ssp} = (0.34 \pm 0.62) \times \log M_{\rm dyn} - (3.06 \pm 6.58). \tag{4.5}$$

The dependence of both stellar and dynamical mass-to-light ratios on ETG dynamical mass is shown in Figure 4.12.

We investigate the stellar population properties of galaxies along the thickness of the FP by measuring the scatter $\Delta\langle I_e \rangle$ from the best-fit FP. The stellar mass-to-light ratios

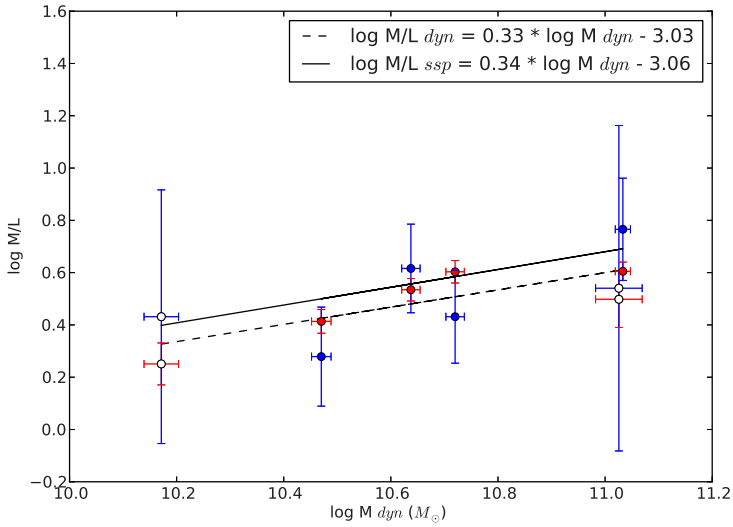

Figure 4.12: Dynamical (red points) and stellar (blue) mass-to-light variation with mass for high-redshift cluster ETGs. Open points correspond to ETGs in GHO 1322+3027, and closed points to ETGs in GHO 1322+3114.

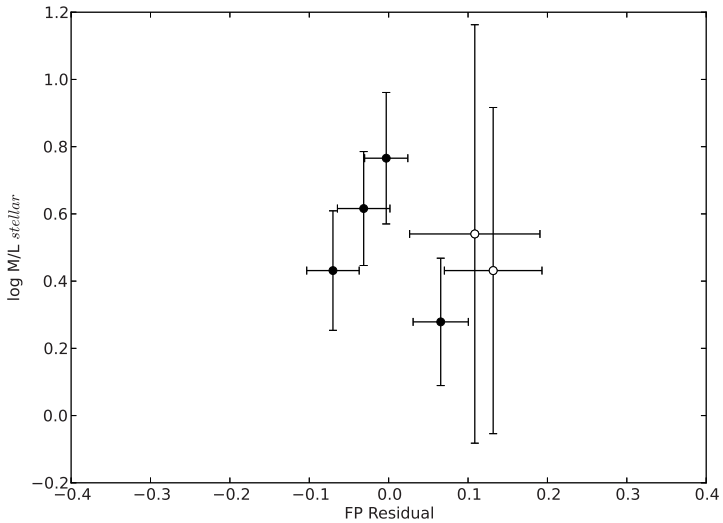

Figure 4.13: The stellar mass-to-light ratios of high-redshift cluster ETGs as a function of their residuals with respect to the Fundamental Plane in the rest-frame B-band. Open points correspond to ETGs from GHO 1322 +3027 galaxy cluster.

derived from stellar population models only weakly correlate with the FP scatter, but the trend is in the same sense as in the lower-redshift clusters (Figure 4.13; see Chapters 2 and 3). We quantify the relation using a least-squares fit, running 1000 Monte Carlo realisations considering the errors in both dimensions.

$$\log M/L_{\rm ssp} = (-0.51 \pm 2.07) \times FP_{\rm Residual} + (0.51 \pm 0.14). \quad (4.6)$$

4.7 Discussion

At a redshift of $z \sim 0.7$, we are observing galaxies in clusters ~ 6 billion years back in time, when the Universe was almost half of its present age. Under the hypothesis that ETGs are passively evolving systems and the assumption that clusters are coeval, ETGs in this cluster should then be ~ 6 billion years younger than ETGs in local Universe clusters like the Coma Cluster. However from our stellar population and dynamical study, we find that ETGs in GHO 1322+3027 and GHO 1322+3114 show dynamical and stellar population properties very similar to the lower-redshift clusters we studied in previous chapters. This result then cannot be explained from simple passive evolution of ETG stellar populations with look-back time. The FP of ETGs in this clusters shows significant scatter. However, unlike the lower-redshift clusters studied in previous chapters, we cannot conclusively argue that the residuals from the FP correlate with the stellar mass-to-light ratios, due to the errors involved in modelling the poor signal-to-noise spectral data. The existence of a mass-to-light–mass relation and its correspondence with stellar mass-to-light ratios shows that we are seeing downsizing trend in the core of these high-redshift clusters.

Further we found that ETGs in these clusters show similar dynamical and stellar population trends to those in Abell 550 at $z \sim 0.1$ (Chapter 2). We point out that the look back time between $z \sim 0.1$ and $z \sim 0.7$ is roughly 5 billion years. ETGs in both clusters show evidence for recent star formation and other similar dynamical correlations based on FP and stellar population studies. This shows that ETGs in these clusters are undergoing similar transformations in line with the cluster assembly process. Such a scenario is difficult to explain based on the hypothesis that ETGs forming at high redshifts and passively evolving to the current epoch.

4.8 Conclusions

We have presented a detailed structural and stellar population analysis for ETGs in two rich galaxy clusters at $z \sim 0.7$. The FP of ETGs in this cluster has an intrinsic scatter comparable to that of ETGs in the Coma Cluster. The stellar and dynamical mass-to-light ratios follow similar trends over the range of ETGs dynamical mass studied in this work.

Chapter 5

Dynamical and Stellar mass-to-light ratio evolution of cluster early-type galaxies from $z \sim 0.7$ to $z \sim 0$

Abstract

We present the dynamical and stellar mass-to-light ratio evolution of early-type galaxies (ETGs) in rich, massive galaxy clusters from $z \sim 0.7$ to $z \sim 0$. The motivation for this study is to check whether the cluster ETGs are passively evolving stellar systems with formation redshifts $z > 2$. We use spectroscopy and photometry to determine the dynamical mass-to-light ratios and estimate the stellar mass-to-light ratios from single stellar population (SSP) modelling. We find that the cluster ETGs within the range of redshifts studied here lack any significant evolution both from dynamical and stellar population analysis. This implies that the ETGs studied here have had complex star formation histories and supports the idea of stellar mass build-up of early-type galaxies over the last 7 Gyrs in galaxy clusters. The classic picture of ETGs as "red and dead" galaxies needs revision in the context of results presented here.

5.1 Introduction

Early-type galaxies (ETGs) in the local universe have long been thought to be old, passively-evolving stellar systems that formed the majority of their mass at high redshifts. This picture has been challenged by stellar population studies of ETGs in the local Universe and photometric surveys from $z \sim 0$ to 1. There is now clear evidence that the stellar mass in ETGs has doubled during the last eight billion years (Bell et al. 2004; Faber et al. 2007). This naturally means ETGs should increase their stellar mass either by merging, accretion or in-situ star formation. All of these processes are

environment and time dependent, the details of which are not yet properly understood.

Galaxy clusters are massive bound structures hypothesised to be formed from the initial density perturbations in the early Universe. The peak of these perturbations collapse to form galaxy clusters and the tiny fluctuations within them form galaxies. Galaxy clusters are observed to be dominated by ETGs which are thought to form at the epoch of cluster formation and finish forming stars by $z \sim 2$ (van Dokkum & Franx 1996; Kelson et al. 1997; van Dokkum et al. 1998). Thus ETGs in galaxy clusters since $z \sim 2$ should be passively-evolving stellar systems, with no signs of recent star formation.

On the other hand, the current paradigm of hierarchical structure formation in a Λ-Cold Dark Matter (ΛCDM) cosmology predicts that galaxy cluster assembly to be ongoing as late as $z \sim 0.4$ (Kauffmann 1995). This implies individual galaxies and galaxy groups should be falling into a common potential well, even at these relatively low redshifts. These galaxies could undergo rapid morphological transformations once they enter the hostile cluster environment. Observationally, many intermediate-redshift galaxy clusters are not relaxed and in fact exhibit on-going mergers (Hsu et al. 2013; Bradač et al. 2008). The end result of this cluster assembly process is a rapid evolution in the morphology and stellar populations of cluster galaxies. The increase of blue galaxies in cluster cores at $z \sim 0.5$ in comparison with local Universe clusters, manifested as the Butcher-Oemler effect, lends further support to this paradigm (Butcher & Oemler 1978a,b).

However, studies of the Fundamental Plane (FP) of ETGs in dense galaxy clusters, like the Coma Cluster, in the local Universe (Jorgensen et al. 1996) and in comparison with clusters at high redshifts demonstrate that ETGs (particularly the massive ones) in galaxy clusters are passively-evolving stellar systems with a formation redshift of $z > 2$ (van Dokkum & Franx 1996; Kelson et al. 1997; van Dokkum et al. 1998). This was further probed up to $z \sim 1.2$ by van Dokkum & Stanford (2003), who showed that the mass-to-light ratios of cluster ETGs are compatible with passive evolution. The mass-to-light ratio evolution in these studies relied on measuring the changing zero-point offsets of the FP at different redshifts with respect to the FP of ETGs in the Coma cluster. These studies showed that ETGs, particularly those in dense galaxy cluster cores, have a high formation redshift and are passively evolving as "red and dead" galaxies to the current epoch. However all these studies were made with the rather extreme assumption that all clusters follow the same evolutionary path in time. We do not know the nature of the underlying stellar populations for these cluster ETGs and their evolution, due to the lack of high signal-to-noise spectral data. Thus we need both dynamical and stellar population mass-to-light at different redshift bins from $z \sim 1$ to understand the formation, evolution, and stellar mass build up of cluster ETGs.

We have carried out a detailed dynamical and stellar population study of cluster ETGs at $z \sim 0.1$–0.7 to understand their stellar mass assembly history (Chapters 2–4). The clusters are similar to the Coma cluster in terms of the richness and mass. Imaging and multi-slit spectral data of galaxies observed with telescopes from space (WFPC2/ACS/HST) and ground (VIMOS/VLT, LRIS/Keck) have been reduced and analysed. Our ultimate goal for these data is to measure dynamical and stellar mass to

Cluster	z	N_{ETGs}
Abell 1656	0.02	12
Abell 550	0.10	15
Abell 851	0.40	12
GHO 1322+3114	0.69	4
GHO 1322+3027	0.75	2

Table 5.1: Details of cluster ETGs studied in this work.

light ratios from structural parameters and line strengths. Our spectral data are of high quality (S/N > 50) and the imaging data is from HST, except for the lowest-redshift cluster, for which VLT/VIMOS imaging data taken under good seeing conditions are used. The FP is constructed for all the clusters studied here, and we use this to determine the dynamical mass-to-light ratios of the individual galaxies. We determine single stellar population (SSP) ages and metallicities using the measured line strengths with the aid of stellar population models and then transform these to stellar mass-to-light ratios. We then study the evolution of these (stellar and dynamical) mass-to-light ratios.

Our study is based on massive ETGs ($M > 10^{10.3}\,M_{\odot}$) belonging to five rich, optically-selected clusters in four redshift bins. The ETGs are selected based on their early-type morphology or colour and are situated at the cluster core or very close to the core. Our photometry is in the Vega magnitude system and all magnitudes and mass-to-light ratios are transformed to the R_c filter pass band. The velocity dispersions of ETGs in all clusters are corrected to a uniform aperture sizes following the prescription in Jorgensen et al. (1995).

This chapter is organised as follows: the evolution of dynamical mass-to-light ratios of the cluster ETGs is examined in section 2 and the evolution of stellar population parameters and stellar mass-to-light ratios is examined in section 3. This is followed by a discussion in Section 4 and a future outlook in section 5.

Table 5.1 shows the redshifts and the number of galaxies used in the clusters studied in this chapter. In the following, we adopt a flat Universe cosmology with $H_o = 71\,\mathrm{km\,s^{-1}\,Mpc^{-1}}$, $\Omega_M = 0.27$, $\Omega_\Lambda = 0.73$ (Komatsu et al. 2011).

5.2 Dynamical mass-to-light ratio evolution of cluster ETGs

In this section we examine dynamical mass-to-light ratios of ETGs from the four clusters studied in previous chapters and ETGs from the Coma Cluster (Trager et al. 2008). We are interested in studying the evolution of mass-to-light ratios of ETGs in these clusters. The offsets in the FP of cluster ETGs can be expressed as the offsets in mass-to-light ratios. Figures 5.1 and 5.2 demonstrate the offsets of cluster ETGs studied in this work. The offset in mass-to-light ratios of cluster ETGs should increase with look-back time, provided the ETGs and the galaxy clusters are coeval and formed uniformly at one epoch. The FP zero-point offset with respect to a local Universe reference like the Coma

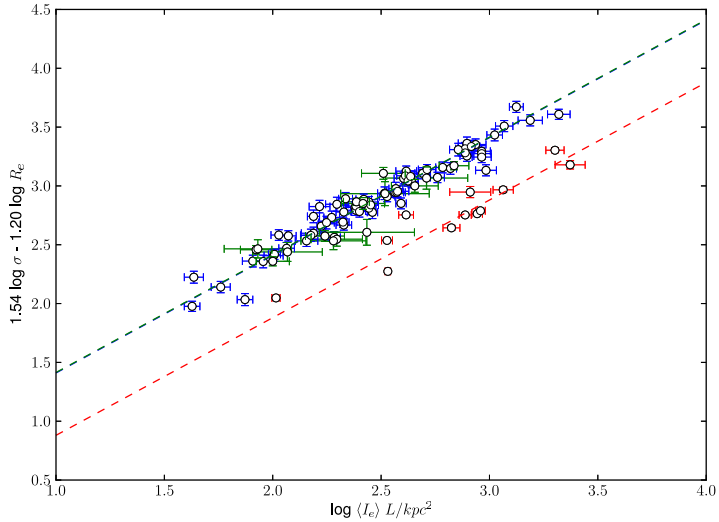

Figure 5.1: The R_c-band FP of ETGs in the Coma ($z \sim 0.02$, blue points), Abell 550 ($z \sim 0.1$, green points), and Abell 851 ($z \sim 0.4$, red points) clusters. The best-fit edge-on projections of the planes are shown as dashed lines of the appropriate colour. Note the offset of the FP projection for different clusters.

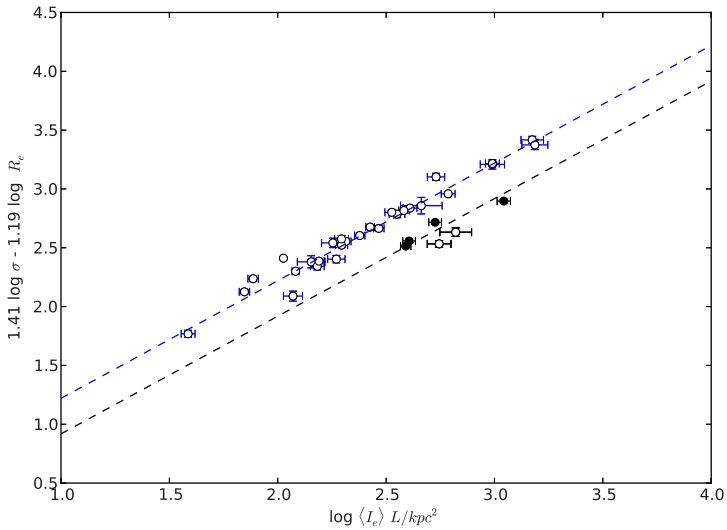

Figure 5.2: The B-band FP of ETGs in the Coma ($z \sim 0.02$, blue points), GHO 1322+3027 ($z \sim 0.75$, open points) and GHO 1322+3114 ($z \sim 0.7$, closed points) clusters. The best-fit edge-on projections of the planes are shown as dashed lines of the appropriate colour. Note the offset of the FP projection for different clusters.

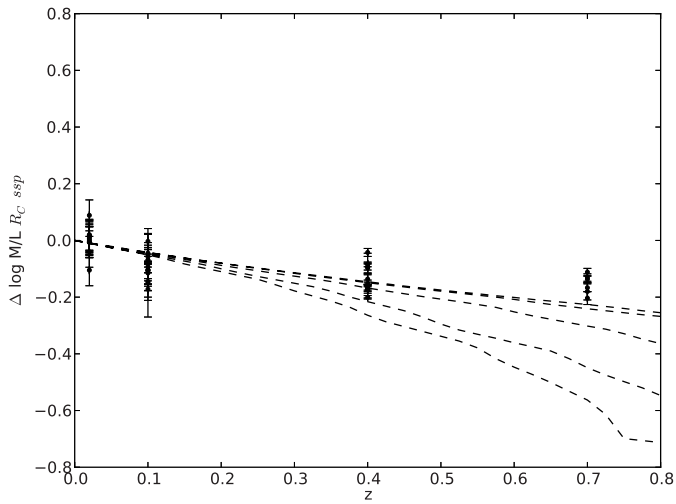

Figure 5.3: The evolution of dynamical mass-to-light ratios in ETGs in the Coma ($z \sim 0.02$), Abell 550 ($z \sim 0.1$), Abell 851 ($z \sim 0.4$), and GHO 1322+3027 and GHO 1322+3114 ($z \sim 0.7$) clusters. Points correspond to individual cluster ETGs. The evolution of the mass-to-light ratios of single stellar populations with various formation redshifts with respect to $z = 0$ is shown with dashed lines: from the bottom to the top, formation redshifts of $z_f = 1$, 1.25, 2, 4, 6.

Cluster can then be used to study the relative change in dynamical mass-to-light ratios and the corresponding evolution with time (Treu et al. 2005). However if ETGs are not formed at one epoch and the galaxy clusters are still assembling over the range of look back time, this will not be the case, as *change* in the mass-to-light ratio will depend on the mass-to-light ratios of the local Universe reference. To be precise, if (say) the Coma Cluster galaxies are the same (average) age as the higher-redshift cluster galaxies, the differential evolution will be weaker than expected. Following previous works (van Dokkum & Franx 1996; Kelson et al. 1997; van Dokkum et al. 1998; van Dokkum & Stanford 2003) we adopt Coma as the local Universe reference point for studying the mass-to-light evolution of cluster ETGs. However, we caution the reader that stellar populations of the Coma Cluster ETGs used here *are* in fact young, with an average SSP-equivalent age of ~ 5 Gyr (Trager et al. 2008).

We relate the offset of a galaxy from the FP to an offset in its mass-to-light ratios following Treu et al. (2005):

$$\Delta \log M/L = -\Delta\gamma/2.5, \tag{5.1}$$

where γ is the FP zero point and the offset of cluster ETGs FP with respect to Coma cluster is $\Delta\gamma = \gamma_{\rm coma} - \gamma_{\rm cluster}$. The evolution of $\Delta \log M/L$ is demonstrated in Figure 5.3. We compare these with the evolution of single-burst, single-metallicity stellar

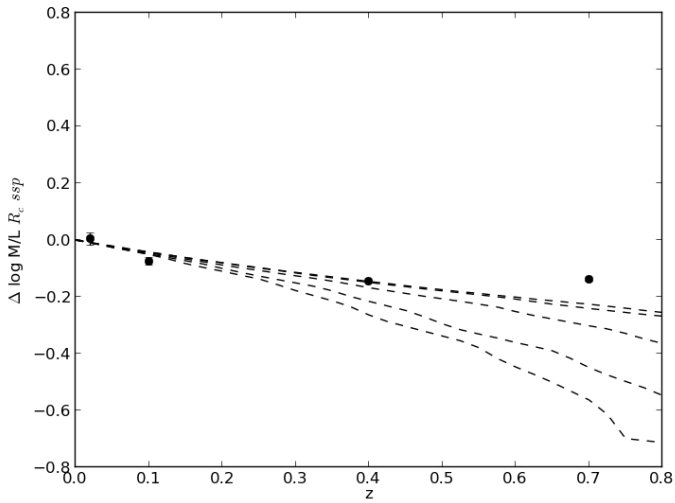

Figure 5.4: The evolution of dynamical mass-to-light ratios of ETGs in the Coma, Abell 550, Abell 851, GHO 1322+3027 and GHO 1322+3114 clusters. Points are the average of galaxies with dynamical masses $M > 10^{10.3}\,M_{\odot}$. The evolution of the mass-to-light ratios of single stellar populations with various formation redshifts with respect to $z = 0$ is shown with dashed lines: from the bottom to the top, formation redshifts of $z_f = 1$, 1.25, 2, 4, 6.

populations with formation redshifts of $z = 1$–6, computed from Bruzual & Charlot (2003, hereafter BC03) models with solar metallicity, Chabrier IMF, Padova isochrones (Bertelli et al. 1994), and stellar fluxes corresponding to Kurucz atmosphere models. We then computed the evolution of the cluster-averaged mass-to-light ratios of ETGs with dynamical masses $M > 10^{10.3}\,M_{\odot}$, as shown in Figure 5.4. There is no evolution between $z \sim 0.7$ and 0.4, but considerable evolution between $z \sim 0.4$ and 0.02. The cluster ETGs clearly do not follow the expectation from SSP models. This is surprising since dynamical mass-to-light ratios of ETGs are very dependent on their constituent stellar populations (see, e.g., Cappellari et al. 2006; Graves et al. 2009; Graves & Faber 2010). We therefore need to analyse the stellar population properties in order to determine the stellar mass-to-light ratios of these ETGs and to understand whether they follow the same trend as dynamical mass-to-light ratios.

5.3 Stellar population parameter evolution of cluster ETGs

We next examine the evolutionary trends of SSP-equivalent parameters of the cluster ETGs, to understand the apparent lack of evolution of their FP-inferred dynamical mass-to-light ratios. We infer SSP-equivalent parameters age (t_{SSP}), metallicity

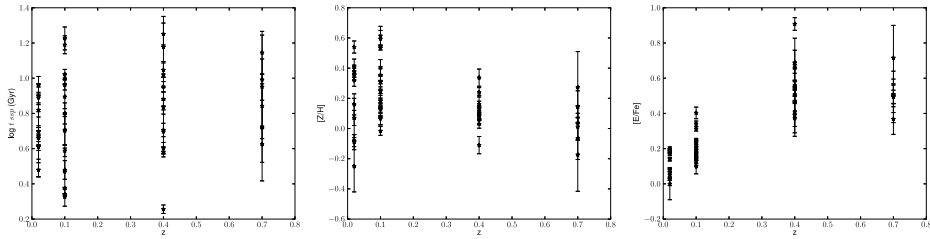

Figure 5.5: The evolution of SSP-equivalent age, metallicity, and α-element enhancement in ETGs in the Coma, Abell 550, Abell 851, GHO 1322+3027 and GHO 1322+3114 clusters. Small points correspond to individual cluster ETGs. Note the lack of evolution in the typical SSP-equivalent age of the cluster galaxies, while a mild evolution in metallicity and a strong evolution in α-element enhancement are apparent.

([Z/H]), and α-element enhancement ratio ([E/Fe]) using the BC03 models with Padova isochrones (Bertelli et al. 1994) and a Chabrier IMF, following the prescriptions and methodology described in detail in Trager et al. (2008, see Chapters 2–4).

Figure 5.5 shows the results of this analysis. We find that the SSP age (t_{SSP}) is fairly uniform for ETGs in all these five clusters. However the metallicity of ETGs decreases and the α-element enhancement increases as one goes to higher redshift.

We then use the SSP-equivalent stellar population parameters described above to infer the stellar mass-to-light ratios in the R_c-band (M/L_{R_c}) with the aid of the BC03 models. However we have used a combination of different indices to derive the stellar mass-to-light ratios, which can create systematic biases as shown in Chapters 3 and 4. We therefore need to bring the stellar mass-to-light ratios to a common system before performing a quantitative comparison. We adopted the line strengths we used for Abell 550 cluster ETGs as the reference system and converted other ETGs stellar mass-to-light using the transformation we computed from ETGs in Coma cluster data (Trager et al. 2008). The transformations are summarised below:

$$\log M/L_{\mathrm{R_c(Abell851)(SSP)}} = \log M/L_{\mathrm{R_c(Abell550)(SSP)}} + (0.04 \pm 0.01) \quad (5.2)$$

$$\log M/L_{\mathrm{R_c(GHO3122+3027)(SSP)}} = \log M/L_{\mathrm{R_c(Abell550)(SSP)}} + (0.02 \pm 0.02) \quad (5.3)$$

$$\log M/L_{\mathrm{R_c(GHO3122+3114)(SSP)}} = \log M/L_{\mathrm{R_c(Abell550)(SSP)}} + (0.04 \pm 0.01) \quad (5.4)$$

We then compared the stellar mass-to-light ratios of our cluster ETGs with those of Coma Cluster ETGs from Trager et al. (2008), and calculated the evolution of stellar mass-to-light ratios for ETGs in different clusters taking the Coma Cluster as a reference point. Figures 5.6 shows the individual ETGs and 5.7 show the average evolution of stellar mass-light ratio of cluster ETGs with $M > 10^{10.3}\,M_{\odot}$. It is clear from these figures that, as with the dynamical mass-to-light ratios, the stellar mass-to-light ratios of cluster ETGs clearly do not follow the expectation from SSP models. We address the possible reasons for these results in the next section.

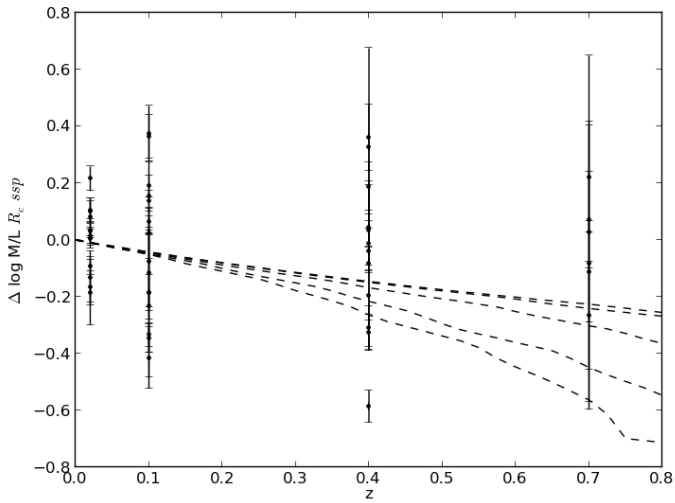

Figure 5.6: The evolution of stellar mass-to-light ratios in ETGs in the Coma, Abell 550, Abell 851, GHO 1322+3027 and GHO 1322+3114 clusters. Points correspond to individual cluster ETGs. The evolution of the change in mass-to-light ratio of single stellar population with various formation redshifts with respect to $z = 0$ is shown with dashed lines: from the bottom to the top, formation redshifts of $z_f = 1$, 1.25, 2, 4, 6.

5.4 Discussion

We have studied the mass-to-light ratios and stellar populations of ETGs in four rich galaxy clusters from ~ 0.7, a look-back time of ~ 7 Gyr, until the current epoch. This time span is large enough for considerable stellar population evolutionary effects appear if ETGs are purely passively evolving stellar systems. Previous studies based on the dynamical mass-to-light ratios of ETGs have claimed considerable evolution in the time interval probed in this work (van Dokkum & Stanford 2003). However, as demonstrated in Figure 5.4 there is no evolution in dynamical mass-to-light ratios between the extreme look back times ($z = 0.7$ and $z = 0.4$) in our study. The implication of this result is that complex processes need to be invoked in these stellar systems to preserve the same dynamical mass-to-light ratios at two different epochs separated by 3 Gyrs.

We have therefore examined the stellar population properties of the cluster ETGs in an effort to determine if such processes are driven by (a lack of) stellar population evolution. We found that the cluster ETGs show a range of SSP ages, with some galaxies having very recent star formation, *at all epochs*. The mean SSP ages of ETGs in clusters studied here are fairly constant within the errors. This is possible only if the ETGs had suffered from star formation events within the last 2 Gyrs at each epoch. The average metallicity of the ETGs decrease as we go to higher redshifts, but the average α-element enhancement ratios increase with higher redshifts, suggesting

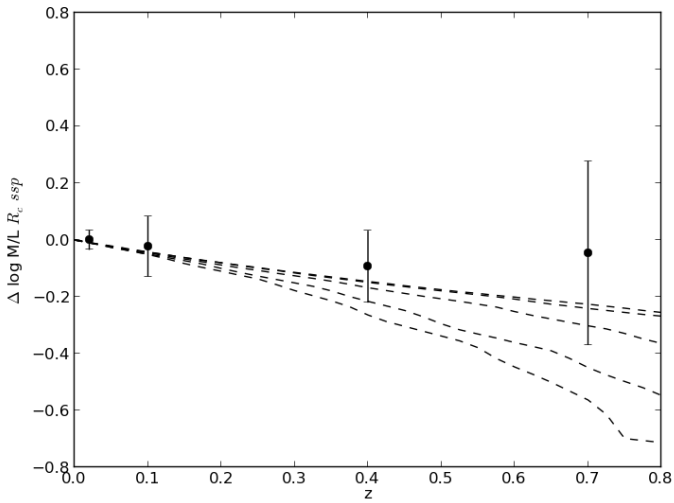

Figure 5.7: The evolution of stellar mass-to-light ratios in ETGs in the Coma, Abell 550, Abell 851, GHO 1322+3027 and GHO 1322+3114 clusters. Points correspond to the average of galaxies with dynamical masses $> 10^{10.3}\,M_{\odot}$. The evolution of the change in mass-to-light ratio of single stellar population with various formation redshifts with respect to $z = 0$ is shown with dashed lines: from the bottom to the top, formation redshifts of $z_f = 1$, 1.25, 2, 4, 6.

on-going build-up of chemical elements from recently-terminated star formation in the clusters at each epoch. It may be that the derived stellar population parameters are dependent on the aperture size used to observe the galaxies, given the fact that for a given aperture size the effective area covered on the galaxy rest frame increases with increasing redshift. However, we note that the age and metallicity sensitive indices and the derived SSP-equivalent ages and metallicity have negative gradients (such that galaxies get older and more metal-poor as a function of radius), whereas the α-element enhancement ratio stays constant for ETGs in the local Universe (Trager et al. 2000a). We found that our ages and α-element enhancement ratios show a different trend, which we suggest is due to recent star formation episodes in these cluster ETGs. We therefore argue that the stellar populations of these cluster ETGs are complex, with recent star formation at all epochs.

The stellar mass-to-light ratio evolution of cluster ETGs is found to be fairly constant. However one should keep in mind that the stellar mass-to-light ratios are single stellar population (SSP) equivalents. This is a very simple approximation of the true underlying population—and as we suggest above, likely to be unreasonable—hence these will differ from the dynamical mass-to-light ratios. SSP-equivalent stellar mass-to-light ratios are very sensitive to the temperature of the main-sequence turn-off of the stellar systems under study. This means that stellar mass-to-light ratios are more affected by

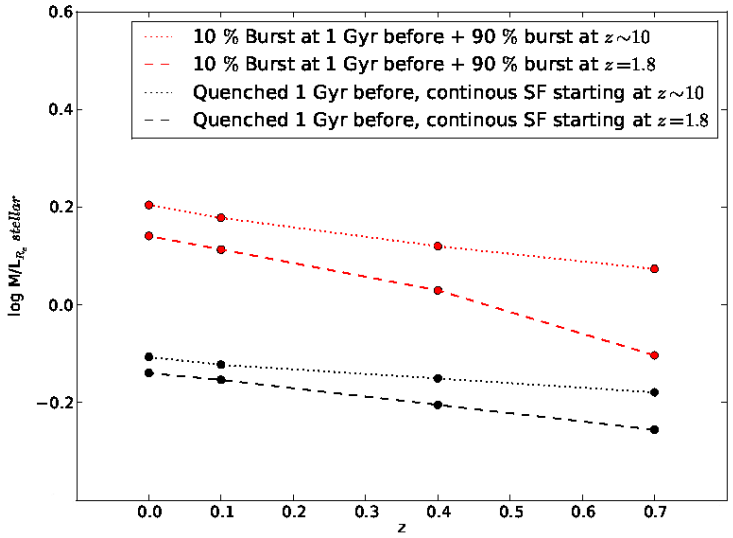

Figure 5.8: The evolution of stellar mass-to-light ratios for complex star formation scenarios.

recent star formation than dynamical mass-to-light ratios (Trager et al. 2008). Given the fact that our average stellar mass-to-light ratios are constant for all the cluster ETGs, we again suggest that we are witnessing the aftermath of recent star formation events in all these clusters.

Both the dynamical and stellar mass-to-light ratios for cluster ETGs do not follow the $\Delta \log M/L$ evolution computed for single stellar populations with different formation redshifts. The cluster-average mass-to-light ratios at $z \sim 0.4$ and 0.7 are well above the expectations of SSPs with formation redshifts of $z \sim 2$. Given our arguments above, we suggest that this is due to recent star formation in ETGs in all of the clusters that we have studied, *including the local Universe reference,* the Coma Cluster. Detailed composite stellar population synthesis analysis techniques are required to completely disentangle the underlying complexity of the stellar population. We therefore modelled the complex star formation histories in galaxies considering two scenarios: a small burst of recent star formation on top of a massive old population and rapid truncation (quenching) of (previously) constant star formation, both happening 1 Gyr before the epoch of observation. Figure 5.8 demonstrates the behaviour of mass-to-light ratios in these two scenarios. We modelled the M/L_{R_c} evolution using Bruzual & Charlot (2003, BC03) models with Padova 1994 isochrones (Bertelli et al. 1994) and a Chabrier IMF for solar metallicity and solar abundance ratios (see Trager et al. 2008, for more details on the models). For each scenario, we considered two cases for the initial star formation burst: either the initial burst happens at or the initiation of star formation begins at $z \sim 10$ (chosen to make the oldest stars nearly as old as the Universe), or at $z = 1.8$ (chosen to make the oldest star have an age of 10 Gyr if observed at $z = 0$). In the two-

burst case, the initial population is assumed to have 90% of the mass, and the recent burst to have 10% of the mass. It is clear from Figure 5.8 that both cases have a *much* flatter evolution in $\Delta \log M/L_{R_c}$ than the single-burst case shown in previous figures, especially the cases of very-high-redshift ($z \sim 10$) star formation followed by recent star formation or continuous star formation beginning at very-high-redshift followed by recent quenching. In fact, the latter case has the shallowest slope of all of the simplified complex star formation models, similar to the observed clusters, but the resulting M/L_{R_c} ratios are particularly low, due to the very recent star formation in these models suppressing the mass-to-light ratios (cf. Trager et al. 2008). In any case, the trends in these composite stellar population models match our observations better than the passively-evolving models shown in previous figures, suggesting that our idea that these cluster ETGs have had complex star formation histories has some merit.

One of the possible caveat in our analysis is the dependence of α-element enhancement ratios on the dynamical and stellar mass-to-light ratios. Super-solar α-element enhancement ratios can change the stellar population colours, making them redder and therefore decreasing the mass-to-light ratios in redder passbands, like the R_c-band used here (Pietrinferni et al. 2006). However as shown in Figures 5.4 and 5.7, the stellar population models we computed are for solar values of [α/Fe]. This may be part of the reason why the relative evolution of both the dynamical and stellar mass-to-light ratios of the ETGs is considerably offset from the expectations of the models of SSP evolution.

Summarising, we find that the cluster ETGs above a dynamical mass of $M > 10^{10.3}\,M_\odot$ over the range of redshifts studied here have complex star formation histories. This is supported by the evolution of their dynamical and stellar mass-to-light ratios and their stellar populations. The reason for these recent star formation episodes can be qualitatively explained due to morphological and stellar population transformations arising from the ongoing assembly of galaxy clusters as late as $z \sim 0$. The virialisation time for massive galaxy clusters within a virial radius of 1 Mpc is ~ 1 Gyr, and the cluster crossing time of galaxies inside such a cluster is ~ 1 Gyr. The key time period within which recent star formation, more specifically the temperature of main-sequence turn-off, can alter the apparent age of the stellar population is also ~ 1 Gyr. Thus recently-virialised clusters will have galaxies which take one billion year to complete one cluster crossing, which may then show the effects of the last intense star bursts due to their interaction with the hostile cluster environment. This implies many galaxies in a relaxed cluster core might actually be on their first cluster crossing phase. These galaxies will have the atomic gas stripped and at the same time may retain cold, molecular gas in their centres, even near to cluster cores, which can form stars due to instabilities in the discs formed out of molecular gas (CO) or due to tidal interactions with in the cluster potential.

The question remains how others (e.g., van Dokkum & Stanford 2003) see a trend of passive evolution for cluster ETGs over the same epochs we have studied. This could largely be due to the properties of the clusters they probed. Our clusters are of similar richness and mass but are known to be dynamically young. This "youth" may explain the recent star formation in the cluster ETGs. The building of galaxy clusters in the

hierarchical formation scenario is a complex process. Galaxies in the field are typically found in groups, within which galaxies can undergo interactions due to low velocity dispersion of groups (150–250 $\mathrm{km\,s^{-1}}$). Giant ellipticals from the field can survive the interactions within the group and may even undergo minor gas-rich mergers, whereas late-type galaxies are likely transformed into S0's or even merge to form ellipticals. Galaxy groups, within which galaxies undergoing morphological and stellar population transformations merge to form Galaxy cluster over time. This point towards a scenario in which galaxy groups are responsible for the stellar population evolution of ETGs, which we observe in cluster ETGs as recent star formation (Tran et al. 2005; Kautsch et al. 2008; Mahajan 2013). Thus the recent star formation events we observe in cluster ETGs in this work over the past 7 Gyrs may be a natural consequence of the hierarchical processes in which field galaxies cluster in groups, which later merge with massive galaxy clusters.

In short the cluster ETGs studied here appear to have complex star formation histories and support the idea of the stellar mass build-up of early-type galaxies over the last 7 Gyrs. The classic picture of ETG formation and evolution as "red and dead" galaxies needs revision in the context of the results presented in this thesis.

5.5 Future Outlook

The results presented in this thesis are based on combined dynamical and stellar population studies of ETGs in galaxy clusters over a range of look-back times. The study lacks statistical significance as we are limited by one or two clusters per redshift bin, with smaller and smaller galaxy samples per cluster as the redshifts increase. This study should be extended to more clusters and more galaxies per cluster, particularly at intermediate redshifts where galaxy clusters are in their last stages of assembly process in a ΛCDM universe.

A survey of early-type galaxies in intermediate redshift clusters will help to understand the role of hierarchical build-up in cluster formation. The stellar population properties can be derived from multi-object spectroscopy or integral-field spectral data now obtainable from 8m class telescopes. Furthermore the availability of gas reservoirs in galaxies for star formation in such dense environments at intermediate redshift can be studied using existing/upcoming radio (APERTIF) and sub-mm (ALMA) facilities. Such a survey will be unique as it aims to understand the detailed stellar population properties of a large sample of ETGs in dense environments, giving an insight into the formation and evolution of ETGs, and then using them to understand the assembly history of clusters hosting them.

Bibliography

Baldry, I. K., Glazebrook, K., Brinkmann, J., Ivezić, Ž., Lupton, R. H., Nichol, R. C., & Szalay, A. S. 2004, ApJ, 600, 681

Bell, E. F., Wolf, C., Meisenheimer, K., Rix, H.-W., Borch, A., Dye, S., Kleinheinrich, M., Wisotzki, L., & McIntosh, D. H. 2004, ApJ, 608, 752

Bender, R., Burstein, D., & Faber, S. M. 1992, ApJ, 399, 462

Bertelli, G., Bressan, A., Chiosi, C., Fagotto, F., & Nasi, E. 1994, A&AS, 106, 275

Binney, J. 1977, ApJ, 215, 483

Blanton, M. R. & Roweis, S. 2007, AJ, 133, 734

Blumenthal, G. R., Faber, S. M., Primack, J. R., & Rees, M. J. 1984, Nature, 311, 517

Bolton, A. S., Burles, S., Treu, T., Koopmans, L. V. E., & Moustakas, L. A. 2007, ApJ, 665, L105

Bower, R. G., Lucey, J. R., & Ellis, R. S. 1992, MNRAS, 254, 601

Bradač, M., Allen, S. W., Treu, T., Ebeling, H., Massey, R., Morris, R. G., von der Linden, A., & Applegate, D. 2008, ApJ, 687, 959

Bruzual, G. & Charlot, S. 2003, MNRAS, 344, 1000

Burstein, D., Bender, R., Faber, S., & Nolthenius, R. 1997, AJ, 114, 1365

Burstein, D., Faber, S. M., Gaskell, C. M., & Krumm, N. 1984, ApJ, 287, 586

Butcher, H. & Oemler, Jr., A. 1978a, ApJ, 219, 18

—. 1978b, ApJ, 226, 559

Cappellari, M., Bacon, R., Bureau, M., Damen, M. C., Davies, R. L., de Zeeuw, P. T., Emsellem, E., Falcón-Barroso, J., Krajnović, D., Kuntschner, H., McDermid, R. M., Peletier, R. F., Sarzi, M., van den Bosch, R. C. E., & van de Ven, G. 2006, MNRAS, 366, 1126

Castander, F. J., Ellis, R. S., Frenk, C. S., Dressler, A., & Gunn, J. E. 1994, ApJ, 424, L79

Ciotti, L., Lanzoni, B., & Renzini, A. 1996, MNRAS, 282, 1

Conroy, C. & van Dokkum, P. 2012, ApJ, 747, 69

Djorgovski, S. & Davis, M. 1987, ApJ, 313, 59

Dressler, A. 1980, ApJ, 236, 351

Dressler, A. & Gunn, J. E. 1990, in Astronomical Society of the Pacific Conference Series, Vol. 10, Evolution of the Universe of Galaxies, ed. R. G. Kron, 200–208

Dressler, A. & Gunn, J. E. 1992, ApJS, 78, 1

Dressler, A., Lynden-Bell, D., Burstein, D., Davies, R. L., Faber, S. M., Terlevich, R., & Wegner, G. 1987, ApJ, 313, 42

Dressler, A., Oemler, Jr., A., Couch, W. J., Smail, I., Ellis, R. S., Barger, A., Butcher, H., Poggianti, B. M., & Sharples, R. M. 1997, ApJ, 490, 577

Dressler, A., Oemler, Jr., A., Sparks, W. B., & Lucas, R. A. 1994, ApJ, 435, L23

Dressler, A., Rigby, J., Oemler, Jr., A., Fritz, J., Poggianti, B. M., Rieke, G., & Bai, L. 2009, ApJ, 693, 140

Faber, S. M. 1973a, ApJ, 179, 731

—. 1973b, ApJ, 179, 731

Faber, S. M., Dressler, A., Davies, R. L., Burstein, D., & Lynden-Bell, D. 1987, in Nearly Normal Galaxies. From the Planck Time to the Present, ed. S. M. Faber, 175–183

Faber, S. M., Willmer, C. N. A., Wolf, C., Koo, D. C., Weiner, B. J., Newman, J. A., Im, M., Coil, A. L., Conroy, C., Cooper, M. C., Davis, M., Finkbeiner, D. P., Gerke, B. F., Gebhardt, K., Groth, E. J., Guhathakurta, P., Harker, J., Kaiser, N., Kassin, S., Kleinheinrich, M., Konidaris, N. P., Kron, R. G., Lin, L., Luppino, G., Madgwick, D. S., Meisenheimer, K., Noeske, K. G., Phillips, A. C., Sarajedini, V. L., Schiavon, R. P., Simard, L., Szalay, A. S., Vogt, N. P., & Yan, R. 2007, ApJ, 665, 265

Gebhardt, K., Faber, S. M., Koo, D. C., Im, M., Simard, L., Illingworth, G. D., Phillips, A. C., Sarajedini, V. L., Vogt, N. P., Weiner, B., & Willmer, C. N. A. 2003, ApJ, 597, 239

Giovannini, G., Bonafede, A., Feretti, L., Govoni, F., Murgia, M., Ferrari, F., & Monti, G. 2009, A&A, 507, 1257

Graves, G. J. & Faber, S. M. 2010, ApJ, 717, 803

Graves, G. J., Faber, S. M., & Schiavon, R. P. 2009, ApJ, 698, 1590

Gunn, J. E., Hoessel, J. G., & Oke, J. B. 1986, ApJ, 306, 30

Holden, B. P., van der Wel, A., Kelson, D. D., Franx, M., & Illingworth, G. D. 2010, ApJ, 724, 714

Hsu, L.-Y., Ebeling, H., & Richard, J. 2013, MNRAS, 429, 833

Jorgensen, I., Franx, M., & Kjaergaard, P. 1995, MNRAS, 276, 1341

—. 1996, MNRAS, 280, 167

Kauffmann, G. 1995, MNRAS, 274, 153

Kautsch, S. J., Gonzalez, A. H., Soto, C. A., Tran, K.-V. H., Zaritsky, D., & Moustakas, J. 2008, ApJ, 688, L5

Kaviraj, S. 2010, MNRAS, 408, 170

Kelson, D. D. 2003, PASP, 115, 688

Kelson, D. D., Illingworth, G. D., Franx, M., & van Dokkum, P. G. 2006, ApJ, 653, 159

Kelson, D. D., van Dokkum, P. G., Franx, M., Illingworth, G. D., & Fabricant, D. 1997,

ApJ, 478, L13

Kodama, T., Smail, I., Nakata, F., Okamura, S., & Bower, R. G. 2001, ApJ, 562, L9

Koleva, M., Prugniel, P., Bouchard, A., & Wu, Y. 2009, A&A, 501, 1269

Komatsu, E., Smith, K. M., Dunkley, J., Bennett, C. L., Gold, B., Hinshaw, G., Jarosik, N., Larson, D., Nolta, M. R., Page, L., Spergel, D. N., Halpern, M., Hill, R. S., Kogut, A., Limon, M., Meyer, S. S., Odegard, N., Tucker, G. S., Weiland, J. L., Wollack, E., & Wright, E. L. 2011, ApJS, 192, 18

Koyama, Y., Kodama, T., Nakata, F., Shimasaku, K., & Okamura, S. 2011, ApJ, 734, 66

Le Fèvre, O., Saisse, M., Mancini, D., Brau-Nogue, S., Caputi, O., Castinel, L., D'Odorico, S., Garilli, B., Kissler-Patig, M., Lucuix, C., Mancini, G., Pauget, A., Sciarretta, G., Scodeggio, M., Tresse, L., & Vettolani, G. 2003, in Society of Photo-Optical Instrumentation Engineers (SPIE) Conference Series, Vol. 4841, Society of Photo-Optical Instrumentation Engineers (SPIE) Conference Series, ed. M. Iye & A. F. M. Moorwood, 1670–1681

Mahajan, S. 2013, MNRAS

Maraston, C. & Strömbäck, G. 2011, MNRAS, 418, 2785

Monachesi, A., Trager, S. C., Lauer, T. R., Hidalgo, S. L., Freedman, W., Dressler, A., Grillmair, C., & Mighell, K. J. 2012, ApJ, 745, 97

O'Connell, R. W. 1986, in Stellar Populations, ed. C. A. Norman, A. Renzini, & M. Tosi, 167–189

Oemler, Jr., A., Dressler, A., & Butcher, H. R. 1997, ApJ, 474, 561

Oemler, Jr., A., Dressler, A., Kelson, D., Rigby, J., Poggianti, B. M., Fritz, J., Morrison, G., & Smail, I. 2009, ApJ, 693, 152

Oke, J. B., Cohen, J. G., Carr, M., Cromer, J., Dingizian, A., Harris, F. H., Labrecque, S., Lucinio, R., Schaal, W., Epps, H., & Miller, J. 1995, PASP, 107, 375

Peng, C. Y., Ho, L. C., Impey, C. D., & Rix, H.-W. 2002, AJ, 124, 266

Pietrinferni, A., Cassisi, S., Salaris, M., & Castelli, F. 2006, ApJ, 642, 797

Pimbblet, K. A., Smail, I., Kodama, T., Couch, W. J., Edge, A. C., Zabludoff, A. I., & O'Hely, E. 2002, MNRAS, 331, 333

Renzini, A. 2006, ARA&A, 44, 141

Sandage, A. & Visvanathan, N. 1978, ApJ, 223, 707

Sarzi, M., Falcón-Barroso, J., Davies, R. L., Bacon, R., Bureau, M., Cappellari, M., de Zeeuw, P. T., Emsellem, E., Fathi, K., Krajnović, D., Kuntschner, H., McDermid, R. M., & Peletier, R. F. 2006, MNRAS, 366, 1151

Schindler, S., Belloni, P., Ikebe, Y., Hattori, M., Wambsganss, J., & Tanaka, Y. 1998, A&A, 338, 843

Schindler, S. & Wambsganss, J. 1996, A&A, 313, 113

Sersic, J. L. 1968, Atlas de galaxias australes

Thomas, D., Maraston, C., Bender, R., & Mendes de Oliveira, C. 2005, ApJ, 621, 673

Trager, S. C., Faber, S. M., & Dressler, A. 1996, in IAU Symposium, Vol. 171, New Light on Galaxy Evolution, ed. R. Bender & R. L. Davies, 455

Trager, S. C., Faber, S. M., & Dressler, A. 2008, MNRAS, 386, 715

Trager, S. C., Faber, S. M., Worthey, G., & González, J. J. 2000a, AJ, 120, 165

—. 2000b, AJ, 119, 1645

Trager, S. C. & Somerville, R. S. 2009, MNRAS, 395, 608

Trager, S. C., Worthey, G., Faber, S. M., Burstein, D., & Gonzalez, J. J. 1998, ApJS, 116, 1

Tran, K.-V. H., Moustakas, J., Gonzalez, A. H., Bai, L., Zaritsky, D., & Kautsch, S. J. 2008, ApJ, 683, L17

Tran, K.-V. H., van Dokkum, P., Illingworth, G. D., Kelson, D., Gonzalez, A., & Franx, M. 2005, ApJ, 619, 134

Treu, T., Ellis, R. S., Liao, T. X., van Dokkum, P. G., Tozzi, P., Coil, A., Newman, J., Cooper, M. C., & Davis, M. 2005, ApJ, 633, 174

Trujillo, I., Burkert, A., & Bell, E. F. 2004, ApJ, 600, L39

van der Wel, A., Franx, M., van Dokkum, P. G., Rix, H.-W., Illingworth, G. D., & Rosati, P. 2005, ApJ, 631, 145

van Dokkum, P. G. & Franx, M. 1996, MNRAS, 281, 985

van Dokkum, P. G., Franx, M., Kelson, D. D., & Illingworth, G. D. 1998, ApJ, 504, L17

van Dokkum, P. G. & Stanford, S. A. 2003, ApJ, 585, 78

Vazdekis, A., Ricciardelli, E., Cenarro, A. J., Rivero-González, J. G., Díaz-García, L. A., & Falcón-Barroso, J. 2012, MNRAS, 424, 157

Vazdekis, A., Sánchez-Blázquez, P., Falcón-Barroso, J., Cenarro, A. J., Beasley, M. A., Cardiel, N., Gorgas, J., & Peletier, R. F. 2010, MNRAS, 404, 1639

White, S. D. M. & Rees, M. J. 1978, MNRAS, 183, 341

Worthey, G. 1994, ApJS, 95, 107

Wuyts, S., van Dokkum, P. G., Kelson, D. D., Franx, M., & Illingworth, G. D. 2004, ApJ, 605, 677

Nederlandse Samenvatting

Traditioneel gezien worden sterrenstelsels geclassificeerd op basis van hun waargenomen morfologie als elliptisch, lensvorming of spiraalvormig sterrenstelsel. Edwin Hubble zette deze verschillende klassen van stelsels uit in het zogenaamde 'stemvorkdiagram' zoals afgebeeld in Figuur 1. Elliptische stelsels (E) bevinden zich aan de linkerkant van de stemvork, lensvormige stelsels (S0) precies in het midden en spiraal stelsels met balk (SB) en zonder balk (S) op de twee tanden van de vork. Het is tegenwoordig gebruikelijk om de stelsels aan de linkerkant van Figuur 1 vroeg-type te noemen (elliptische en lensvormige stelsels), en sterrenstelsels aan de rechterkant laat-type (spiralen). Vroeg-type sterrenstelsels worden gedomineerd door stellaire populaties met rode kleuren. Dit heeft astronomen doen veronderstellen dat deze stelsels hun formatie al afgerond hadden toen het Heelal nog niet eens de helft van haar huidige leeftijd had bereikt. Vroeg-type stelsels waren onderhevig aan een korte en intensieve periode van stervorming, waarna ze een passieve evolutie ondergingen tot aan hun huidige verschijning. Spiraalstelsels daarentegen worden juist gedomineerd door blauwe populaties van sterren. Deze sterren leveren een sterke bijdrage aan het uitgezonden licht en impliceren een continue vorming van nieuwe sterren. Dit schetst een plaatje waarin vroeg-type stelsels 'rode en dode' populaties van sterren bezitten.

Volgens het huidige paradigma van een Λ-Cold Dark Matter (ΛCDM) kosmologie bouwen structuren zich hiërarchisch op. Kleine klompen van donkere materie smelten samen en vormen op deze wijze grote halos van donkere materie. De baryonen binnen deze halos van donkere materie koelen dissipatief af en vormen stellaire systemen die we nu waarnemen als sterrenstelsels. Sterrenstelsels zijn dus het resultaat van een condensatie proces in het centrum van grote halos van donkere materie. De formatie en evolutie van vroeg-type stelsels is binnen dit paradigma ook hiërarchisch, waarbij botsingen, accretie en *lokale* stervorming allemaal een belangrijke rol spelen.

Een van de voornaamste problemen bij het bestuderen van de sterren in vroeg-type stelsels is dat deze stelsels te ver weg staan om hun individuele sterren waar te kunnen nemen (M32 – een compact elliptisch satelliet stelsel van de Andromeda nevel – is de uitzondering). Men moet daarom het geïntegreerde licht en de kleuren van deze stelsels bestuderen om de eigenschappen van de stellaire populaties te kunnen begrijpen. Zulke studies worden bemoeilijkt door de afhankelijkheid van zowel leeftijd als chemische

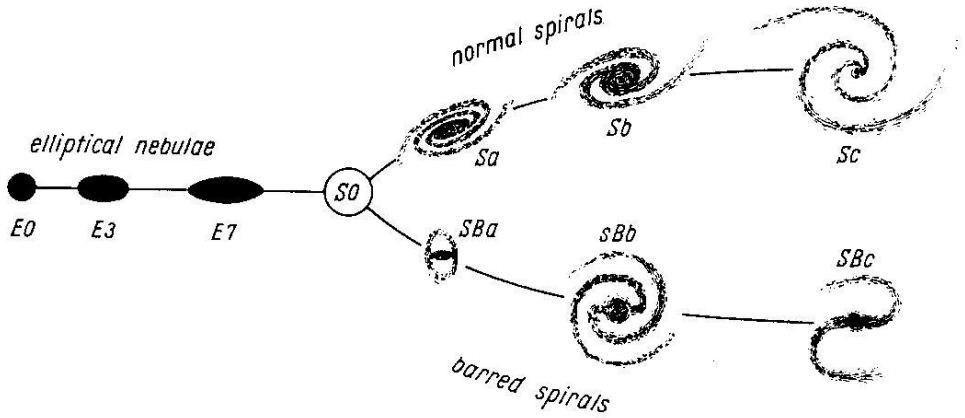

Figuur 1: Het stemvorkdiagram van Edwin Hubble. Sterrenstelsels aan de linkerkant van de vork (elliptische en lensvormige stelsels) worden vroeg-type sterrenstelsels genoemd. Stelsels aan de rechterkant (spiralen) worden laat-type stelsels genoemd. [Figuur: Hubble E.P., The Realm of the Nebulae (New Haven, 1936.)

compositie op eigenschappen van stellaire populaties: in oude populaties van sterren kunnen verandering in leeftijd *of* chemische compositie van een ster identieke verschillen in kleur opleveren. Kleuren kunnen derhalve niet worden gebruikt om recente periodes van sterformatie te bestuderen die langer dan 1–2 miljard jaar geleden plaats vonden. De rode kleur van een oud sterrenstelsel impliceert dus niet noodzakelijkerwijs dat dit stelsel *volledig* uit oude sterren bestaat. Zonder extra informatie weerhoudt het samenspel van leeftijd en chemische compositie ons er van om de sterformatie geschiedenis van een vroeg-type stelsel te bestuderen door middel van kleuren. De bijdrage van leeftijd en chemische compositie kan gelukkig geïsoleerd worden door een combinatie van absorptie lijnen in het spectrum van geïntegreerd licht waar te nemen die voornamelijk gevoelig zijn voor leeftijd *of* chemische compositie.

Waarnemingen hebben tevens laten zien dat vroeg-type stelsels een driedimensionale correlatie volgen die de 'Fundamental Plane' (FP) genoemd wordt. Deze correlatie geeft het verband weer tussen de snelheidsdispersie (σ), effectieve straal (R_e) en gemiddelde oppervlaktehelderheid ($\langle I_e \rangle$) van vroeg-type stelsels. De viriaalstelling leert ons dat vroeg-type stelsels allemaal op een plat vlak in deze driedimensionale ruimte zouden moeten liggen. Echter, men heeft gevonden dat de FP gekanteld is ten opzichte van dit verwachte vlak; we zullen later bespreken hoe deze kanteling samenhangt met de sterformatie in sterrenstelsels. De intrinsieke spreiding rondom de FP van vroeg-type stelsels in lokale clusters is $\sim$10–15%. De locatie van een stelsels op de FP wordt slechts licht beïnvloed door het samenspel van leeftijd en chemische compositie. De FP kan daarom goed gebruikt worden om de formatie en evolutie van vroeg-type stelsels beter te leren begrijpen. Het (σ, R_e, $\langle I_e \rangle$) coördinaat van een sterrenstelsel kan bijvoorbeeld direct in verband worden gebracht met de recente sterformatie van het stelsel. Onlangs gevormde sterren verhogen de helderheid van een stelsel – en derhalve ook de opper-

Figuur 2: Observatie van het lokale sterrenstelselcluster Abell 1656 (Coma). De waarneming is uitgevoerd met de 32-inch telescoop van de Misti Mountain Observatory, Northwestern Arizona, USA. De kern van het cluster wordt gedomineerd door vroeg-type stelsels. [Figuur: Jim Misti (Misti Mountain Observatory)].

vlaktehelderheid – en doen het stelsel van de FP vandaan bewegen. De positie van sterrenstelsels op de FP, in combinatie met kennis over de stellaire populaties, kan op deze wijze gebruikt worden om een fundamentele vraag te beantwoorden: zijn vroege stelsels passief evoluerende systemen? In dit proefschrift proberen we deze vraag te beantwoorden doormiddel van het bestuderen van vroeg-type stelsels die zich bevinden in de hoge dichtheid gebieden van clusters van sterrenstelsels.

Clusters van sterrenstelsels zijn gebonden structuren met een hoge massa en dichtheid. Ze zijn waarschijnlijk gevormd op een roodverschuiving $z > 2$ en bestaan uit honderden, zo niet duizenden sterrenstelsels. De relatie tussen morfologie en dichtheid, gevonden door Fritz Zwicky en later opnieuw gedefinieerd door Alan Dressler, leert ons dat des te drukker de omgeving, des te groter de kans dat stelsels in die omgeving vroeg-type stelsels zijn. Clusters van sterrenstelsels, onafhankelijk van roodverschuiving de gebieden met de hoogste dichtheid in het Heelal, zijn perfecte locaties om de formatie en evolutie van vroeg-type stelsels beter te leren begrijpen. Het nabijgelegen cluster met de meeste sterrenstelsels – vaak ook gebruikt als een referentiepunt voor ons lokale Universum– is het Coma cluster, afgebeeld in Figuur 2. Het Coma cluster is een massief ($M \sim 10^{15}\, M_{\odot}$) cluster van sterrenstelsels, bestaande uit duizenden stelsels; de stelsels die zich in de kern van deze cluster bevinden zijn voornamelijk vroeg-type stelsels.

In dit proefschrift bestuderen we vroeg-type sterrenstelsels die onderdeel zijn van vier optisch geselecteerde clusters (gelijk aan het Coma cluster) op drie verschillende roodverschuivingen. Vroeg-type stelsels zijn geselecteerd op basis van hun morfologie, kleur en hun positie ten opzichte van de kern van het cluster. We herleiden de geschiedenis van sterformatie van elk vroeg-type stelsel door gebruik te maken van state-of-the-art stellaire populatie modellen en procedures voor het reduceren van data.

In hoofdstuk 2 bestuderen we de invloed van stellaire populaties op de FP van vroeg-type stelsels in Abell 550, een cluster op roodverschuiving $z \sim 0.1$. We construeren de FP door gebruik te maken van afbeeldingen en spectra van de vroeg-type stelsels in Abell 550, waargenomen met de Very Large Telescope. Deze waarnemingen geven ons de structurele parameters en de snelheidsdispersie van elk stelsel. We bepalen de dynamische massa-lichtkracht verhouding door gebruik te maken van onze kinematische waarnemingen en de stellaire massa-lichtkracht verhouding door gebruik te maken van de stellaire populatie modellen. De bepaling van leeftijd, chemische compositie en de abundantie van α-elementen van de stellaire populaties wordt verkregen door gebruik te maken van absorptielijnen in de waargenomen spectra. Onze waarnemingen laten zien dat de spreiding rond de FP van de vroeg-type stelsels in Abell 550 veroorzaakt wordt door variaties in de *stellaire* massa-lichtkracht verhouding. Recente formatie van sterren kan de verhouding tussen massa en lichtkracht doen verlagen en doet de spreiding rond de FP toenemen. Verder vinden we dat de kanteling van de vroeg-type stelsels in dit cluster ten opzichte van de voorspellingen van de viriaalstelling ook toegeschreven kan worden aan recente formatie van nieuwe sterren: de stellaire massa-lichtkracht verhouding varieert systematisch met de dynamische massa-lichtkracht verhouding. Beide resultaten geven weer dat de vroeg-type stelsels in Abell 550, op een roodverschuiving van $z \sim 0.1$, de FP nog niet volledig volgen. Dit staat in schril contrast met de hypothese dat alle vroeg-type stelsels op roodverschuivingen $z < 2$ een passieve evolutie ondergaan.

In hoofdstuk 3 gaan we verder terug in de tijd en bestuderen we vroeg-type stelsels in het bekende samenklonterende cluster Abell 851, gelegen op een roodverschuiving van $z \sim 0.4$. Onze analyse van de FP en stellaire populaties leveren ook voor dit cluster sterk bewijs voor recente formatie van nieuwe sterren: de spreiding van vroeg-type stelsels in de FP is gecorreleerd aan de stellaire massa-lichtkracht verhouding gevonden met behulp van stellaire populatie modellen. De stellaire massa-lichtkracht verhouding laat een constante trend zien voor alle bestudeerde dynamische massa's. Deze empirische resultaten geven weer dat alle vroeg-type stelsels in Abell 851 onlangs een periode van sterformatie hebben ondergaan, ongeacht hun massa. De recente periode van sterformatie is verantwoordelijk voor de toegenomen spreiding rondom de FP, middels de verandering in de stellaire massa-lichtkracht verhouding. Deze resultaten kunnen verklaard worden aan de hand van een transformatie in morfologie en stellaire populatie van de vroeg-type stelsels in Abell 851, veroorzaakt door een continue accretie van materie op het cluster. Ze kunnen echter niet verklaard worden door middel van vroeg-type stelsels die reeds gevormd waren op hoge roodverschuiving waarna ze slechts passieve evolutie ondergingen.

In hoofdstuk 4 gaan we nog een stap verder terug in de tijd en bestuderen we vroeg-

type stelsels in twee clusters op roodverschuiving $z \sim 0.7$, GHO 1322+3027 en GHO 1322+3114. Ook in deze clusters hebben de vroeg-type stelsels een grote intrinsieke spreiding in de FP. De vroeg-type stelsels in de twee bestudeerde clusters volgen een gelijke trend tussen stellaire en dynamische massa-lichtkracht verhouding en dynamische massa. Evenals in de vorige twee hoofdstukken, zien we dat vroeg-type stelsels in GHO 1322+3027 en GHO 1322+3114 een recente periode van sterformatie hebben ondergaan. Deze recente sterformatie kan verklaard worden door veranderingen in de morfologie en stellaire populatie van de stelsels in de kern van deze clusters, veroorzaakt door een continue accretie van materie op de clusters.

In hoofdstuk 5 bespreken we de resultaten van alle voorgaande hoofdstukken in het licht van onze fundamentele vraag: zijn vroeg-type stelsels passief evoluerende stellaire systemen? We focussen op de evolutie van de dynamische en stellaire massa-lichtkracht verhouding van vroeg-type stelsels in clusters als functie van hun roodverschuiving. We nemen hierbij niet alleen de vroeg-type stelsels in de vier bestudeerde massieve clusters in beschouwing, maar ook die van het Coma cluster. De bestudeerde stelsels beslaan een tijdsbestek in roodverschuiving van $z = 0$ tot $z \sim 0.7$. Onze resultaten kunnen als volgt worden samengevat: de door ons bestudeerde vroeg-type stelsels tonen geen significante evolutie in hun gemiddelde dynamische of stellaire massa-lichtkracht verhouding. De gemiddelde leeftijd van de sterren in de vroeg-type stelsels zoals bepaald met stellaire populatie modellen is constant binnen de foutmarge. Hun chemische compositie neemt af naarmate de roodverschuiving toeneemt. De gemiddelde abundantie van α-elementen neemt toe naarmate de roodverschuiving hoger wordt. Dit laatste wekt de suggestie van een toename in de chemische elementen met dank aan de onlangs beëindigde sterformatie in de bestudeerde clusters.

Deze resultaten zijn slechts mogelijk wanneer de vroeg-type stelsels, op hun eigen respectievelijke roodverschuiving, in de afgelopen 2 miljard jaar een periode van sterformatie hebben ondergaan. De vroeg-type stelsels, allen op hun eigen roodverschijning waargenomen in clusters met een dynamische massa van $M > 10^{10.3}\,M_{\odot}$, hebben inderdaad allemaal een complexe stervorming geschiedenis. Dit wordt ondersteund door de waargenomen evolutie in hun dynamische en stellaire massa-lichtkracht verhouding. Kwalitatief kunnen we de oorzaak van deze recente periodes van sterformatie verklaren als een gevolg van veranderingen in de morfologie en stellaire populatie van de sterrenstelsels. Deze veranderingen vloeien voort uit de accretie van materie op de clusters; deze evolutie is aanwezig op alle bestudeerde roodverschuivingen, wat betekent dat vroeg-type stelsels tot vandaag de dag blijven evolueren.

Voor een massief cluster is de tijdsduur om binnen een viriële straal van 1 Mpc gevirialiseerd te raken ongeveer 1 miljard jaar. Dit is ongeveer gelijk aan de tijd die een stelsel nodig heeft om een massief cluster te doorkruisen. Het tijdsbestek waarbinnen recente vorming van nieuwe sterren de schijnbare leeftijd van stellaire populaties kan veranderen is ook ongeveer 1 miljard jaar. De combinatie van deze tijdschalen betekent dat sterrenstelsels in een cluster dat onlangs gevirialiseerd is voor nog eens ongeveer 1 miljard jaar interactie kunnen ondergaan met de omgeving binnen dit cluster. De stelsels in de kern van een gevirialiseerd cluster kunnen namelijk nog bezig zijn met hun eerste doorkruising van het cluster. Toen deze stelsels het cluster binnen vielen zijn ze

hun atomaire gas kwijt geraakt, maar hebben ze nog wel een hoeveelheid moleculair gas vast weten te houden. Dit gas kan worden omgezet in sterren als gevolg van verstoringen in de schijf van moleculair gas of als gevolg van getijde interacties met de potentiaal van het cluster. Als dit scenario correct is, zouden vroeg-type stelsels in clusters tekenen moeten laten zien van een recente periode van sterformatie, in overeenstemming met onze waarnemingen. Dit onderschrijft het idee van een toename in de stellaire massa van vroeg-type sterrenstelsels in clusters in de laatste 7 miljard jaar. De resultaten in dit proefschrift laten daarom zien dat het klassieke idee dat vroeg-type stelsels "rood en dood" zijn aan een herziening toe is.

Summary

Traditionally, galaxies have been classified according to their observed morphology as ellipticals, lenticulars, and spirals. Hubble placed these classes along the "tuning fork" diagram shown in Figure 1. Ellipticals (E) are situated to the left, lenticulars (S0) at the base of the fork, and spirals with (SB) and without (S) bar structures are separated along the two prongs. It is now customary to call those galaxies falling on the left of Figure 1 early-type galaxies (ellipticals and lenticulars), whereas those on the right are referred to as late-type galaxies (spirals). Early-type galaxies (ETGs) are dominated by red stellar populations, on the basis of which astronomers have hypothesized these galaxies completed their formation process when the Universe was much less than half of its current age. The idea is that ETGs had a burst of star formation very early in the history of the Universe, followed by simple passive evolution until the current epoch. On the contrary, late-type galaxies exhibit blue stellar populations, implying a strong contribution of young stars to their emission and a history of continuous star formation. This picture presents ETGs as having "red and dead" stellar populations.

However, according to the current paradigm of a Λ-Cold Dark Matter (ΛCDM) cosmology, structures form hierarchically, with small dark matter clumps merging together to form large dark matter halos. The associated baryons within the dark matter halos cool down dissipatively to form stellar systems, which we observe as galaxies. In this picture, galaxies are baryonic condensates at the center of large dark matter halos. ETG formation and evolution should then be hierarchical in nature with merging, accretion and *in situ* star formation all playing major roles in shaping this baryonic content.

A major problem in studying the stellar content of the ETGs is that these galaxies are too distant to resolve into individual stars using current optical telescopes. (M32 – a compact elliptical galaxy satellite of the Andromeda Galaxy – is the exception.) Therefore, one must study the integrated light and broad-band colors of these galaxies to understand the underlying properties of their stellar populations. Such studies are significantly limited by the degeneracy between age and metallicity of a given stellar population: in old populations, one can find equivalent changes in broad-band color by adjusting its metallicity *or* its age. This degeneracy implies that colors cannot be used to detect recent star-formation episodes occurring longer than 1–2 Gyr ago. Indeed, the red color of an ETG does not necessarily imply that it is *purely* composed of old

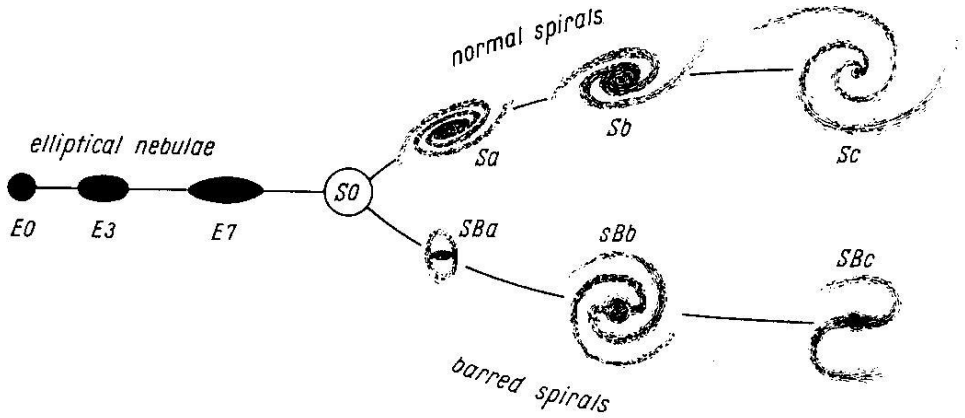

Figure 1: The Hubble tuning fork diagram. Galaxies to the left (ellipticals and lenticulars) are called early-type galaxies and those to the right (spirals) are called late-type galaxies. [Image credit: Hubble E.P., The Realm of the Nebulae (New Haven, 1936.)]

stars. Unless broken by additional information, the age–metallicity degeneracy prohibits studying the star-formation histories of ETGs via broad-band colors. Fortunately, one can isolate the effects of age and metallicity by observing a combination of absorption lines in integrated-light spectra that are primarily sensitive to either age *or* metallicity.

Additionally, ETGs are observed to follow a tight scaling relation called the Fundamental Plane (FP), a plane in the three-dimensional phase space relating velocity dispersion (σ) to effective radius (R_e) and mean surface brightness ($\langle I_e \rangle$). The virial theorem predicts that ETGs should lie along a single plane in this space. However, it has been found that the FP is tilted with respect to this expectation; we discuss this tilt in the context of star-formation below. The intrinsic scatter about the FP is $\sim$10–15% for ETGs in local galaxy clusters. The FP is only weakly affected by the age–metallicity degeneracy and can therefore be used to understand ETG formation and evolution over cosmic times. The (σ, R_e, $\langle I_e \rangle$) coordinate of a galaxy can be related to its star-formation history in the sense that recent star formation should enhance the luminosity of that galaxy – and therefore its surface brightness – and can move the galaxy off the plane. In this way, the combination of the position of a galaxy on the FP and a knowledge of its stellar content can be used to answer a fundamental question: are ETGs passively evolving stellar systems? In this thesis, we attempt to answer this question by studying ETGs in the very dense environments of galaxy clusters.

Galaxy clusters are dense, massive, and bound structures thought to form at $z > 2$ and consisting of hundreds to thousands of galaxies. The morphology–density relation first discovered by Fritz Zwicky and later refined by Alan Dressler states that the more crowded ("denser") the environment, the more likely the galaxies found in that environment are ETGs. Thus galaxy clusters, the densest environments at any redshift, are ideal laboratories to understand the formation and evolution of ETGs. The richest nearby galaxy cluster – often used as a local-Universe reference point – is the Coma

Figure 2: Ground based image of the local-Universe galaxy cluster Abell 1656 (Coma) located in the constellation Coma Berenices. The image was taken with a 32-inch telescope at Misti Mountain Observatory, Northwestern Arizona, USA. The core of the cluster is dominated by galaxies with early-type morphology. [Image credit & copyright: Jim Misti (Misti Mountain Observatory)].

cluster, shown in Figure 2. The Coma cluster is a massive ($M \sim 10^{15}\,M_{\odot}$) galaxy cluster consisting of thousands of galaxies; the galaxies that occupy its dense core region are primarily ETGs.

In this thesis, we have studied ETGs belonging to four rich, optically-selected clusters (like the Coma cluster) in three redshift bins. We have selected ETGs for this study based on their early-type morphology, color, and their position relative to the cluster core. We have used state-of-the-art data-reduction procedures and stellar-population models to derive the star-formation history of each ETG.

In Chapter 2, we studied the impact of stellar populations on the FP of ETGs in Abell 550, a galaxy cluster at $z \sim 0.1$. We constructed the FP using structural parameters from Very Large Telescope (VLT) imaging and velocity dispersion measurements from VLT spectra of each ETG. We calculated dynamical mass-to-light ratios using our kinematic measurements and stellar mass-to-light ratios using stellar-population models. Our stellar-population measurements yield ages, metallicities, and α-element enhancements derived from absorption-line strengths measured from our high signal-to-noise spectra. We found that the ETGs in Abell 550 exhibit a scatter about the FP due to the intrinsic variations of their *stellar* mass-to-light ratios: recent star formation

decreases the stellar mass-to-light ratios and increases the scatter of galaxies about the FP, yielding a finite thickness of the FP for this cluster. Additionally, we found that the tilt of the FP for this cluster can also be attributed to recent star formation: the stellar mass-to-light ratios vary systematically with their dynamical mass. Both results indicate that the ETGs in Abell 550 are still falling onto the FP relation at $z \sim 0.1$, strongly conflicting with the hypothesis that all ETGs should be passively evolving at $z < 2$.

In Chapter 3, we went further back in time by studying ETGs in the well-known merging cluster Abell 851 at $z \sim 0.4$. Our FP and stellar population analysis also resulted in strong evidence for recent star formation in this cluster: the FP residual is correlated with the stellar mass-to-light ratio derived from stellar-population modeling. The stellar mass-to-light ratios have a constant trend over the range of measured dynamical masses. These two empirical results imply that all ETGs in Abell 851 have undergone recent star-formation episodes regardless of their mass, and that this recent star formation is responsible for the increased scatter in the FP via the change in the stellar mass-to-light ratios. Our results can be explained by morphological and stellar-population transformations of the ETGs in Abell 851 due to the on-going cluster assembly at $z \sim 0.4$. They cannot be explained by ETG formation at high redshifts followed by completely passive evolution to the epoch of observation.

In Chapter 4, we extend our study to higher redshifts by studying ETGs in two galaxy clusters at $z \sim 0.7$, GHO 1322+3027 and GHO 1322+3114. We found that the FP of ETGs in these clusters also has a large intrinsic scatter. The stellar and dynamical mass-to-light ratios follow similar trends over the range of calculated dynamical mass. Thus, similar to the results in the previous two chapters, we find the ETGs in GHO 1322+3027 and GHO 1322+3114 have undergone recent star-formation episodes. The reason for this recent star formation can be explained by morphological and stellar-population transformations happening in the cluster core due to the on-going cluster assembly processes.

In Chapter 5, we discuss the results from the previous chapters in the context of our fundamental question: are ETGs passively evolving stellar systems? Our discussion focusses on the evolution of the dynamical and stellar mass-to-light ratios in cluster ETGs as a function of redshift from our study. This analysis includes ETGs from all four rich, massive clusters studied here and the Coma Cluster, over the full redshift range of $0 < z < 0.7$. The results may be briefly summarized as follows: the ETGs in our study exhibit no significant evolution in the mean dynamical or stellar mass-to-light ratios. The mean SSP ages of the ETGs are constant within the errors, whereas their mean metallicity decreases toward higher redshifts. The average α-enhancement increases toward higher redshift, suggesting on-going build-up of chemical elements from recently terminated star formation in the clusters at each epoch.

These results are only possible if these ETGs, at their respective epochs, experienced star-formation events within the last 2 Gyr. Indeed, the cluster ETGs at all redshifts with dynamical mass of $M > 10^{10.3}\,M_{\odot}$ exhibit complex star-formation histories, as supported by the evolution of their dynamical and stellar mass-to-light ratios. We qualitatively explain the origin of these recent star formation episodes as being due to

morphological and stellar-population transformations arising from the ongoing assembly of galaxy clusters; this evolution is seen at all redshifts meaning ETGs continue to evolve well into the current epoch ($z \sim 0$).

The virialisation time for massive galaxy clusters within a virial radius of 1 Mpc is ~ 1 Gyr, which is approximately the cluster crossing time. The key time period within which recent star formation can alter the apparent age of the stellar population, more specifically the luminosity-weighted temperature of the main-sequence turn-off, is also ~ 1 Gyr. This correspondence implies that recently virialized clusters will have galaxies that continue to interact with the hostile cluster environment for ~ 1 Gyr, which may lead to final and intense star-formation events. That is, galaxies in a relaxed cluster core might actually be on their first cluster crossing phase. These galaxies will have had their atomic gas stripped, due to ram-pressure stripping, upon entering the cluster, but they may retain molecular gas at their centers. This gas can then form stars due to instabilities in the discs formed out of the molecular gas or due to tidal interactions with the cluster potential. In this scenario, our study of cluster ETGs would show signs of recent star-formation episodes, supporting the idea of stellar mass build-up of early-type galaxies over the last 7 Gyrs in galaxy clusters. Therefore, the classic picture of ETGs as "red and dead" galaxies needs revision given the results presented in this thesis.

Acknowledgements

Finally the time has come to end this thesis with the traditional ritual. I can see the ray of hope at the end of the long tunnel. These past years here in the Netherlands under the pretext of doing research have had a great impact on my scientific and personal life. The scientific environment provided by the staff and management team along with the international ambience of the Kapteyn Astronomical Institute have impressed me over the years. Life was not always easy during these years. There were happy times of exploration: places, food, weather and people; tough times of dealing with cultural differences; and gloomy days in which the entire enterprise of life itself was a struggle. I have done my best in enjoying and overcoming whatever happened during these years, not alone, but with the help of many people that I would like to mention here.

Scott, I remember the time we first talked over the phone for an hour. It was the coolest interview I had ever given in my life. We then met at Groningen Centraal for the first time. You could easily identify me due to obvious reasons, which I don't want to mention here. It was a great time doing science with you. I should admit that it was not easy for you, due to my taking-things-for-granted attitude combined with an over-enthusiasm that led to the many careless mistakes I made and weird conclusions I came to. It was quite a challenge for you to change me to be careful and critical while doing science. I will say, up to some extent, you succeeded in that endeavor. Thank you for allowing me to have the scientific freedom to explore my own ideas and for stepping in many times when I had completely derailed myself. Thanks for your strong understanding of the situation when tough times kicked in, letting me go on short and long breaks to India. You are one of the few people I have met here with a strong empathy. This thesis would not have been finished without your support, encouragement and guidance. Thanks for everything!

Kate, it was really nice meeting you here in Groningen. Thanks for hosting me for my first dinner in Groningen and the many other dinners that followed. Catriona, it was very nice to see you growing over the years. I enjoyed the chats with you and the fun of playing the AH card game.

Reynier, from the very beginning you were interested in my research. I was intimidated many times in the beginning by your strong opinion on my way of doing science. Being from a culture where these things are considered negative, it took me a while to

understand you. Over the years I have realised your intentions, which were always kind and helpful. I am very glad that we met here. Thanks for our numerous interactions, which many times happened in corridors. They gave me many new ideas regarding the topics covered in this thesis. Thanks for the time we spent during the conference in Munich and the winter school in the Canary Islands.

Saleem, you are one of those rare personalities that gives me both hope and happiness. Thanks for your good advice and help on many occasions.

I would like to express my gratitude to the current and former PBC of the Kapteyn Institute which includes Rien, Amina, Reynier, Inga, Saleem, and Eline.

I thank my reading committee members — Marc, Saleem and Reynier — for their input that improved the content of this thesis.

Gergö, I know translating the Dutch summary was not an easy task, but I am sure that you now know a good deal of what my thesis is all about. Thank you very much!

Niels, I am very impressed by your design skills. Your implementation of the design for my thesis cover was more than what I could have expected. Thanks a lot "Buurman".

I thank my native English speaking friends, Robyn and Kyle for checking my writing.

I would like to express my gratitude to the secretariat at the Kapteyn Institute — Hennie, Jackie, Gineke, and Christa — and the Computer group — Wim, Eite and Martin — for always being very helpful. Hennie, thanks for all the help with travel declarations. You were always very nice to me. Jackie, thanks for those many Dutch translations you did for me in the beginning. Lucia, thanks for all the help with the administrative procedures dealing with all the paperwork starting in India and continuing throughout the years here. Your efficient way of dealing with the ISD and the University bureaucracy put me at ease.

I thank Stuart, Renzo, Mariano, Peter, Piet, Thijs and Bob for the many interactions over the coffee table and in the corridors. Thanks to Hugo van Woerden for always being curious about my well being here.

I decided that I wanted to continue in science while completing my master thesis. Prof.K.Indulekha from the School of Pure and Applied Physics is largely responsible for that, by giving me a recommendation letter to attend a summer school at IUCAA in Pune. I then did my master's thesis work with Prof.A.N.Ramaprakash of IUCAA, which further increased my interest in astronomy. I'd like to express my gratitude to them. This was followed by brief stints at the Physical Research Laboratory, Ahmedabad, and the ISRO Satellite Center, Bangalore. I thank Prof.T.Chandrasekhar for guidance and support. Prof.N.M.Ashok and Prof.D.P.K.Banerjee were my close collaborators during the time I spent at PRL. I thank them for encouraging my scientific curiosity and enthusiasm. I thank Dr.K.Sankarasubramanian of ISRO Satellite Center, Bangalore, for introducing me to astronomical instrumentation.

To my current and former group members: Thanks for the discussion and group meetings. It was fun to see you guys evolve during the years. I wish you good luck with future group meetings. :)

Mathias, thanks for our many scientific discussions during the initial phase of this work. Antonela, we had many discussions on resolved stellar population, which gave me a first level understanding for integrated stellar populations. Yanping, I have never

seen such a hard working person. Your thesis should be called "Life of Ping". Chiara, you are so enthusiastic about the IMF. I enjoyed all our scientific and non-scientifc chats. Thanks for the last-minute help with pPXF errors. Sofia, you should keep watching "The Big Bang Theory", which I think is very useful with your thesis work. Gergö, I still remember our discussion about your future plans when you were a master's student, and eventually you joined our group and became a vital part. Thanks for those many scientific interactions we had over the last years. Your semi-analytic feeling for galaxy formation and evolution helped in understanding my observations. Wouter, I am amazed by your questioning nature and criticality.

My current and former officemates, Antonela: Thanks for your cool, easy going nature. It was fun to share an office with you. Facu, I couldn't think of our office in those days without your frequent visits. I have many things to say here, but I better stop.:) Matthijs: Thanks for the nice company in our office. Bee it was really nice to meet you here in Groningen. I was very happy to be there at your wedding and see you guys growing as a big family over the years, with two more members by now. I enjoyed our officemate dinners.

Rosina: You are the only soft spoken person who shared an office with me.:) Thanks for the time I could spend with Toby, Blanka and Fleur. Hans: When you first came to the office, it was like Pearl Harbor. I was not prepared for it and I thought it is going to be a disaster. Your need to make things according to your own way was unacceptable for me. But we got out of that very fast. We both are good at breaking silences in our office, which was later overtaken by the addition of Robyn. Robyn, you are one of the most cheerful ladies I ever met in my life. Yet, I could see you struggle over the years commuting between Paris and Groningen. Andrew and you should get a job at one place together soon. Thank you guys, for the fun, laughter, candies, cakes, tea supply, particularly during the last crazy periods of thesis writing.

Rajat, Laura, Simona, Vibor, and Panos were the first to incorporate me into their social activities outside of the institute. Rajat thanks for those replies for my mails from India. It was nice meeting you here. Your help during my first weeks here is very much appreciated. Laura Sales, "machi" it was fun hanging out with you. Your opinions on many things made me laugh like crazy. I won't forget the early morning call I got from Canada asking to break into your apartment. Luckily I was wise enough that I didn't do it.:) Simona: There are numerous things to say about you. Thanks for the first Italian dish you made for me on my first days here. I was really struggling to eat it, with my spicy Indian tastes, and politeness at the same time to say I liked it.:) It is nice to see you again and again here in Groningen over the years. Vibor, "macha" thanks for those Croatian delights and your many stories, which still make me laugh. Thanks to you and Katarina for many dinners. Panos, Panos, "macha" you have explanations and excuses for everything. You are one of the nerdiest guys I met here.:) Thanks for the company and our many car rides together. The one through Germany was really crazy.

Leon (Koopmans), we became good friends over the years. Thanks for the time at the Pacific or at the Greek restaurant or at the Mr. Mofongo. Your explanations for things and facts were always supported by scientific theories. I am amazed by the way

your scientific perceptive mind works. Thanks for the company, Leon.

Carlos, you are a rare species. You were hiding in your office for one year and then you started interacting with people. It was nice to meet you here. Your arguments were always right in the end. Thanks for many scientific and non-scientific discussions and the support during many difficult times.

Kyle, we became good friends over the years. I enjoyed your company on numerous occasions, parties, dinners, game nights. Thanks for always being very willing to help in time of need.

John, thanks for the time we spend together with the "usual suspects" at the Pacific.

Shoko, though we knew each other only for the past year, it was really nice to have your company on many occasions and particularly to complain about the "wonderful" Dutch weather.

Boris, thanks for being a nice office neighbour and for checking in many times.

Harish and Iva, you guys are great explorers. Thanks for those many dinners. I am looking forward to the day when you settle in India. :)

Gergö and Anke, thanks for the dinners and game nights.

Mark (den Brok), we went on many bike rides in the first years. I was always puzzled by the fact that, how little you knew about the world outside the Netherlands.:) Hope you are enjoying life in Utah. Thanks for the company.

Amina, thanks for the friendship and inviting me for those many cocktail parties. I will never forget the day I scared you in the corridor. :)

Parisa, it was always fun talking to you. I wish you good luck with your future endeavors.

Sofia and Thomas, it was nice to see you people getting together and fun to be there for your semi-Dutch wedding.

German, thanks for the chocolates and chats, particularly in sharing the "fun" of thesis writing in these last months.

Andrea, thanks for making real Italian coffee (from a machine) on many lazy afternoons.

Johan, thanks for those many coffees. Hugo, thanks for the computational tips and to be a true "Buurman".

Andre, Ajinkya, Maarten, Facundo, Thomas Martinsson, Teffie, Johnson, Else, Tjiske, Guobao, Giacomo, Katinka, Federico, Pratyush, Esra, Burcu, Aycin, Paolo, Oscar, Oscar, Teresa, Stephanie, Stefania, Silvia, Linda, Leon, Soobash, Abhik, Yunhee, Patrick, Alexandros, Marius, Jeffrey, Eva, Beth, Seyit, Stephan, Gert, Gijs, and many more I am forgetting here, thanks for many chats during coffee times, lunch, or dinners.

Pandey and Sweta, thanks for the dinners. I am glad to see you people getting merged into the Dutch culture. :)

My friends from India, Blesson and Sreeja. Thanks for being there over the years. Blesson, we have known each other for a long time, but in Bangalore we became good friends. I am glad that you are enjoying life in Melbourne. Ramya, Vigeesh, Bharat, Uday, Malay, Nagaraj, Sreejith, Debbijoy, Smitha, Bhavya, Anusha, Ajith, Toney, Shaiju, and many more, I have appreciated your company over the years.

My "mallu" friends in the Netherlands: Shahina and Musthafa, thanks for hosting me at your place on many occasions over the years. It was really nice to have someone with whom I can talk Malayalam. :) Sheeba and Rajesh, thanks for those interactions that always happened at Musthafa's. Shaji, I badly miss you for the last one year. Hope you are enjoying life in Norway. Aunty Kamala and Uncle Berny, thanks for the time I spent with you. The dinners and get togethers at your place were always amusing.

Wim, it was really nice meeting you here. Thanks for introducing me to the Christian assembly in Groningen. Thanks for your companionship and advice on many occasions.

Jelle, it was nice to see how you changed over the years. I am glad that you got Eunice and I enjoyed the day-long typical Dutch wedding.

Janneke, thanks for the house. Marten and Carien, you guys have expanded your family since I came here. Thanks for the times we spent together.

Eduard and Tineke, I always enjoyed visiting familie Bus in Sappemeer. Thanks for the time I could spend with you during harvests, barbecues and many dinners.

Familie Brug, thanks for being such a nice, cool neighbour and landlord, both at the same time. I enjoyed my stay at your place over the years.

Finally I thank my family back in India for their support and encouragement over the years.

All's Well That Ends Well, this thesis is not an exception.

Koshy George
Groningen
April, 2013